UNIVERSITY OF CALIFORNIA SAN DIEGO

Neuron Growth Estimation and Control

A dissertation submitted in partial satisfaction of the
requirements for the degree Doctor of Philosophy

in

Engineering Sciences (Aerospace Engineering)

by

Cenk Demir

Committee in charge:

Professor Miroslav Krstić, Chair
Professor Jorge Cortés
Professor Mamadou Diagne
Professor Padmini Rangamani
Professor Ruth J. Williams

2024

The Dissertation of Cenk Demir is approved, and it is acceptable in quality and form for publication on microfilm and electronically.

University of California San Diego

2024

DEDICATION

I dedicate this dissertation to my family and friends.

EPIGRAPH

İstikbal göklerdedir. / The future is in the skies.

–Mustafa Kemal Atatürk

TABLE OF CONTENTS

Dissertation Approval Page iii

Dedication iv

Epigraph v

Table of Contents vi

List of Figures ix

List of Tables x

Acknowledgements xi

Vita xiv

Abstract of the Dissertation xv

Chapter 1 The Foundation of Neuronal Growth and Control 1
1.1 Understanding Neuronal Functionality 1
1.2 Why Neuron Growth Matters: From Development to Disease 2
1.3 Modeling the Mysteries: Mathematical Approaches to Neuron Growth 4
1.3.1 Transport-limited models 4
1.3.2 Mechanically mediated growth models 6
1.4 Literature Review for Neuron Growth Control 7
1.5 Literature Review for PDE Control 7
1.6 Research Objectives and Contributions 9
1.6.1 Innovations in neuron growth control 9
1.6.2 Theoretical advances in boundary control of PDEs 10
1.7 Organization of the Dissertation 11

Chapter 2 Moving Boundary Neuron Growth Model 15
2.1 Introduction to the Moving Boundary PDE-ODE Coupled Model 15
2.2 Reference Error System and Control Objective 17
2.2.1 Reference error system 17
2.2.2 Linearized error system 19
2.3 Towards Closed-loop Feedback Control 20
2.3.1 Control objective 20
2.3.2 Basic idea of Stefan type of PDE control 21

Chapter 3 State Feedback Control Design 27
3.1 Backstepping Control of Neuron Growth Problem 27
3.1.1 Transformation into target system 28
3.1.2 Gain kernel solutions 29

3.1.3 Backstepping control law 31
3.2 Stability proof under state-feedback control 31
3.2.1 Nonlinear target system. 31
3.2.2 How to ensure local stability on a non-constant spatial interval. 32
3.2.3 Inverse Transformation. 33
3.2.4 Lyapunov analysis 33
3.2.5 Ensuring bounds on axon length and growth rate. 40
3.3 Simulations 42
3.3.1 Parameter Values 42
3.3.2 Axon elongation by up to *three orders of magnitude* 43

Chapter 4 Neuron Growth State Estimation 46
4.1 Observer Design 47
4.1.1 Observer Error System 48
4.1.2 Backstepping Transformation 49
4.1.3 Well-posedness of backstepping transformations 50
4.2 Stability proof of designed observer 56
4.2.1 Inverse Transformation 56
4.2.2 Lyapunov analysis 57
4.3 Simulations: Estimation of unmeasured tubulin concentration profile in a 4× growth 62

Chapter 5 Observer-based Neuron Growth Control 65
5.1 Output-feedback design 65
5.1.1 Reference error states 66
5.1.2 Target reference error states 67
5.2 Stability under output-feedback control 67
5.2.1 Lyapunov Analysis 67
5.3 Simulations: Axon elongation by up to *three orders of magnitude* 71
5.4 Robustness to Large Uncertainty in Diffusion, Advection, and Reaction 74

Chapter 6 Input Delay Compensation 77
6.1 Axon Growth Model with Input Delay 78
6.1.1 The reference error system with input delay 78
6.1.2 Input delay as transport PDE 79
6.1.3 Linearized reference error system 80
6.2 Backstepping Design of Delay Compensated Control 80
6.2.1 Transformation into target system 81
6.2.2 Gain kernel solutions 83
6.2.3 Delay compensated backstepping control law 83
6.3 Stability proof under delay compensated control 84
6.3.1 Transformed nonlinear target system 84
6.3.2 Inverse transformation 85
6.3.3 System property to ensure local stability on a non-constant interval 87

6.3.4 Lyapunov analysis . . . 87
6.3.5 Guaranteeing the conditions for all time . . . 94

Chapter 7 Event-triggered Control . . . 98
7.1 Axon Growth Model with Actuation at Robin Boundary Condition . . . 98
7.2 Sample-based Control of Neuron Growth Problem . . . 100
7.2.1 Transformation into target system . . . 100
7.2.2 Gain kernel solutions . . . 101
7.2.3 Continuous-time and sampled-data control law . . . 101
7.3 Event-Triggered based Control . . . 102
7.4 Avoidance of zeno phenomena and stability proof under event-triggering Control 106
7.4.1 Avoidance of Zeno phenomena . . . 106
7.4.2 Stability proof under event-triggering control law . . . 108
7.4.3 Nonlinear target system . . . 109
7.4.4 Lyapunov analysis . . . 109
7.5 Simulations . . . 115

Chapter 8 Periodic Event-triggered Control . . . 118
8.1 Periodic event-triggered based control . . . 118
8.1.1 Selection of the sampling period . . . 119
8.1.2 Design of the periodic event triggering function $\Gamma^p(t)$ . . . 120
8.2 Convergence proof under periodic event-triggering control law . . . 125
8.2.1 Nonlinear target system . . . 126
8.2.2 Lyapunov analysis . . . 126
8.3 Simulations . . . 129

Chapter 9 Conclusion and Future Work . . . 132
9.1 Summary . . . 132
9.2 Future Work . . . 135

Bibliography . . . 137

LIST OF FIGURES

Figure 2.1. Schematic of neuron and state variables 16

Figure 3.1. The closed-loop response of the designed full-state feedback control system. 43

Figure 3.2. The closed-loop response of the designed full-state feedback control system for long-range elongation $l_s = 1$. 44

Figure 4.1. Increase of the observer gain throughout the growth of the axon length. . . 62

Figure 4.2. Open-loop responses of the plant and observer. 63

Figure 5.1. Block diagram of observer design and output feedback system 65

Figure 5.2. Close-loop response of the plant and observer. 72

Figure 5.3. The estimated tubulin concentration, $\hat{c}(x,t) = \hat{u}(x,t) + c_{\text{eq}}(x)$, generated by the observer in (4.1)-(4.5), converges to the unmeasured tubulin concentration, $c(x,t)$, generated by nonlinear plant dynamics (2.1)-(2.5), and then both converge to the steady-state solution, $c_{\text{eq}}(x)$ by about $t = 15$ hours. . . 73

Figure 5.4. The estimation error, $\tilde{c}(x,t)$, between the estimated tubulin concentration $\hat{c}(x,t)$ and the plant tubulin concentration $c(x,t)$ converges to 0 uniformly along the axon length. 74

Figure 5.5. Robustness study of the proposed observer and the output feedback control under parameters' mismatch between the plant and the estimator. 75

Figure 7.1. The closed-loop response of the continuous-time and event-triggered control law for $l_s = 12\mu m$ 116

Figure 7.2. The closed-loop response of the designed full-state feedback control system for continuous-time and event-triggered control law. 117

Figure 8.1. Comparison between periodic-event triggering control input $U_k^p(t)$, continuous time event triggering control input $U_k^c(t)$ and the continuous control law $U(t)$ 130

Figure 8.2. The tubulin concentration governed by (2.1)-(2.5), $c(x,t)$, converges to the steady-state tubulin concentration, $c_{\text{eq}}(t)$ by about $t = 4.5$min for both continuous control input, CETC and PETC. The axon length, $l(t)$, also converges to the desired axon length, l_s, by about $t = 4$min. 131

LIST OF TABLES

Table 1.1. Mathematical models of neuron growth 4

Table 3.1. Biological constants and control parameters 42

ACKNOWLEDGEMENTS

As my advisor, Prof. Krstic has been a constant source throughout my academic journey. Over the past five years, I have also had the privilege of serving as his teaching assistant, which has further deepened my appreciation for his expertise and approach to both teaching and research. His exceptional knowledge and willingness to address my questions, regardless of the time, have been invaluable in shaping my research. I have particularly admired his ability to explain complex concepts with clarity, a skill that has significantly influenced my own ability to articulate and present my work. Prof. Krstic's mentorship has not only directed the course of my research but has also inspired me to strive for excellence in clarity and precision.

I want to express my sincere thanks to Shumon Koga who introduced this dissertation topic to me and for his unwavering support and dedication throughout this journey. His time and effort have been vital to my progress, and his encouragement, along with the supportive environment he creates, has been invaluable. I am truly grateful for the positive influence he has had on both my academic and personal growth.

I would like to express my gratitude to Prof. Mamadou Diagne, who has always been a source of inspiration and support. His insightful guidance and encouragement have greatly contributed to my development, both as a researcher and as an individual.

I would also like to express my gratitude to Bhathiya Rathnayake, who not only developed event-triggering mechanisms for the Stefan problem but also consistently engaged in generous and selfless discussions on event-triggered control, greatly enhancing my understanding of the subject. Beyond our academic collaborations, I am truly thankful for his wonderful friendship.

Throughout my academic journey, I have had the opportunity to serve as a teaching assistant for many classes, and I have gained valuable insights from each of the instructors. I would like to extend my sincere thanks to Prof. Sylvia Herbert, Prof. Boris Kramer, Prof. Jorge Cortes, Prof. Mauricio de Oliveira, and Prof. Robert Bitmead for their guidance and the knowledge they have imparted.

Thanks to my father Nihat Demir, my mother Tulay Demir, my aunt Gulay Yerlikaya and

my dear brothers, Mert and Berk Demir for their constant support and encouragement throughout my life. I'm deeply grateful to my girlfriend's family—Cindi Viviano, Daniel Metz, Jasmina Sing, Jeffrey Metz, and Annette Aerenson—for their support and for being my family here.

Also thanks to my friends for your support and all of the memories: Gokhan Gultepe, Ismail Ocak, Basar Kutukcu, Ebru Evcen, Merve Basaranbilek, Berat Gulecyuz, Korkut Eken, Ayse Betul Kolemen, Onur Tepencelik, Saygin Artiran, Yigit Korkmaz and many other friends that I met during this journey. I would not have been able to find the motivation throughout the years without you all.

I would like to thank my labmates, Drew Steves, Imoleayo Abel, Alan Williams, Huan Yu, Tugrul Yilmaz, Carina Veil, Kwang Hak Kim, Brad Ratto, Varun Ramadurai, Stephen Chen, Leobardo Camacho, Mostafa Bagheri, Evelia Zapien Ramos, Mohammad AlSuwaidan, and visiting professors Fatma Yıldız Taşcıkaraoğlu and Akın Taşcıkaraoğlu. I'm grateful to have been in such a supportive and easygoing lab, which helped me stay focused and balanced during this journey, and I appreciate the insightful conversations, great coffee, and all the laughs we shared during lunches and trips.

Finally, I want to express my deepest gratitude to my girlfriend, Elana Metz. She has become an essential part of my life, sharing in both the everyday moments and the adventures, and bringing a sense of joy and warmth to each day. Her steady support, bright smiles, and genuine love have made this journey not only possible but also far more rewarding than I could have ever imagined. Having her by my side has made every challenge easier to face and every achievement more meaningful.

To my committee, thank you for your time, effort, and interest in reviewing my work.

Chapter 2 and 3 have been published with the title "Neuron growth control and estimation by PDE backstepping" C. Demir, S. Koga, M. Krstic. Chapter 2 and 3 also contain a partial adaptation of the work contained in the conference paper "Neuron growth control by PDE backstepping: Axon length regulation by tubulin flux actuation in soma" C.Demir, S.Koga, M. Krstic, presented at the IEEE Conference on Decision and Control 2021. The dissertation author

was the primary investigator and author of these two papers.

Chapter 4 and 5 have been published with the title “Neuron growth control and estimation by PDE backstepping” C. Demir, S. Koga, M. Krstic. Chapter 4 and 5 also contain a partial adaptation of the work contained in the conference paper “Neuron growth output-feedback control by pde backstepping” C. Demir, S. Koga, M. Krstic, presented at the American Control Conference 2022. The dissertation author was the primary investigator and author of these two papers.

Chapter 6 contains a partial adaptation of the work contained in the conference paper “Input Delay Compensation for Neuron Growth by PDE Backstepping” C. Demir, S. Koga, M. Krstic, presented at the 17th IFAC Workshop on Time Delay Systems 2022. The dissertation author was the primary investigator and author of these two papers.

Chapter 7 contains a partial adaptation of the work contained in the conference paper “Event-Triggered Control of Neuron Growth with Actuation at Soma” C. Demir, S. Koga, M. Krstic, presented at the American Control Conference 2024. The dissertation author was the primary investigator and author of these two papers.

Chapter 8 contains a partial adaptation of the work contained in the conference paper “Periodic Event-Triggered Boundary Control of Neuron Growth with Actuation at Soma” C. Demir, S. Koga, M. Krstic, accepted and will be presented at IEEE Conference on Decision and Control 2024. The dissertation author was the primary investigator and author of these two papers.

Chapter 1 contains snippets of introduction sections and literature gathered from the previously mentioned publications (or submitted publications).

VITA

2013	B. S. in Electrical and Electronics Engineering, Pamukkale University
2018	M. S. in Electrical and Computer Engineering, University of Delaware
2024	Ph.D. in Engineering Sciences (Aerospace Engineering), University of California San Diego

PUBLICATIONS

C. Demir, M. Diagne, M. Krstic, "Adaptive Event-Triggered and Periodic Event-Triggered Boundary Control of Neuron Growth with Actuation at Soma" in preparation for publication 2024.

C. Demir, M. Diagne, M. Krstic, "Periodic Event-Triggered Boundary Control of Neuron Growth with Actuation at Soma" Accepted in the Proceedings of the 63rd IEEE Conference on Decision and Control 2024.

C. Demir, S. Koga, M. Krstic, "Event-Triggered Control of Neuron Growth with Dirichlet Actuation at Soma" American Control Conference 2024.

C. Demir, S. Koga, M. Krstic, "Neuron growth control and estimation by PDE backstepping" Automatica 2024.

S. Koga, C. Demir, M. Krstic, "Event-triggered safe stabilizing boundary control for the Stefan PDE system with actuator dynamics" American Control Conference 2023.

C. Demir, S. Koga, M. Krstic, "Neuron growth output-feedback control by pde backstepping" American Control Conference 2022.

C. Demir, S. Koga, M. Krstic, "Input Delay Compensation for Neuron Growth by PDE Backstepping" IFAC-PapersOnLine 55.36, 2022.

C. Demir, S. Koga, M. Krstic, "Neuron growth control by PDE backstepping: Axon length regulation by tubulin flux actuation in soma" The 60th IEEE Conference on Decision and Control 2021.

ABSTRACT OF THE DISSERTATION

Neuron Growth Estimation and Control

by

Cenk Demir

Doctor of Philosophy in Engineering Sciences (Aerospace Engineering)

University of California San Diego, 2024

Professor Miroslav Krstić, Chair

This dissertation introduces a control mechanism for addressing neuronal growth problems, which can be applied to neurological disorders such as spinal cord injuries, Parkinson's disease, and Alzheimer's disease that limit neuronal functionality. We consider a recent medical therapy, Chondroitinase ABC (ChABC), as a control mechanism for these conditions. ChABC aims to treat these conditions by restoring neuron functionality through axon growth for damaged neurons. It manipulates the extracellular matrix (ECM), a network of macromolecules and minerals that surrounds neurons and regulates their activity. As a result, neurons produce tubulin proteins, which cause the axon to elongate. This process is modeled as a Partial Differential Equation (PDE), representing the behavior of tubulin concentration along the axon, with a moving

boundary governed by Ordinary Differential Equations (ODE) consisting of the dynamics of the axon length and tubulin concentration in the growth cone. In this dissertation, we propose nonlinear design methods for a novel state feedback control law, an observer, and an output feedback control law for a one-dimensional model of axonal elongation. We demonstrate the robustness of the model to parameter changes of up to 40% relative to the original design and analysis framework. We also address potential challenges, such as input delay, and propose a compensation mechanism to overcome these issues. In addition to theoretical challenges, we enhance the practical applicability of the proposed control law by introducing an event-triggered control mechanism that allows users to update the control law in a sample-based manner. We ensured local exponential stability and convergence of the closed-loop system, integrating the plant dynamics with the proposed control law across all these techniques. The performance of the designed control methods was validated through numerical simulations, demonstrating neuron elongation by up to three orders of magnitude. These advancements offer promising avenues for enhancing neural regeneration therapies and contribute significantly to the understanding of neural growth dynamics, while also advancing theoretical control of Stefan-type moving boundary PDE-ODE coupled systems.

Chapter 1

The Foundation of Neuronal Growth and Control

1.1 Understanding Neuronal Functionality

Neuroscience is a leading multidisciplinary field focused on understanding neuronal functionality, drawing interest from medical science, engineering, biology, mathematics, and other disciplines [44, 3, 43, 16, 93, 57]. Each of these disciplines play a role in understanding how neurons function, how they are structured, and how to cure neuron-based diseases [87, 81]. To comprehensively study these aspects, researchers categorize neuronal functionality into two major anatomical systems in vertebrate animals: the central nervous system (CNS) and the peripheral nervous system (PNS).

The CNS is a complex network that integrates sensory information from the PNS and coordinates bodily functions by sending commands back to the PNS. Essentially, it serves as the control center for vertebrate animals, managing everything from basic reflexes to higher-order cognitive processes. It consists of the brain and spinal cord. The PNS acts as the sensory and motor interface of the nervous system. It gathers sensory signals from the environment and transmits them to the CNS for processing. The PNS also carries commands from the CNS to muscles and glands, enabling both voluntary and involuntary actions [4].

All this information is carried and processed by specialized cells known as neurons. Neurons are the main cells in the nervous system whose objective is to obtain perception by

transmitting electrical signals. This transmission process begins when a signal enters the neuron through its dendrites and ends when the signal is relayed to another neuron at the axon terminal. Dendrites are branch-like structures that extend from the soma, or cell body, which houses the nucleus and organelles. The soma is crucial for maintaining the cell's functions, as it manages essential activities such as protein synthesis, ATP production, and RNA synthesis. When a neuron receives a signal, the growth cone seeks chemical cues in the extracellular matrix. The growth cone, a dynamic structure at the tip of the axon, plays a crucial role in sensing the cues. These molecules create a pathway for the neuron to locate its target (post-synaptic) neuron, where a synapse will form, allowing for the transmission of signals either electrically or chemically [26]. After detecting the path, the axon of the transmitter neuron elongates towards that direction, and electrical signals propagate along the axon. Such elongation and propagation occur because of a specific protein called "tubulin" that extends the axon towards the target neuron. Free tubulin monomers and dimers assemble and create microtubules which form the neuron's cytoskeleton. Finally, with the elongation of the axon and the formation of synapses, the transmission of the signal is completed. The combination of these signals brings information to the central nervous system (CNS), where it is processed. The CNS then produces a response, which is transmitted back to the muscles to elicit an appropriate action.

1.2 Why Neuron Growth Matters: From Development to Disease

Neuronal growth, the process described in the previous section, is vital for the nervous system's development and function in vertebrate animals. Specifically, it is crucial for brain development [84], learning, memory formation [10], and recovery from injury [31]. During embryonic development, neurons grow and extend their axons and dendrites, forming a complex network within the brain and spinal cord. In addition, learning and memory formation are closely related to neuron growth, particularly the synapses created during signal transmission. This

process, known as synaptic plasticity, refers to the ability of synapses to strengthen or weaken over time. These changes modify the connections between neurons based on the signals they receive. Another key purpose of neuron growth is to repair injured neurons and regenerate new ones. However, due to neurological disorders such as Alzheimer's disease[64], Huntington's disease [13], Parkinson's disease [14] and spinal cord injuries [63], neurons start to degenerate, which causes neuronal growth to stop or to shrink. In Alzheimer's disease, the buildup of amyloid plaques and neurofibrillary tangles interferes with signal transmission, ultimately causing synaptic dysfunction and the loss of neurons. Understanding and enhancing the neuron growth process can slow down the progression of amyloid plaques and restore neural connectivity [88]. With certain therapies, it may be possible to remove this accumulation of material and promote neuron growth to form synapses with target neurons. In Parkinson's disease, neurons in the midbrain and forebrain are gradually lost over time due to genetic and environmental factors, as shown by clinical research. According to [68], both short- and long-distance axon growth can help rebuild damaged neuronal circuits, such as those between the midbrain and forebrain, after cell transplantation. When neurons are transplanted, axons typically grow only a short distance from the transplants, and few axons reach their final target unless growth factor pathways are used. Similarly, there can be regions in the spinal cord where neurons can be damaged because of various factors such as injury, disease, or degenerative conditions. Damage to these neurons can disrupt communication between the brain and the rest of the body, affecting movement, sensation, and reflexes [85]. Therapeutic interventions that promote axonal growth for this injured lesion have huge promises to solve this communication problem between the spinal cord and the body [92]. However, solutions to these problems are still in the early stages, and mathematical models are essential for improving our understanding and developing effective solutions.

1.3 Modeling the Mysteries: Mathematical Approaches to Neuron Growth

In this section, we introduce mathematical models of neuron growth. Two distinct models describe this phenomenon: the transport-limited model and the mechanical forces model. The transport-limited model uses the concept of mass uptake to explain neuronal growth [34]. The mechanical forces model describes neuronal growth as being influenced by physical forces [90]. In the literature, these two models are represented using both ordinary differential equations (ODE) and partial differential equations (PDE). Table 1.1 lists the literature for these models along with the year they appeared. Recent research explores the interaction between these two processes, proposing a model that couples mechanical and transport-limited mechanisms to explain axonal growth. While experiments support the correlation between these processes [72, 90, 2], as of our knowledge, no comprehensive systematic model currently exists.

Table 1.1. Mathematical models of neuron growth

	Transport Limited Models	**Mechanically Mediated Growth**
ODE Models	Van Veen et al. (1994), Samuels et al. (1996), Miller et al. (1997), Van Ooyen et al. (2001), Zubler et al. (2009), Koene et al (2009)	Dennerll et al. (1989), Li et al. (1995, 1996), Goriely et al. (2015, 2017), Anthonisen et al. (2019)
PDE Models	Hely et al. (2001), McLean et al. (2004), Graham et al. (2006), Diehl et al. (2014)	O'Toole et al. (2008), Recho et al. (2016),

1.3.1 Transport-limited models

The transport-limited models are based on diffusion and active transport of the proteins specifically tubulin protein. They describe the movement of tubulin from soma to the end of the neuron where the growth takes place. The authors of [82] and [96] propose that compartments contain specific tubulin concentrations, and that these concentrations are exchanged between

compartments through the diffusion and active transport of proteins. After diffusion and active transport processes, tubulin monomers and dimers assemble and disassemble at the tip of the neuron, causing elongation. The length of the neuron is determined by the distance between compartments. This proposed model is also known as the zero-dimensional model, and it is described by ordinary differential equations (ODEs). This model extended for neurons with multiple branches [95]. In addition, the slow transport velocity of tubulin proteins sets theoretical limits on axon length, as proposed by the model in [69]. Subsequently, these models were adapted to apply to large-sclae neural networks, as detailed in [99]. Later, a tool for modeling the growth and connectivity of these networks, NetMorph, is introduced in [47]. However, these models are inadequate for explaining axon growth as they do not account for protein degradation. Therefore, it was necessary to develop a model that captures protein concentration along the entire length of the axon. The first attempt to create a model for this problem was made by [40]. The authors considered the concentrations of tubulin and intracellular calcium (Ca) as key factors responsible for the growth and branching of axons and dendrites. In their model, the concentration changes of tubulin and Ca were explicitly modeled using PDEs. The PDE spatial domain represents the length of the axon or dendrite and is divided into compartments to capture variations in concentration along its length. This model fell short of representing axon growth as a continuous process. The first continuum PDE-ODE model addressing axon growth driven by tubulin was introduced in [67]. This model successfully incorporates both the production of tubulin in the soma and its transport to the growth cone. The proposed model consists of a reaction-advection-diffusion PDE that describes the dynamics of tubulin concentration along the axon and an ODE that represents the axon length as a function of tubulin concentration at the axon tip. This model identifies three distinct regimes of axon growth: short, moderate, and long. Following this model, the authors of [36] analyze these three regimes and the transitions between them with respect to changes in parameters. However, this model is inconsistent in representing biological behavior because it does not account for the elongation of the axon, which implies a moving boundary for the PDE. Instead, the model assumes a stationary PDE boundary. The

authors of [26] address the issue by representing the growth cone as a finite volume. This allows them to track the concentration of tubulin more accurately within the axon. They also handle tubulin polymerization separately with an ordinary differential equation (ODE). They effectively incorporate the moving boundary of the PDE, making the model more aligned with the actual biological processes of axon growth. Due to these advancements, we have adopted this model in this dissertation and provide a detailed explanation of it in Chapter 2.

1.3.2 Mechanically mediated growth models

In this modeling strategy, the forces acting on axons or dendrites are considered the key factors influencing neuron growth. Axonal growth is hypothesized to result of the application of tension to the surface of the neuron's cell body. This process is often described by well-known spring-and-dashpot-type models which capture how the applied forces have both fluid and solid-like properties and the neuron is a single unit without any spatial variation [24, 61, 60]. Following this model, a more comprehensive approach has been proposed, which considers the neuron as a morphoelastic tubular compartment [35, 34]. In another model, the morphoelasticity framework separates the applied stretch into an elastic component, representing immediate deformation, and a growth component, reflecting long-term changes associated with neuronal growth [5]. These models are at the cutting edge of research, with rapid advancements continually enhancing our understanding of neuronal growth. Due to the presence of dissipative forces, elongation driven by the growth cone does not meet the assumption of uniform longitudinal tension. Therefore, a model that accounts for variations in longitudinal tension is needed. A PDE model has been developed that integrates force generation at the growth cone, the viscoelastic properties of the axon, and adhesions between the axon and the substrate, where longitudinal tension varies [71]. This model is expanded by incorporating a three-compartment approach that describes the three key states: collapsed, static, and motile [80]. These states come from the interaction between the forces inside the neurite's core and the surrounding membrane.

1.4 Literature Review for Neuron Growth Control

As highlighted earlier, neural functionality is fundamental to the well-being of vertebrate animals. However, conditions such as neurodegenerative diseases and spinal cord injuries can severely impair this functionality. To address these disruptions, therapies are being developed that focus on promoting axon elongation. This approach is crucial because elongating axons can help restore lost connections within the nervous system, thereby recovering essential neural functions and improving overall outcomes for affected individuals. Extensive research has been conducted to promote neuron growth, with key techniques including the use of neurotrophic factors [41], stem cell therapies [62], gene therapies [70], electrical stimulation, [37] and pharmacological treatments [7]. Recently developed therapies such as ChABC have promising potential to cure these disorders, specifically spinal cord injuries [6, 46]. ChABC therapy involves injecting bacterial enzymes into the area where the degenerated neurons are located, which digest the axon growth inhibitors [59, 32, 58]. After this therapy, axon growth sustains for a short distance, starting from approximately 70 μm and extending to 274.5 μm for Dorsal Root Ganglia neurons, as reported in [15]. However, this study does not provide any results related to long-distance axon regeneration, a crucial factor for achieving functional recovery in spinal cord injury, where growth spans from micrometers to millimeters. This mechanism motivates our design of the control law in this paper to enhance axon elongation, aiming to achieve desired lengths in both millimeters and micrometers.

1.5 Literature Review for PDE Control

PDE control, or in other words, control of infinite-dimensional systems, is typically divided into two categories: in-domain control and boundary control. **In-domain control** refers to the control of PDEs where the control inputs are applied directly within the spatial domain of the system which influences the system's dynamics at various spatial points. Some research in this area, such as the work [94], has explored backstepping techniques for in-domain control

by applying an additional differential transformation to cancel the residual term. This approach aimed to address a common limitation in in-domain control strategies, where the control input often fails to fully cancel the residual term, thereby potentially compromising the effectiveness of the control strategy. In another work, the authors of [97], developed a state transformation that reformulates the control input to function as a boundary control. They then applied the classical boundary backstepping technique. However, in-domain control requires the control input to influence the entire spatial domain which makes the mathematical analysis complicated. Another drawback of in-domain control is actuation and sensing are non-intrusive, making it challenging to effectively measure and influence the system without interfering with its natural behavior. **Boundary control** of PDE systems has been intensively studied over the last two decades [56]. Specifically, the utilization of the method of successive approximation in [86] for backstepping transformation has enabled to obtaining of numerical and symbolic solutions for kernel PDEs. Following this initial contribution, backstepping-based boundary control for PDEs has been extended to the class of coupled PDE-ODE systems [53, 89, 91]. Following this extension, [55] introduced input delay compensation for boundary control by considering an input delay as a transport PDE. [54] also provides input delay compensation and control for unstable reaction-diffusion PDE for arbitrarily long input delays. Although most studies including the aforementioned ones considered a constant domain size in time, several prior work have focused on the boundary control of the Stefan problem, formulated as a parabolic PDE with a moving boundary governed by ODE, see [27, 73, 74, 66, 9, 28, 42] for instance. Recent study [50] [51] have designed a backstepping-based control strategy for the Stefan problem, where the authors have provided the global stability results for the nonlinear closed-loop systems by virtue of the maximum principle. On the other hand, the local stability results for nonlinear hyperbolic PDEs have been developed in several work [12, 8, 98]. However, without utilizing the maximum principle, even the local stability results had not been achieved for nonlinear parabolic PDEs with moving boundary besides our prior work [19].

While the aforementioned control designs operate in continuous time, certain technologies

require control actions only when necessary due to energy, communication, and computation constraints [38]. To address this, an event-triggered control strategy is proposed for PID controllers in [1], and for state feedback and output feedback controllers for linear and nonlinear time-invariant systems in [39] and [48]. In the context of PDEs, [83] introduced the first event-triggered control design. Building on this foundation, [45] introduced a dynamic event-triggering mechanism for hyperbolic PDEs and later for parabolic PDEs, where they proposed sampled-data boundary control. The first event-triggered boundary control for parabolic PDEs was developed by [29]. For Stefan problem, both static and dynamic event-triggered boundary control laws were developed by the authors of [77] and [76]. Meanwhile, a new method called periodic event-triggered control has emerged, where the triggering function is checked only periodically, while the control input is updated aperiodically. In this area, the authors of [79] introduced a periodic event-triggering mechanism for parabolic PDEs, followed by its application to moving boundary PDEs in [78]. Additionally, an event-triggering mechanism was employed to transition between safety, using Control Barrier Functions (CBFs), and stability for the Stefan problem with actuator dynamics, as discussed in [49].

1.6 Research Objectives and Contributions

1.6.1 Innovations in neuron growth control

With the recent discovery of axon regenerability as discussed in the background section, there is a significant potential for the application of control systems to regulate and guide this regeneration toward achieving desired outcomes. Consequently, this dissertation represents the pioneering research in the field of control systems related to axon regeneration, as it provides the design and analysis of control laws and observers for neuronal axon growth. By connecting theoretical control systems with biological processes, it provides a mathematical framework for manipulating axon growth by controlling the flow of tubulin from the soma to the axon. This approach allows researchers to systematically influence how axons grow, potentially leading to

breakthroughs in treating neurodegenerative diseases, spinal cord injuries, and other conditions where nerve regeneration is essential. Additionally, this innovation also opens up possibilities for creating advanced prosthetics and artificial neural networks that work better with our nervous system.

1.6.2 Theoretical advances in boundary control of PDEs

The advancement in this dissertation is not only valuable for neuroscience, but also it introduces methodological and theoretical advances in the control of the Stefan-type moving-boundary PDE-ODE systems. In our earlier work [50], where we developed control and state estimators for the classical Stefan model, the relation from heat flux at the phase interface to the position of the interface was of relative degree one. In our extension [52], in which advection and reaction appear, as do in axon growth, the relative degree remained one. But in the axon growth, the relation arising at the growth cone, from protein flux to the axon end location, is of relative degree two. In addition, the ODE that represents the dynamics of tubulin concentration in the growth cone is nonlinear, whereas in the classical Stefan model, it is a simple integrator. The increase in the relative degree from one to two changes everything. First, the maximum principle for parabolic PDEs is no longer applicable, and global stability is not achievable. Second, not needing to meet the condition of the maximum principle, namely, that the inlet flux is above a certain value (analogous to the heat flux needing to be positive in the classical Stefan model of melting), comes as a blessing because there is no risk of model violation from the violation of the maximum principle. In physical terms, the model remains valid even if the axon is a little tubulin-starved relative to the equilibrium profile since the tubulin equilibrium profile at the target length is strictly positive. So, local stability is not as catastrophic as in classical Stefan-type melting where, if stability is not global, an island of solid may develop in the liquid domain [50] and [52]. In the axon, slight undershooting of tubulin does not cause axon death. Some of the contributions described above were presented only for the linearized system in our earlier works, such as [19] and [21]. However, recognizing the limitations of linearization, we

extended this work to a more comprehensive framework that couples partial differential equations (PDEs) with nonlinear ordinary differential equations (ODEs) without relying on linearization, as discussed in [23]. This extension allows for a more accurate representation of the complex, nonlinear dynamics observed in neuronal systems. Furthermore, we introduced a method for compensating input delays in control systems, as detailed in [20], which significantly advanced the field by addressing a critical challenge in the compensating input time delay. Building on these advancements, we continued to refine the theoretical foundations by developing event-triggering [22] and periodic event-triggering mechanisms [18]. These mechanisms are designed to improve the practicality and efficiency of control laws by ensuring that the control actions are triggered only when necessary, rather than continuously. Additionally, we were the first to analyze the closed-loop convergence of these mechanisms in a coupled PDE and nonlinear ODE setting, providing important insights into their stability and effectiveness in complex systems.

1.7 Organization of the Dissertation

This dissertation is structured into nine chapters, each of which delves into different aspects of the control of neuronal growth, with a particular focus on developing and applying advanced control methods for this complex biological process.

- **Chapter 1: The Foundation of Neuronal Growth and Control**

  This chapter presents the moving boundary PDE-ODE coupled model, explaining its relevance to neuron growth. It covers the reference error system, control objectives, and the development of closed-loop feedback control, focusing on Stefan-type PDE control for managing moving boundaries.

- **Chapter 2: Moving Boundary Neuron Growth Model**

  This chapter presents the moving boundary PDE-ODE coupled model, explaining its relevance to neuron growth. It covers the reference error system, control objectives, and

the development of closed-loop feedback control, focusing on Stefan-type PDE control which is critical for managing the moving boundary conditions inherent in the model.

- **Chapter 3: State Feedback Control Design**

  This chapter focuses on designing state feedback control for neuron growth using the backstepping method. It begins by transforming the original neuron growth system into a target system, followed by deriving the gain kernel solutions and the backstepping control law. A detailed stability analysis of the system under state feedback control is presented. The chapter also addresses challenges related to ensuring local stability over a non-constant spatial interval and demonstrates the effectiveness of the control law through simulations.

- **Chapter 4: Neuron Growth State Estimation**

  This chapter addresses the state of neuron growth through observer design that can estimate the unmeasured states of the system. The observer error system is introduced, followed by the application of the backstepping transformation for the desired observer design, with a stability proof ensuring convergence of estimates to true states over time, and a discussion on the well-posedness of the transformations to guarantee the observer's reliability. Finally, the chapter includes simulations that demonstrate the accuracy and robustness of the state estimation process.

- **Chapter 5: Observer-based Neuron Growth Control**

  Building on the observer design, this chapter presents an output-feedback control strategy. It discusses the reference error states, stability under output-feedback control, and robustness against system uncertainties, supported by simulation results.

- **Chapter 6: Input Delay Compensation**

  This chapter extends the neuron growth model to include input delays, modeled as a transport PDE. It adapts the backstepping method for delay-compensated control, providing

stability proofs and ensuring local stability, with a final Lyapunov analysis confirming effectiveness.

- **Chapter 7: Event-triggered Control**

  The chapter introduces event-triggered control for neuron growth, focusing on axon growth models with actuation at Robin boundary conditions. It covers continuous-time and sampled-data control laws, avoidance of Zeno phenomena, and stability proofs, validated by simulations.

- **Chapter 8: Periodic Event-triggered Control**

  This chapter discusses periodic event-triggering mechanisms, where triggering occurs at regular intervals. It covers the design of the periodic event-triggering function, stability analysis, and simulations that demonstrate the advantages of this control approach.

- **Chapter 9: Conclusion**

  The final chapter summarizes the key findings, discusses the implications of the research, and suggests directions for future work, highlighting the broader impact of the control methods developed in this dissertation.

Acknowledgements

This chapter contains partial adaptations and snippets of the following works: C. Demir, M. Diagne, M. Krstic, "Periodic Event-Triggered Boundary Control of Neuron Growth with Actuation at Soma" Accepted in the Proceedings of the 63st IEEE Conference on Decision and Control 2024. C. Demir, S. Koga, M. Krstic, "Event-Triggered Control of Neuron Growth with Actuation at Soma" American Control Conference 2024. C. Demir, S. Koga, M. Krstic, "Neuron growth control and estimation by PDE backstepping" Automatica 2024. C. Demir, S. Koga, M. Krstic, "Neuron growth output-feedback control by pde backstepping" American Control Conference 2022. C. Demir, S. Koga, M. Krstic, "Input Delay Compensation for Neuron Growth

by PDE Backstepping" 17th IFAC Workshop on Time Delay Systems, 2022. C. Demir, S. Koga, M. Krstic, "Neuron growth control by PDE backstepping: Axon length regulation by tubulin flux actuation in soma" The 60th IEEE Conference on Decision and Control 2021. The dissertation author was the primary author of these publications.

Chapter 2

Moving Boundary Neuron Growth Model

2.1 Introduction to the Moving Boundary PDE-ODE Coupled Model

In this section, we introduce the moving boundary model for the neuron growth problem that is proposed in [26]. In this model, axon growth is determined by the dynamic behavior of tubulin proteins, which play a crucial role in the assembly and extension of microtubules that form the structural framework of the axon. This model is based on two key assumptions that form the foundation of its framework: tubulin is treated as a homogeneous continuum due to the small size of free tubulin molecules, and axon growth is assumed to be solely dependent on the dynamics of tubulin. With these assumptions, as proposed in [26, 25], axonal growth driven by tubulin dynamics can be modeled as follows:

$$c_t(x,t) = Dc_{xx}(x,t) - ac_x(x,t) - gc(x,t), \tag{2.1}$$

$$c_x(0,t) = -q_{\mathrm{s}}(t), \tag{2.2}$$

$$c(l(t),t) = c_{\mathrm{c}}(t), \tag{2.3}$$

$$l_{\mathrm{c}}\dot{c}_{\mathrm{c}}(t) = (a - gl_{\mathrm{c}})c_{\mathrm{c}}(t) - Dc_x(l(t),t) - (r_{\mathrm{g}}c_{\mathrm{c}}(t) + \tilde{r}_{\mathrm{g}}l_{\mathrm{c}})(c_{\mathrm{c}}(t) - c_\infty), \tag{2.4}$$

$$\dot{l}(t) = r_{\mathrm{g}}(c_c(t) - c_\infty), \tag{2.5}$$

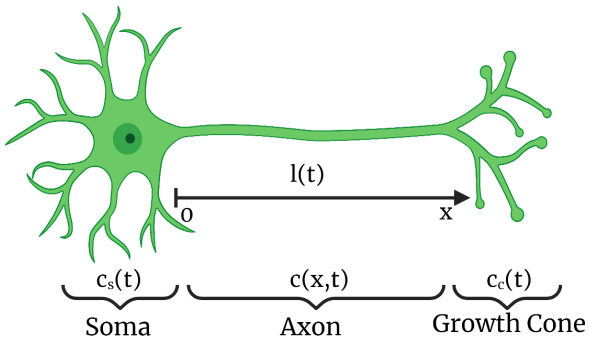

Figure 2.1. Schematic of neuron and state variables

where the tubulin concentration in the axon is $c(x,t)$. Subscript s is used for the soma of the neuron, and subscript c is used for the cone of the neuron. The flux of concentration in the soma is represented as $q_s(t)$ and the tubulin concentration in the cone is denoted as $c_c(t)$. $l(t)$ is the length of axon in x-coordinate. The physical locations of these states and a sample neuron are shown in Figure 2.1. In (2.1), the constants g, D, and a represent tubulin degradation rate, tubulin diffusion constant, and tubulin velocity constant, respectively. The growth ratio is $l_c = \frac{V_c}{A}$ which depends on the cone cross-sectional area A, and a volume of the growth cone V_c. $\tilde{r}_g$ is the reaction rate to create microtubules. r_g is the lumped parameter defined as $r_g := \frac{\tilde{r}_g V_c}{\rho A_g}$ where ρ is the density of assembled microtubules, and A_g is the effective area of created microtubules growth. c_∞ is the equilibrium of the tubulin concentration in the cone. It causes the axon elongation to stop.

Steady-state analysis of the model

To achieve a desired axon length l_s, we examine the steady-state solution $(c_{eq}(x), c_\infty, l_s)$ of the axonal growth model defined by equations (2.1)-(2.5). By setting the time derivative to zero, we derive the steady-state solution as:

$$c_{eq}(x) = c_\infty K_+ e^{\lambda_+(x-l_s)} + c_\infty K_- e^{\lambda_-(x-l_s)}, \tag{2.6}$$

where

$$\lambda_+ = \frac{a+\sqrt{a^2+4Dg}}{2D}, \quad \lambda_- = \frac{a-\sqrt{a^2+4Dg}}{2D}, \tag{2.7}$$

$$K_+ = \frac{1}{2} + \frac{a-2gl_c}{2\sqrt{a^2+4Dg}}, \quad K_- = \frac{1}{2} - \frac{a-2gl_c}{2\sqrt{a^2+4Dg}}. \tag{2.8}$$

The steady-state solution for the concentration flux in the soma, which is an input, is obtained as

$$q_s^* = -c_\infty \left(K_+\lambda_+ e^{-\lambda_+ l_s} + K_-\lambda_- e^{-\lambda_- l_s} \right). \tag{2.9}$$

or readers who are interested, a comprehensive discussion of steady-state solutions for various parameters and their stability analysis can be found in [26].

2.2 Reference Error System and Control Objective

2.2.1 Reference error system

To achieve convergence of the system (2.1)-(2.5) to its steady-state solution, it is necessary to subtract the steady-state solution from the current state of the system. Subsequently, we must demonstrate that the resulting error system, representing the deviation from the steady-state, asymptotically converges to zero. To facilitate this analysis, we introduce $u(x,t)$, $z_1(t)$, $z_2(t)$, and $U(t)$ as the reference error states and the reference error input, respectively, defined as follows:

$$u(x,t) = c(x,t) - c_{\text{eq}}(x), \tag{2.10}$$

$$z_1(t) = c_c(t) - c_\infty, \tag{2.11}$$

$$z_2(t) = l(t) - l_s, \tag{2.12}$$

$$U(t) = -\left(q_s(t) - q_s^*\right). \tag{2.13}$$

The reference error system is obtained by subtracting the steady-state solution (2.6) from the governing equations (2.1)-(2.5), resulting into

$$u_t(x,t) = Du_{xx}(x,t) - au_x(x,t) - gu(x,t), \tag{2.14}$$

$$u_x(0,t) = U(t), \tag{2.15}$$

$$u(l(t),t) = c_{\mathrm{c}}(t) - c_{\mathrm{eq}}(l(t)), \tag{2.16}$$

$$\dot{z}_1(t) = \tilde{a}_1 z_1(t) - \beta u_x(l(t),t) - \kappa z_1(t)^2 + \beta f_1(z_2(t)) - \beta \tilde{a}_2 z_2(t), \tag{2.17}$$

$$\dot{z}_2(t) = r_{\mathrm{g}} z_1(t), \tag{2.18}$$

where the constants in (2.14)-(2.18) are

$$\tilde{a}_1 = \frac{a - r_{\mathrm{g}} c_\infty}{l_{\mathrm{c}}} - g - \tilde{r}_{\mathrm{g}}, \tag{2.19}$$

$$\tilde{a}_2 = c_\infty \left(\lambda_+^2 K_+ + \lambda_-^2 K_- \right), \tag{2.20}$$

$$\beta = \frac{D}{l_{\mathrm{c}}}, \quad \kappa = \frac{r_{\mathrm{g}}}{l_{\mathrm{c}}}, \tag{2.21}$$

and

$$f_1(z_2(t)) = c_\infty \left(\frac{a - g l_{\mathrm{c}}}{D} - K_+ \lambda_+ e^{\lambda_+ z_2(t)} - K_- \lambda_- e^{\lambda_- z_2(t)} \right) + \tilde{a}_2 z_2(t). \tag{2.22}$$

Let $X \in \mathbb{R}^2$ be an ODE state vector for the reference error states $z_1(t)$ and $z_2(t)$, defined by

$$X(t) = [z_1(t) \quad z_2(t)]^\top. \tag{2.23}$$

Rewriting the system (2.16)–(2.18) with respect to $X(t)$, a nonlinear coupled PDE-ODE reference error system is given by

$$u_t(x,t) = Du_{xx}(x,t) - au_x(x,t) - gu(x,t), \tag{2.24}$$

$$u_x(0,t) = U(t), \tag{2.25}$$

$$u(l(t),t) = h(X(t)), \tag{2.26}$$

$$\dot{X}(t) = AX(t) + f(X(t)) + Bu_x(l(t),t), \tag{2.27}$$

where

$$A = \begin{bmatrix} \tilde{a}_1 & -\beta\tilde{a}_2 \\ r_{\mathrm{g}} & 0 \end{bmatrix}, \quad B = \begin{bmatrix} -\beta \\ 0 \end{bmatrix}, \tag{2.28}$$

$$f(X(t)) = -\kappa z_1^2(t) + \beta f_1(z_2(t)), \tag{2.29}$$

$$h(X(t)) = z_1(t) + \tilde{h}(z_2(t)), \tag{2.30}$$

$$\tilde{h}(z_2(t)) = c_\infty \left(1 - K_+ e^{\lambda_+ z_2(t)} - K_- e^{\lambda_- z_2(t)}\right). \tag{2.31}$$

2.2.2 Linearized error system

Applying the linearization of $X(t)$ around zero states to the nonlinear error system (2.24)–(2.27) leads to the following linearized reference error system:

$$u_t(x,t) = Du_{xx}(x,t) - au_x(x,t) - gu(x,t), \tag{2.32}$$

$$u_x(0,t) = U(t), \tag{2.33}$$

$$u(l(t),t) = H^\top X(t), \tag{2.34}$$

$$\dot{X}(t) = A_1 X(t) + Bu_x(l(t),t), \tag{2.35}$$

where the vector $H \in \mathbb{R}^2$ is defined as

$$A_1 = \begin{bmatrix} \tilde{a}_1 & \tilde{a}_3 \\ r_{\mathrm{g}} & 0 \end{bmatrix}, \qquad H = \begin{bmatrix} 1 & -\dfrac{(a - g l_{\mathrm{c}}) c_\infty}{D} \end{bmatrix}^\top, \tag{2.36}$$

where

$$\tilde{a}_3 = \frac{a^2 + Dg - a g l_{\mathrm{c}}}{D^2}. \tag{2.37}$$

2.3 Towards Closed-loop Feedback Control

2.3.1 Control objective

Our main objective is to achieve a specified target axon length $l_s > 0$ by designing an appropriate control law for $q_{\mathrm{s}}(t)$. This involves deriving the steady-state solution $(c_{\mathrm{eq}}(x), l_s)$ for the system governed by equations (2.1)–(2.5), which reflects the equilibrium concentration of tubulin $c_{\mathrm{eq}}(x)$. The control objective is formally defined as ensuring that the axon length $l(t)$ asymptotically approaches the desired length l_{s} and that the tubulin concentration $c(x,t)$ stabilizes at the equilibrium distribution $c_{\mathrm{eq}}(x)$:

$$\lim_{t \to \infty} l(t) = l_s, \tag{2.38}$$

$$\lim_{t \to \infty} c(x,t) = c_{\mathrm{eq}}(x). \tag{2.39}$$

Remark 2.1. *The given axon growth model and its steady-state solution primarily describe axon elongation; however, the axon can retract under certain conditions. The scenario where axon shrinkage occurs is detailed in [26]. This situation can be simplified by satisfying the following inequality. If the inequality below is met for the system parameters and the tubulin concentration*

at the soma, the axon length will retract:

$$K_+ e^{\lambda_+(l_0-l_s)} + K_- e^{\lambda_-(l_0-l_s)} < \frac{c(0,t)}{c_\infty} < 1, \tag{2.40}$$

The inequality (2.40) *indicates that the tubulin concentration at the soma,* $c(0,t)$*, should be lower than the steady-state tubulin concentration at the growth cone,* c_∞*, and that the ratio of these two concentrations should be greater than the expression involving the initial axon length,* l_0*, and the desired axon length,* l_s*. When these conditions are satisfied:*

$$\lim_{t\to\infty} l(t) = l_s \tag{2.41}$$

where $l_s \leq l_0$*. Biologically, when the tubulin concentration at the soma drops below that at the growth cone, the usual balance of transport is disrupted, leading to a potential retraction of the axon. In this scenario, if the diffusive transport back toward the soma is balanced by the active transport toward the growth cone, the axon can stabilize at a new, shorter length that is smaller than the initial axon length. As a result, the axon ceases to grow further and maintains this reduced length over time.*

2.3.2 Basic idea of Stefan type of PDE control

In this section, we present a basic idea of control of moving boundary PDE, Stefan problem, which is adapted from [50]. The Stefan problem is a mathematical model that describes the phase change process involving heat transfer and the movement of the boundary between

phases. The problem is given by the following coupled PDE-ODE system

$$T_t(x,t) = \alpha T_{xx}(x,t), \quad x \in (0, s(t)), \tag{2.42}$$

$$-kT_x(0,t) = q_c(t), \tag{2.43}$$

$$T(s(t),t) = T_m, \tag{2.44}$$

$$\dot{s}(t) = -\beta T_x(s(t),t), \tag{2.45}$$

where $T(x,t)$ explains the temperature evolution along the domain, $x \in [0, L]$, and $s(t)$ is the moving interface between solid and liquid phases. The objective of the control design is to ensure exponential convergence of moving interface, $s(t)$, to a set point, s_r and exponential convergence of the temperature profile, $T(x,t)$, to uniform melting temperature, T_m.

To design a feedback control law for this goal, we define the reference error states as

$$u(x,t) = T(x,t) - T_m, \tag{2.46}$$

$$X(t) = s(t) - s_r \tag{2.47}$$

which gives us

$$u_t(x,t) = \alpha u_{xx}(x,t), \quad x \in (0, s(t)), \tag{2.48}$$

$$u_x(0,t) = -\frac{1}{k} q_c(t), \tag{2.49}$$

$$u(s(t),t) = T_m, \tag{2.50}$$

$$\dot{X}(t) = -\beta u_x(s(t),t). \tag{2.51}$$

The idea behind backstepping is to transform the reference error system into a stable target system, ensuring that the error diminishes over time. The state transformation method known as backstepping (or Volterra transformation) is introduced to convert the original system

into a target system, which takes the form of:

$$w(x,t) = u(x,t) - \int_x^{s(t)} k(x,y)u(y,t)dy - \phi(x)^\top X(t) \tag{2.52}$$

where $k(x,y)$ and $\phi(x)^\top$ are gain kernels that need to be derived, and the desired target system is given by

$$w_t(x,t) = \alpha w_{xx}(x,t) + \frac{c}{\beta}\dot{s}(t)X(t), \tag{2.53}$$

$$w_x(0,t) = 0, \tag{2.54}$$

$$w(s(t),t) = 0, \tag{2.55}$$

$$\dot{X}(t) = -cX(t) - \beta w_x(s(t),t). \tag{2.56}$$

By taking the time and spatial derivatives of (2.52) along with the (2.48)-(2.51), and matching with the target system, one can obtain the gain kernels as

$$k(x,y) = \frac{c}{\alpha}(x-y), \tag{2.57}$$

$$\phi(x) = \frac{c}{\beta}(x - s(t)). \tag{2.58}$$

Next, it is time to derive the control law $q_c(t)$ which is derived by taking the spatial derivative of (2.52) which gives us

$$w_x(x,t) = u(x,t) + k(x,x)u(x,t) - \int_x^{s(t)} k_x(x,y)u(y,t)dy - \dot{\phi}(x - l(t))^\top X(t) \tag{2.59}$$

By substituting $k(x,y)$ and $\phi(x)^\top$, we get

$$w_x(x,t) = u(x,t) - \int_x^{s(t)} \frac{c}{\alpha}u(y,t)dy - \frac{c}{\beta}X(t) \tag{2.60}$$

Finally, substituting $x = 0$ and the boundary condition of Stefan problem and the target system, one can get

$$0 = -\frac{1}{k} q_{\mathrm{c}}(t) - \int_0^{s(t)} \frac{c}{\alpha} \left(T(y,t) - T_{\mathrm{m}}\right) dy - \frac{c}{\beta} \left(s(t) - s_{\mathrm{r}}\right) \tag{2.61}$$

Thus, the control law $q_{\mathrm{c}}(t)$ is

$$q_{\mathrm{c}}(t) = -c \left(\frac{k}{\alpha} \int_0^{s(t)} \left(T(y,t) - T_{\mathrm{m}}\right) dy - \frac{k}{\beta} \left(s(t) - s_{\mathrm{r}}\right) \right) \tag{2.62}$$

The next step is to prove that the target system is stable. However, proving the stability of the target system alone is insufficient, as our ultimate goal is to establish the stability of the original system. To achieve this, we must convert the target system back to the reference error system. This conversion is accomplished using the inverse transformation, which is given by:

$$u(x,t) = w(x,t) + \int_x^{s(t)} l(x,y) w(y,t) dy + \psi(x - s(t)) X(t). \tag{2.63}$$

By using the same strategy that we used to obtain direct transformation gain kernels, we can obtain

$$l(x,y) = \frac{\beta}{\alpha} \psi(x - y), \tag{2.64}$$

$$\psi(x) = \frac{c}{\beta} \sqrt{\frac{\alpha}{c}} \sin\left(\sqrt{\frac{c}{\alpha}} x \right). \tag{2.65}$$

Finally, we can prove the stability of both the target system and the original system. This is achieved using a straightforward method by applying Lyapunov analysis. To begin, we define the Lyapunov functional as:

$$V = \frac{1}{2} \int_0^{s(t)} w(x,t)^2 dx + \frac{1}{2} \int_0^{s(t)} w_x(x,t)^2 dx + \frac{1}{2} X(t)^2 \tag{2.66}$$

By taking the time derivative of this Lyapunov function, applying integration by parts, substituting the boundary conditions, and using Young's, Poincaré's, and Agmon's inequalities, we arrive at:

$$\dot{V} \leq -bV + a\dot{s}(t)V \tag{2.67}$$

where

$$a = \max\left\{1, \frac{8s_{\mathrm{r}}c}{\alpha}\right\}, \tag{2.68}$$

$$b = \min\left\{\frac{\alpha}{4s_{\mathrm{r}}^2}, c\right\} \tag{2.69}$$

Now, by introducing a new Lyapunov function W, defined by $W = Ve^{-as(t)}$, we can conclude that:

$$V(t) \leq e^{as_{\mathrm{r}}}V(0)e^{-bt} \tag{2.70}$$

which finally yields

$$||w||^2_{\mathcal{H}_1} + pX(t)^2 \leq e^{as_{\mathrm{r}}}\left(||w_0||^2_{\mathcal{H}_1} + p(X(0)^2)\right)e^{-bt} \tag{2.71}$$

Using the inverse transformation, it is possible to demonstrate that the original system is exponentially stable.

Motivated by the control law design and stability analysis of the Stefan problem, we develop a control design and conduct a closed-loop analysis for the neuron growth problem.

Acknowledgements

Chapter 2 contains partial adaptations and snippets of the following works: C. Demir, S. Koga, M. Krstic, "Neuron growth control and estimation by PDE backstepping" Automatica 2024. C. Demir, S. Koga, M. Krstic, "Neuron growth output-feedback control by pde backstepping"

American Control Conference 2022 and C. Demir, S. Koga, M. Krstic, "Neuron growth control by PDE backstepping: Axon length regulation by tubulin flux actuation in soma" The 60th IEEE Conference on Decision and Control 2021. The dissertation author was the primary author of these publications.

Chapter 3

State Feedback Control Design

3.1 Backstepping Control of Neuron Growth Problem

This section presents the main theorem of this dissertation. We extended the backstepping method from its application in the classical Stefan problem to a nonlinear moving boundary model that is coupled with a PDE-ODE system. We first state the theorem.

Theorem 3.1. *Consider the closed-loop system consisting of the plant* (2.24)–(2.27) *with the control law*

$$U(t) = \left(\frac{1}{D}H^\top B + \gamma\right)u(0,t) - \frac{1}{D}\int_0^{l(t)} p(x)Bu(x,t)dx + p(l(t))X(t), \tag{3.1}$$

where

$$p(x) = \phi'(-x)^\top - \gamma\phi(-x)^\top \tag{3.2}$$

and $\phi(x)$ represents a gain kernel. Suppose the control parameter $\gamma > 0$ is chosen to satisfy $\gamma \geq \frac{a}{D}$. Then, there exist $\bar{M} > 0$, $c > 0$, and $\kappa > 0$, such that, if $Z(0) < \bar{M}$ then the following norm estimate holds

$$Z(t) \leq cZ(0)\exp(-\kappa t), \tag{3.3}$$

for all $t \geq 0$, in terms of the $\mathcal{H}_1$-norm

$$Z(t) = ||u(\cdot,t)||^2_{\mathcal{H}_1(0,l(t))} + X^\top X, \tag{3.4}$$

namely, the origin of the closed-loop systems is locally exponentially stable.

The proof is presented in the remainder of this section.

3.1.1 Transformation into target system

The state feedback control in this paper is designed by applying a backstepping transformation [56] to the linearized reference error system (2.32)–(2.35). The backstepping transformations and the associated gain kernel functions are given in the remainder of this section. Referring to [50], we consider the following backstepping transformation

$$w(x,t) = u(x,t) - \int_x^{l(t)} k(x,y)u(y,t)dy - \phi(x-l(t))^\top X(t), \tag{3.5}$$

where $k(x,y) \in \mathbb{R}$ and $\phi(x-l(t)) \in \mathbb{R}^2$ are the gain kernel functions to be determined. The desired target system for the linearized error system is proposed as

$$w_t(x,t) = Dw_{xx}(x,t) - aw_x(x,t) - gw(x,t) - \dot{l}(t)F(x,X(t)), \tag{3.6}$$

$$w_x(0,t) = \gamma w(0,t), \tag{3.7}$$

$$w(l(t),t) = 0, \tag{3.8}$$

$$\dot{X}(t) = (A_1 + BK^\top)X(t) + Bw_x(l(t),t), \tag{3.9}$$

where $K \in \mathbb{R}^2$ is a feedback control gain vector chosen to make $A_1 + BK$ Hurwitz. With the system matrices given in (2.28), by setting

$$K = [k_1 \quad k_2]^\top, \quad k_1 > \frac{\tilde{a}_1}{\beta}, \quad k_2 > \frac{\tilde{a}_3}{\beta}, \tag{3.10}$$

we obtain $A_1 + BK^\top$ Hurwitz. The redundant nonlinear term $\dot{l}(t)F(x, X(t)) \in \mathbb{R}$ in (3.6) is present due to the time-dependency of the moving boundary $l(t)$ in the transformation (3.5), which is described by

$$F(x, X(t)) = \left(\phi'(x - l(t))^\top - k(x, l(t))H^\top\right) X(t). \tag{3.11}$$

3.1.2 Gain kernel solutions

By using the solution technique in [53] and [91], we first take the time derivative of (3.5) together with the solution of (2.32)-(2.35), so we get

$$\begin{aligned} w_t(x,t) =& Du_{xx}(x,t) - au_x(x,t) - gu(x,t) \\ & - \int_x^{l(t)} k(x,y)\left(Du_{yy}(y,t) - au_y(y,t) - gu(y,t)\right) dy \\ & - \phi(x - l(t))^T \left(A_1 X(t) + Bu_x(l(t),t)\right) - \dot{l}(t)F(x, X(t)) \end{aligned} \tag{3.12}$$

Then, we take the spatial derivative of (3.12) and substituted $x = l(t)$ in both the transformation (3.5) and its spatial derivative, so (3.12) becomes

$$\begin{aligned} w_t(x,t) + \dot{l}(t)F(x, X(t)) =& Dw_{xx}(x,t) - aw_x(x,t) - gw(x,t) \\ & + u(x,t)\left[-2Dk_y(x,x) - 2Dk_x(x,x)\right] + u_x(l(t),t)\left[-Dk(x,l(t)) - \phi(x - l(t))^T B\right] \\ & + u(l(t),t)\left[-Dk_y(x,l(t)) + ak(x,l(t))\right] \\ & + \int_x^{l(t)} u(y,t)\left[Dk_{xx}(x,y) - Dk_{yy}(x,y) - ak_x(x,y) - ak_y(x,y)\right] dy \\ & + D\phi''(x - l(t))^T X(t) - a\phi'(x - l(t))^T X(t) - \phi(x - l(t))^T \left[gX(t) + A_1 X(t)\right]. \end{aligned} \tag{3.13}$$

Finally, substituting the boundary conditions by matching with the target system (3.6)–(3.9), we have the following PDEs and an ODE for gain kernels.

$$k_{xx}(x,y) - k_{yy}(x,y) = \frac{a}{D}\left(k_x(x,y) + k_y(x,y)\right), \tag{3.14}$$

$$k_x(x,x) + k_y(x,x) = 0, \tag{3.15}$$

$$k(x,l(t)) = -\frac{1}{D}\phi(x-l(t))^\top B, \tag{3.16}$$

$$D\phi''(x-l(t))^\top - a\phi'(x-l(t))^\top - \phi(x-l(t))^\top (gI + A_1) - Dk_y(x,l(t))H^\top + ak(x,l(t))H^\top = 0, \tag{3.17}$$

$$\phi(0) = H, \tag{3.18}$$

$$\phi'(0) = k(l(t),l(t))H^\top + K^\top. \tag{3.19}$$

By the conditions (3.14)–(3.16), the solution of $k(x,y)$ is uniquely given by

$$k(x,y) = -\frac{1}{D}\phi(x-y)^\top B. \tag{3.20}$$

Substituting (3.20) into (3.17)–(3.19), the ODE of $\phi(\cdot)$ becomes

$$D\phi''(x-l(t))^\top - \phi'(x-l(t))^\top \left(BH^\top + aI\right) - \phi(x-l(t))^\top \left(gI + A_1 + \frac{a}{D}BH^\top\right) = 0, \tag{3.21}$$

$$\phi(0) = H, \tag{3.22}$$

$$\phi'(0)^\top = -\frac{1}{D}H^\top BH^\top + K^\top. \tag{3.23}$$

The solution to (3.21)-(3.23) is given by (see [91])

$$\phi(x)^\top = \left[H^\top \; K^\top - \tfrac{1}{D}H^\top BH^\top\right] e^{N_1 x}\begin{bmatrix} I \\ 0 \end{bmatrix}, \tag{3.24}$$

where the matrix $N_1 \in \mathbb{R}^{4\times4}$ is defined as

$$N_1 = \begin{bmatrix} 0 & \frac{1}{D}\left(gI + A_1 + \frac{a}{D}BH^\top\right) \\ I & \frac{1}{D}\left(BH^\top + aI\right) \end{bmatrix}. \tag{3.25}$$

3.1.3 Backstepping control law

From the boundary condition (3.7) of the target system at $x = 0$ and the kernel solutions, we obtain the control law. Substituting $x = 0$ into the transformation (3.5) and its spatial derivative, and substituting (2.33), (3.7) and (3.20) into these equations, and setting the boundary condition (3.7), the control input is described as follows

$$U(t) = \left(\frac{1}{D}H^\top B + \gamma\right)u(0,t) - \frac{1}{D}\int_0^{l(t)} p(x)Bu(x,t)dx + p(l(t))X(t), \tag{3.26}$$

where

$$p(x) = \phi'(-x)^\top - \gamma\phi(-x)^\top. \tag{3.27}$$

One can explicitly deduce the function $p(x) \in \mathbb{R}^2$ by using the kernel solution.

3.2 Stability proof under state-feedback control

In this section, we outline the proof of Theorem 3.1, beginning with the formulation of the nonlinear target system that results from applying the backstepping transformation (3.5).

3.2.1 Nonlinear target system.

While the control design in the previous section is pursued on a linearized reference error system (2.32)–(2.35), we prove the local stability for the original nonlinear system (2.24)–(2.27) under the designed linear control law, which is linear in u and c_c but not in l. The nonlinear target system is obtained by applying the transformation (3.5) to the nonlinear system (2.24)–(2.27),

arriving at

$$
\begin{aligned}
w_t(x,t) =& Dw_{xx}(x,t) - aw_x(x,t) - gw(x,t) - \dot{l}(t)F(x,X(t)) \\
&- \phi(x-l(t))^\top f(X(t)) - \left(\phi'(x-l(t))^\top B + \frac{a}{D}\phi(x-l(t))^\top B\right) h^*(X), \qquad (3.28)\\
w_x(0,t) =& \gamma w(0,t), \qquad (3.29)\\
w(l(t),t) =& h^*(X(t)), \qquad (3.30)\\
\dot{X}(t) =& (A+BK)X(t) + f(X(t)) + Bw_x(l(t),t), \qquad (3.31)
\end{aligned}
$$

where

$$
h^*(X(t)) = z_1(t) + \tilde{h}(z_2(t)) - H^\top X(t). \qquad (3.32)
$$

3.2.2 How to ensure local stability on a non-constant spatial interval.

The stability property of the nonlinear target system (3.28)-(3.31) is equivalent to the closed-loop system consisting of the plant (2.24)-(2.27) with the control law (3.1) when the backstepping transformation (3.5) is invertible. We study the local stability of the target system by imposing the following two properties

$$
0 < l(t) \le \bar{l}, \qquad (3.33)
$$

$$
|\dot{l}(t)| \le \bar{v}, \qquad (3.34)
$$

for some $\bar{l} > l_s > 0$ and $\bar{v} > 0$. We will derive the restricted initial state to satisfy these properties for all $t \ge 0$ later.

3.2.3 Inverse Transformation.

By performing a similar procedure to the derivation of the direct transformation, one can obtain the inverse transformation as

$$u(x,t) = w(x,t) + \int_x^{l(t)} q(x,y)w(y,t)dy + \varphi(x-l(t))^\top X(t), \tag{3.35}$$

where the gain kernel functions $q(x,y) \in \mathbb{R}$ and $\varphi(x-l(t)) \in \mathbb{R}^2$ satisfy

$$q_{xx}(x,y) - q_{yy}(x,y) = \frac{a}{D}\left(q_x(x,y) + q_y(x,y)\right), \tag{3.36}$$

$$q_x(x,x) + q_y(y,y) = 0, \tag{3.37}$$

$$q(x,l(t)) = -\frac{1}{D}\varphi(x-l(t))^\top B, \tag{3.38}$$

$$D\varphi''(x-l(t))^\top + a\varphi'(x-l(t))^\top + \left(gI + A_1 + BK^\top\right)\varphi(x-l(t))^\top = 0, \tag{3.39}$$

$$\varphi(0) = H, \tag{3.40}$$

$$\varphi'(0) = K. \tag{3.41}$$

The same solution technique employed in the previous chapter is equally applicable to (3.36)–(3.41). Therefore, we can explicitly obtain the solution for (3.36)–(3.41).

3.2.4 Lyapunov analysis

Throughout the dissertation, norms on non-constant intervals are denoted as

$$||u(.,t)||_{L_2(0,l(t))} = \sqrt{\int_0^{l(t)} u(.,t)^2 dx}, \quad ||u(.,t)||_{\mathcal{H}_1(0,l(t))} = \sqrt{\left(\int_0^{l(t)} u(.,t)^2 + u_x(.,t)^2 dx\right)},$$

and the L_2 norm is further shortened as $||w|| := ||w(\cdot,t)||_{L_2}$. Consider the following Lyapunov functionals

$$V_1 = \frac{1}{2}||w||^2, \quad V_2 = \frac{1}{2}||w_x||^2, \quad V_3 = X(t)^\top P X(t), \tag{3.42}$$

where $P > 0$ is a positive definite matrix satisfying the Lyapunov equation:

$$(A + BK^\top)^\top P + P(A + BK^\top) = -Q, \tag{3.43}$$

for some positive definite matrix $Q > 0$. We define the total Lyapunov function as

$$V = d_1 V_1 + V_2 + \frac{\gamma}{2} w(0,t)^2 + d_2 V_3, \tag{3.44}$$

where $d_1 > 0$ and $d_2 > 0$ are to be determined.

Lemma 3.1. *Assume that* (3.33)–(3.34) *are satisfied with*

$$\bar{v} = \min\left\{\frac{g}{4\gamma}, \frac{D}{8\bar{l}}\right\}, \tag{3.45}$$

for all $t \geq 0$*. Then, for sufficiently large* $d_1 > 0$ *and small* $d_2 > 0$*, there exist positive constants* $\beta_i > 0$ *for* $i \in \{1,2,3,4\}$ *such the following norm estimate holds for all* $t \geq 0$*:*

$$\dot{V} \leq -\alpha V + \left(\sum_{i=1}^{4} \beta_i V^{1+\frac{i}{2}}\right), \tag{3.46}$$

where $\alpha = \min\left\{2g + \frac{D}{4\bar{l}}, \frac{4g+d_1 D}{2}, \frac{\lambda_{\min}(Q)}{2\lambda_{\max}(P)}, \frac{d_2(2d_1 D+g)}{4}\right\}$.

Proof. Taking the time derivative of the Lyapunov functions in (3.42) along the target system,

one can obtain

$$\dot{V}_1 = -D||w_x||^2 - g||w||^2 - \left(\gamma D - \frac{a}{2}\right) w(0,t)^2 + \dot{l}(t) \int_0^{l(t)} F(x, X(t)) w(x,t) dx$$
$$+ \frac{1}{2}\dot{l}(t) w(l(t),t)^2 + \int_0^{l(t)} w(x,t)\phi(x - l(t))^\top f(X(t)) dx$$
$$- \int_0^{l(t)} w(x,t)\phi'(x - l(t))^\top B h^*(X) dx - \frac{1}{D}\int_0^{l(t)} w(x,t)\phi(x - l(t))^\top B h^*(X) dx, \tag{3.47}$$

$$\dot{V}_2 = -D||w_{xx}||^2 + a\int_0^{l(t)} w_{xx}(x,t) w_x(x,t) dx - \gamma g w(0,t)^2 - g||w_x||^2 - \gamma w(0,t) w_t(0,t)$$
$$- \dot{l}(t) F(l(t), X(t)) w_x(l(t),t) + \dot{l}(t)\gamma F(0, X(t)) w(0,t) - \frac{1}{2}\dot{l}(t) w_x(l(t),t)^2$$
$$+ \dot{l}(t)\int_0^{l(t)} F_x(x, X(t)) w_x(x,t) dx - \int_0^{l(t)} w_{xx}(x,t)\phi(x - l(t))^\top \left(f(X(t)) + \frac{a}{D} B h^*(X)\right) dx$$
$$- \int_0^{l(t)} w_{xx}(x,t)\phi'(x - l(t))^\top B h^*(X) dx, \tag{3.48}$$

$$\dot{V}_3 = -X(t)^\top Q X(t) + \frac{\partial w}{\partial x}(l(t),t) 2B^\top P X(t) + \kappa X(t)^\top \left(P e_1 e_1^\top X(t) e_1^\top + e_1 X(t)^\top e_1 e_1^\top P\right) X(t)$$
$$+ f_1(X(t)) P X(t) + X(t)^\top P f_1(X(t)). \tag{3.49}$$

Note that we selected k_2 such that

$$k_2 \geq \max\{-\tilde{a}_2, \frac{\tilde{a}_3}{\beta}\}, \tag{3.50}$$

in order to demonstrate Hurwitz matrices of both $A + BK^\top$ and $A_1 + BK^\top$. Then, applying Agmon's inequality as

$$w_x(l(t),t)^2 \leq 2 w_x(0,t)^2 + 4\bar{l}||w_{xx}||^2, \tag{3.51}$$

Poincare's inequalities as

$$||w||^2 \leq 2\bar{l}w(l(t),t)^2 + 4\bar{l}^2||w_x||^2, \tag{3.52}$$

$$||w_x||^2 \leq 2\bar{l}w_x(0,t)^2 + 4\bar{l}^2||w_{xx}||^2, \tag{3.53}$$

and Young's inequality to (3.47)-(3.49) leads to

$$\begin{aligned}\dot{V}_2 \leq & -\frac{D}{4}||w_{xx}||^2 - \frac{\gamma g}{2}w(0,t)^2 - (g - \frac{a^2}{D})||w_x||^2 - \gamma w(0,t)w_t(0,t) + \dot{l}(t)\gamma F(0,X(t))w(0,t) \\ & + \dot{l}(t)\int_0^{l(t)} F_x(x,X(t))w_x(x,t)dx + \frac{|\dot{l}(t)|}{2}F(l(t),X(t))^2 \\ & - \int_0^{l(t)} w_{xx}(x,t)\phi(x-l(t))^\top \left(f(X(t)) + \frac{a}{D}Bh^*(X)\right)dx \\ & - \int_0^{l(t)} w_{xx}(x,t)\phi'(x-l(t))^\top Bh^*(X)dx,\end{aligned} \tag{3.54}$$

and

$$\begin{aligned}\dot{V}_3 \leq & -\frac{\lambda_{\min}(Q)}{2}X^\top X + \frac{4\left|B^\top P\right|^2\gamma^2}{\lambda_{\min}(Q)}w(0,t)^2 + \frac{8\left|B^\top P\right|^2\bar{l}||w_{xx}||^2}{\lambda_{\min}(Q)} \\ & + \kappa X(t)^\top \left(Pe_1e_1^\top X(t)e_1^\top + e_1X(t)^\top e_1e_1^\top P\right)X(t) \\ & + f_1(X(t))PX(t) + X(t)^\top Pf_1(X(t)).\end{aligned} \tag{3.55}$$

We choose the constants d_1 and d_2 to satisfy

$$d_1 \geq \frac{2a^2}{D^2}, \quad d_2 \leq \min\left\{\frac{D\lambda_{\min}(Q)}{64\bar{l}\left|B^\top P\right|^2}, \frac{gD\lambda_{\min}(Q)}{16a\left|B^\top P\right|^2}\right\}. \tag{3.56}$$

Taking the square of (3.11), it follows that the redundant nonlinear terms that appear in (3.47), (3.54) and (3.55) can be bounded by a quadratic norm of the ODE state. Namely, there exist

positive constants $L_1 > 0$, $L_2 > 0$, $L_3 > 0$ and $L_4 > 0$ such that

$$F(0, X(t))^2 \leq L_1 X^\top X, \tag{3.57}$$

$$F(l(t), X(t))^2 \leq L_2 X^\top X, \tag{3.58}$$

$$\int_0^{l(t)} F_x(x, X(t))^2 dx \leq L_3 X^\top X, \tag{3.59}$$

$$\int_0^{l(t)} F(x, X(t))^2 dx \leq L_4 X^\top X. \tag{3.60}$$

In addition, following (2.18), $\dot{l}(t)$ can be rewritten as

$$\dot{l}(t) = r_g e_1 X, \tag{3.61}$$

where $e_1 = [1, 0]$ is the unit vector. Moreover, the following inequalities are given

$$\int_0^{l(t)} \left(\phi'(x - l(t))^\top B + \frac{1}{D} \phi(x - l(t))^\top B \right)^2 dx \leq L_{n_1}, \tag{3.62}$$

$$\int_0^{l(t)} \left(\phi(x - l(t))^\top \right)^2 dx \leq L_{n_2}, \tag{3.63}$$

$$\int_0^{l(t)} \left(\phi'(x - l(t))^\top B + \frac{a}{D} \phi(x - l(t))^\top B \right)^2 dx \leq L_{n_3}. \tag{3.64}$$

By using (3.62)-(3.64) and applying Cauchy-Schwarz inequality, and using (3.47), (3.54) and (3.55), recalling $\gamma \geq \frac{a}{D}$, the time derivative of the total Lyapunov function (3.44) satisfies the following inequality

$$\begin{aligned} \dot{V} \leq & -\alpha V + \beta_1 V^{3/2} + 8 d_1^2 D L_{n_1} h^*(X)^2 + d_1 \frac{1}{2} \left| r_g e_1^\top X \right| h^*(X)^2 + 8 d_1^2 D L_{n_2} f(X(t))^2 \\ & + 8 D L_{n_2} f(X(t))^2 + 8 D L_{n_3} h^*(X)^2, \end{aligned} \tag{3.65}$$

where

$$\beta_1 = \frac{r_g\left(L_2 + L_1\gamma + \sqrt{2}(L_3 + L_4)\right)}{2d_2\lambda_{\min}(P)^{3/2}} + \frac{r_g(2 + d_1^2)}{2\lambda_{\min}(P)^{1/2}} + \frac{2\kappa|P|}{\lambda_{\max}(P)^{3/2}}. \tag{3.66}$$

The next step is to bound the nonlinear terms in (3.65) which is defined in (3.32). Using the exponential inequality

$$e^x - x - 1 \leq x^2 \quad \text{for} \quad x \leq 1.79, \tag{3.67}$$

we can first bound the nonlinear term $h^*(X)$ term. By recalling $h^*(X)$ from (3.32),

$$h^*(X) = c_\infty\left(1 - K_+ e^{\lambda_+ z_2(t)} - K_- e^{\lambda_- z_2(t)}\right) + \frac{(a - gl_c)c_\infty}{D} z_2(t), \tag{3.68}$$

We can derive this bound by first showing that

$$\frac{a - gl_c}{D} = \lambda_+ K_+ + \lambda_- K_-, \tag{3.69}$$

which leads to

$$h^*(X) = c_\infty\left(K_+(1 + \lambda_+ z_2 - e^{\lambda_+ z_2}) + K_-(1 + \lambda_- z_2 - e^{\lambda_- z_2})\right). \tag{3.70}$$

It's clear that both $(1 + \lambda_+ z_2 - e^{\lambda_+ z_2})$ and $(1 + \lambda_- z_2 - e^{\lambda_- z_2})$ are upper-bounded by 0 because

$$1 + x - e^x \leq 0 \tag{3.71}$$

for any x value. Since we need to take square of $h^*(X(t))$, we can write

$$h^*(X)^2 = c_\infty^2\left(K_+|1 + \lambda_+ z_2 - e^{\lambda_+ z_2}| + K_-|1 + \lambda_- z_2 - e^{\lambda_- z_2}|\right)^2. \tag{3.72}$$

By using Young's inequality, we get

$$h^*(X)^2 \leq 2c_\infty^2 K_+^2 |1+\lambda_+ z_2 - e^{\lambda_+ z_2}|^2 + 2c_\infty^2 K_-^2 |1+\lambda_- z_2 - e^{\lambda_- z_2}|^2. \tag{3.73}$$

Since $1+x-e^x \leq 0$, we can write

$$h^*(X)^2 \leq 2c_\infty^2 K_+^2 \left(-1-\lambda_+ z_2 + e^{\lambda_+ z_2}\right)^2 + 2c_\infty^2 K_-^2 \left(-1-\lambda_- z_2 + e^{\lambda_- z_2}\right)^2. \tag{3.74}$$

because $-1-x+e^x \geq 0$ for all x. By using this argument and using (3.67), we can show that

$$e^x - 1 - x \leq x^2 \text{ for } x \leq 1.79 \tag{3.75}$$

Similarly, we have

$$|h^*(X)|^2 \leq 2c_\infty^2 \left(K_+^2(\lambda_+ z_2)^4 + K_-^2(\lambda_- z_2)^4\right). \tag{3.76}$$

Then, we define

$$k_n = \max\{c_\infty K_+ \lambda_+^2, c_\infty K_- \lambda_-^2\}, \tag{3.77}$$

and this allows us to conclude that

$$|h^*(X)| \leq 2k_n X^\top X, \tag{3.78}$$

Applying the same strategy, we also derive

$$f(X(t)) \leq \kappa X^\top X + 2k_m |X^\top X|^{3/2}, \tag{3.79}$$

where

$$k_m = \max\{c_\infty K_+ \lambda_+^3, c_\infty K_- \lambda_-^3\} \tag{3.80}$$

for a sufficiently small norm of X. Applying (3.78) and (3.79) to (3.65), we have the following inequality

$$\dot{V} \leq -\alpha V + \beta_1 V^{3/2} + \beta_2 V^2 + \beta_3 V^{5/2} + \beta_4 V^3, \tag{3.81}$$

where

$$\beta_2 = \frac{8d_1^2 D\left(L_{n_1} 4k_n^2 + L_{n_2}\kappa^2\right) + 8D\left(L_{n_2}\kappa^2 + L_{n_3} 4k_n^2\right)}{\lambda_{\min}(P)^2}, \tag{3.82}$$

$$\beta_3 = \frac{d_1 r_{\mathrm{g}}}{2\lambda_{\min}(P)^{5/2}}, \tag{3.83}$$

$$\beta_4 = \frac{32DL_{n_2} k_m^2 |P|^2 (d_1^2 + 1)}{\lambda_{\min}(P)^3}, \tag{3.84}$$

which completes the proof of Lemma 3.1. □

3.2.5 Ensuring bounds on axon length and growth rate.

In this subsection, we prove important lemmas to conclude with Theorem 1 ensuring the local stability of the closed-loop system. First, we give the following lemma.

Lemma 3.2. *There exists a positive constant $M_1 > 0$ such that in the region $\Omega_1 := \{(w, X) \in \mathcal{H}_1 \times \mathbb{R}^2 | V(t) < M_1\}$ the conditions* (3.33) *and* (3.34) *are satisfied.*

Proof. By using (2.23) and the plant equation (2.5), $X(t)$ can be described as

$$X(t) = \begin{bmatrix} \dfrac{\dot{l}(t)}{r_{\mathrm{g}}(t)} & l(t) - l_{\mathrm{s}} \end{bmatrix}^\top. \tag{3.85}$$

For any $r > 0$, if $|X| < r$ then the following two inequalities hold:

$$\left|\frac{\dot{l}(t)}{r_{\mathrm{g}}}\right| < r, \quad \left|l(t) - l_{\mathrm{s}}\right| < r. \tag{3.86}$$

The first inequality tells that if $r < \frac{\bar{v}}{r_{\mathrm{g}}}$ then the property of the system, (3.33), holds. Moreover, the second inequality can be written as $-r + l_{\mathrm{s}} < l(t) < r + l_{\mathrm{s}}$, and thus if both $r < l_{\mathrm{s}}$ and $r < \bar{l} - l_{\mathrm{s}}$ hold, then the condition (3.34) holds. Therefore, the constant, r, is chosen as

$$r = \min\left\{\frac{\bar{v}}{r_{\mathrm{g}}}, l_{\mathrm{s}}, \bar{l} - l_{\mathrm{s}}\right\}. \tag{3.87}$$

Since we know $|X|^2 \leq \frac{1}{\lambda_{\min}(P)} X^\top P X \leq \frac{d_2}{\lambda_{\min}(P)} V$, we derive the setting $M_1 = \frac{\lambda_{\min}(P)}{d_2} r^2$. If $V(t) < M_1$ holds then $|X| < r$ and thus the properties of the system, (3.33) and (3.34), are satisfied, by which we can conclude Lemma 3.2. □

Lemma 3.3. *There exists a positive constant $M > 0$ such that if $V(0) < M$ then the conditions* (3.33) *and* (3.34) *are satisfied and the following norm estimate holds:*

$$V(t) \leq V(0) \exp\left(-\frac{\alpha}{2} t\right). \tag{3.88}$$

Proof. For a positive constant $M > 0$, let $\Omega := \{(w, X) \in \mathcal{H}_1 \times \mathbb{R}^2 | V(t) < M\}$. By Lemma 3.2, it is easily shown that if $M \leq M_1$ then $\Omega \subset \Omega_1$, and thus the conditions (3.33) and (3.34) are satisfied in the region Ω. Thus, by Lemma 1, the norm estimate (3.46) holds. Moreover, we set $M \leq p^*$ where p^* is the root of the following polynomial with respect to V (except $p^* = 0$)

$$-\frac{\alpha}{2} V + \beta_1 V^{3/2} + \beta_2 V^2 + \beta_3 V^{5/2} + \beta_4 V^3 \leq 0. \tag{3.89}$$

Since $\alpha > 0$, $\beta_i > 0$ for $i = \{1, 2, 3, 4\}$ exist, the root of the polynomial always exists. Now, we

can see that applying $V(t) < M$ to (3.46) leads to

$$\dot{V} \leq -\frac{\alpha}{2}V, \tag{3.90}$$

by which the norm estimate (3.88) is deduced. Since (3.88) is a monotonically decreasing function in time, by setting $M = \min\{M_1, p^*\}$, the region Ω is shown to be an invariant set. Thus, if $V(0) < M$, then $V(t) < M$ for all $t \geq 0$, and one can conclude with Lemma 3.3. □

Due to Lemma 3.3, and the equivalent norm estimate in the $\mathcal{H}_1$-norm between the target system and the closed-loop system, one can obtain the local stability of the closed-loop system, which completes the proof of Theorem 1.

3.3 Simulations

3.3.1 Parameter Values

We perform simulations for the axon growth model by incorporating the biological parameters proposed by [26], which are shown in Table 3.1. The state-feedback controller remains unaffected by the desired length, denoted as l_s. However, it is worth noting that the desired length is employed in the steady-state solution for the concentration flux in the soma, which serves as an input. In the simulation of the state-feedback control, as specified in (3.1), the initial conditions are set as $c_0(x) = 2c_\infty$ for tubulin concentration along the axon and $l_0 = 1\mu$m for the axon length. The gain parameters of the closed-loop system are set as $k_1 = -0.1$, and $k_2 = 10^{13}$.

Table 3.1. Biological constants and control parameters

Parameter	Value	Parameter	Value
D	$10\times10^{-12}m^2/s$	$\tilde{r}_{\mathrm{g}}$	0.053
a	$1\times10^{-8}m/s$	γ	10^4
g	$5\times10^{-7}\ s^{-1}$	l_{c}	$4\mu m$
r_{g}	$1.783\times10^{-5}\ m^4/(mols)$	l_s	$12\mu m$
c_∞	$0.0119\ mol/m^3$	l_0	$1\mu m$

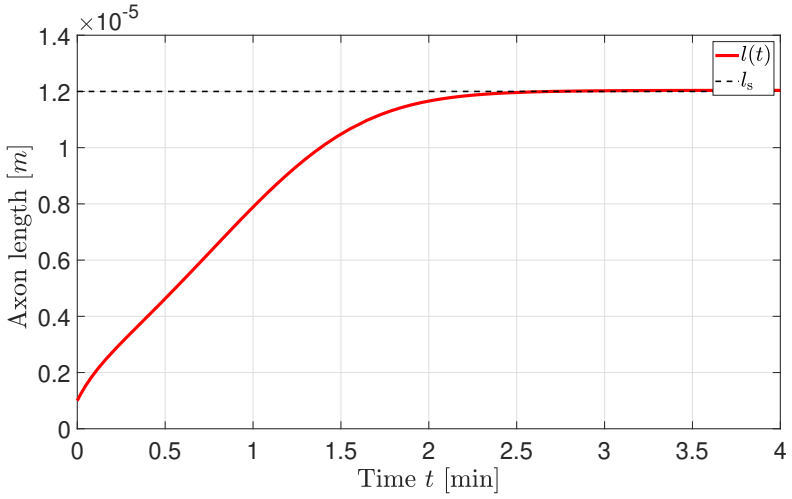

(a) The axon length $l(t)$ governed by the nonlinear ODE dynamics converges to the desired length l_s within $t = 3$min.

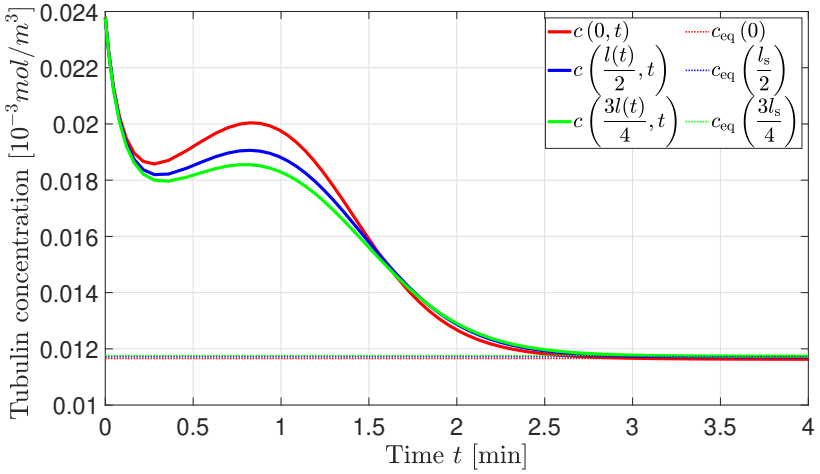

(b) Tubulin concentration $c(x,t)$ governed by the nonlinear PDE-ODE dynamics converges to the steady-state tubulin concentration, $c_{eq}(x)$ along the axon within $t = 3$ min.

Figure 3.1. The closed-loop response of the designed full-state feedback control system.

3.3.2 Axon elongation by up to *three orders of magnitude*

When the state feedback control law is applied to the nonlinear dynamics in (2.1)-(2.2), the axon length, $l(t)$, successfully converges to the desired axon length, l_s in Figure 3.1a. Moreover, Figure 3.1b demonstrates that the tubulin concentration along the axon also converges to the equilibrium profile.

Simulation in Figure 3.1a and 3.1b are informative to understand how the proposed

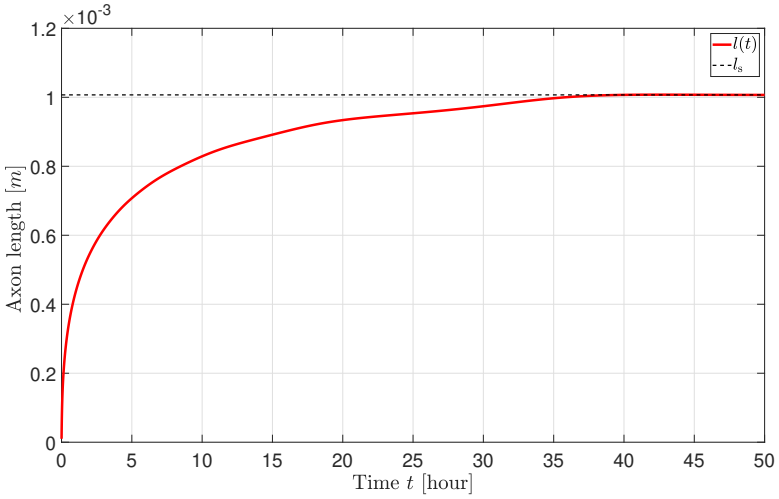

(a) The axon length $l(t)$ governed by the nonlinear ODE dynamics converges to the desired length by about $t = 36$ hours.

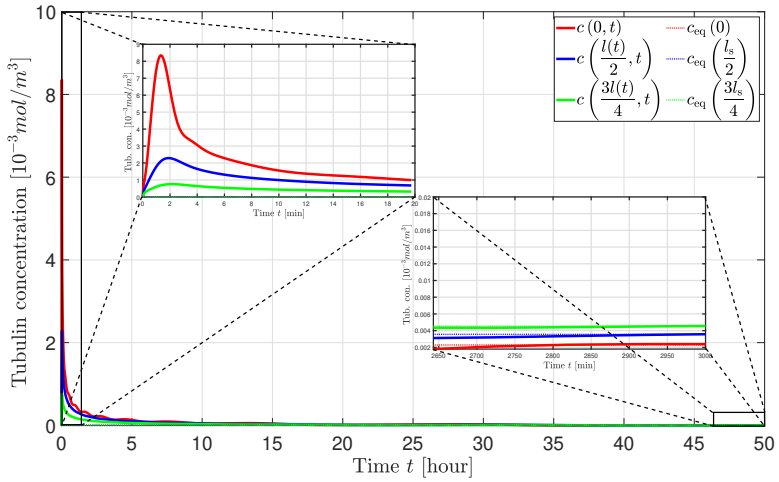

(b) Tubulin concentration $c(x,t)$ governed by the nonlinear PDE-ODE dynamics converges to the steady-state tubulin concentration, $c_{\text{eq}}(x)$ along the axon by about $t = 10$ hours.

Figure 3.2. The closed-loop response of the designed full-state feedback control system for long-range elongation $l_{\text{s}} = 1$.

control methods are effective to elongate the axon within one order of magnitude. However, axon lengths for inhibitory interneurons in the spinal cord are around 1 mm [17]. In Figure 3.2a and 3.2b, we apply our proposed state feedback controller to elongate the axon from the very small initial length, $l_0 = 1$ μm to three orders of magnitude of desired axon length, $l_{\text{s}} = 1$ mm for biological parameters in Table 3.1 and the equilibrium of the tubulin concentration in the

cone, c_∞. c_∞ is chosen as $5.95 \times 10^{-3}\ mol/m^3$. The state feedback control law is applied to the nonlinear dynamics in (2.1)-(2.2) by choosing the gains $k_1 = -5.3 \times 10^5$ and $k_2 = 1 \times 10^{13}$. The axon length, $l(t)$, successfully converges to the desired long-range axon length, l_s in Figure 3.2a. Moreover, Figure 3.2b demonstrates that the tubulin concentration along the axon also converges to equilibrium.

Acknowledgements

Chapter 3 has been published in Automatica 2024 with the title "Neuron growth control and estimation by PDE backstepping" C. Demir, S. Koga, M. Krstic. Chapter 3, 'also contains a partial adaptation of the work contained in the conference paper"Neuron growth control by PDE backstepping: Axon length regulation by tubulin flux actuation in soma" C. Demir, S. Koga, M. Krstic, presented in the 60th IEEE Conference on Decision and Control 2021. The dissertation author was the primary author of these publications.

Chapter 4

Neuron Growth State Estimation

In the state feedback control law designed in the previous section, measurements of both the distributed tubulin concentration $c(x,t)$ along the domain and axon length $l(t)$ are required for the computation of the controller. The requirement of measuring the entire spatial concentration profile limits the practical applicability of the controller. These measurements can be obtained using advanced techniques. Immunofluorescence microscopy, for example, allows for the quantification of tubulin concentration along the axon by detecting fluorescently labeled antibodies that specifically target tubulin [33]. Axon length can be measured using either manual tracing from microscopy images or automated image analysis software, both of which offer accurate and reliable measurements [75]. However, accurately measuring tubulin concentration along the entire length of an axon can be challenging [33]. To resolve the issue, we develop a nonlinear observer to reconstruct the entire concentration profile from the boundary measurements. The measured states are axon length $l(t)$ and the tubulin flux at the cone, $c_x(l(t),t)$.

4.1 Observer Design

In this section, we introduce the observer design of the tubulin concentration profile along the axon. The observer model with measured states is described by

$$\hat{c}_t(x,t) = D\hat{c}_{xx}(x,t) - a\hat{c}_x(x,t) - g\hat{c}(x,t) + p_1(x,l(t))\left(c_x(l(t),t) - \hat{c}_x(l(t),t)\right), \tag{4.1}$$

$$\hat{c}_x(0,t) = U(t), \tag{4.2}$$

$$\hat{c}(l(t),t) = \hat{c}_c(t), \tag{4.3}$$

$$l_c\dot{\hat{c}}_c(t) = (a - gl_c)\hat{c}_c(t) - \left(r_g\hat{c}_c(t) + \tilde{r}_g l_c\right)(\hat{c}_c(t) - c_\infty) - Dc_x(l(t),t) + l_1(l(t) - \hat{l}(t)), \tag{4.4}$$

$$\dot{\hat{l}}(t) = r_g(\hat{c}_c(t) - c_\infty) + l_2(l(t) - \hat{l}(t)), \tag{4.5}$$

with the measurements

$$y_1(t) = c_x(l(t),t), \quad y_2(t) = C\begin{bmatrix} c_c(t) \\ l(t) \end{bmatrix}, \tag{4.6}$$

where $C = [0 \quad 1]$. Denoting the estimates of the tubulin concentration, $\hat{c}(x,t)$, the following theorem holds:

Theorem 4.1. *Let the system properties* (3.33) *and* (3.34) *hold. Let* $c_c(t)$ *be bounded as*

$$\underline{c} \le c_c(t) \le \bar{c}, \tag{4.7}$$

where $\bar{c} > \underline{c} > 0$. *Consider the plant* (2.32)-(2.35) *and the observer* (4.1)-(4.5) *with available measurements* (4.6)*, let* $L = [l_1 \quad l_2]$ *be chosen as*

$$l_1 > \frac{\tilde{a}l_2}{r_g}, \quad l_2 \ge |\tilde{a}| + \frac{2r_g\bar{c}}{l_c} + 4r_g + \frac{1}{2}, \tag{4.8}$$

and let the observer gain be $p_1(x,l(t)) = DP(x,l(t))$ *where* $P(x,l(t))$ *is the solution to the*

following PDE

$$DP_{yy}(x,y) - DP_{xx}(x,y) + aP_x(x,y) - aP_y(x,y) = \lambda P(x,y), \tag{4.9}$$

$$P(x,x) = \frac{\lambda}{2D}x + \gamma_1, \tag{4.10}$$

$$P_x(0,y) = 0, \tag{4.11}$$

where $\lambda > 0$ *is an arbitrary constant, and* γ_1 *is a constant satisfying* $\frac{D}{a} \leq \gamma_1$*. Then, the observer error system is locally exponentially stable in the* $\mathcal{H}_1$*-norm, i.e., there exist* $\tilde{M}$*,* $c_2 > 0$ *and* $\kappa > 0$ *such that if* $\tilde{\Phi}(0) < \tilde{M}$ *then the following norm estimate holds:*

$$\tilde{\Phi}(t) \leq c_2 \tilde{\Phi}(0) e^{-\kappa t}, \tag{4.12}$$

where $\tilde{\Phi}(t) := ||c - \hat{c}||_{\mathcal{H}_1(0,l(t))} + |X - \hat{X}|$.

In the remainder of this section, we provide the proof of Theorem 4.1.

4.1.1 Observer Error System

In order to prove Theorem 4.1, we first derive the observer error system. This is a critical step because the observer error system captures the difference between the actual system states and the estimated states provided by the observer. These states are given by

$$\tilde{c}(x,t) = c(x,t) - \hat{c}(x,t), \tag{4.13}$$

$$\tilde{c}_c(t) = c_c(t) - \hat{c}(t), \tag{4.14}$$

$$\tilde{l}(t) = l(t) - \hat{l}(t). \tag{4.15}$$

Thus, we have

$$\tilde{c}_t(x,t) = D\tilde{c}_{xx}(x,t) - a\tilde{c}_x(x,t) - g\tilde{c}(x,t) - p_1(x,l(t))\left(c_x(l(t),t) - \hat{c}_x(l(t),t)\right), \tag{4.16}$$

$$\tilde{c}_x(0,t) = 0, \tag{4.17}$$

$$\tilde{c}(l(t),t) = [1 \quad 0]\tilde{X}(t), \tag{4.18}$$

$$\dot{\tilde{X}}(t) = \left(\tilde{A} - LC\right)\tilde{X}(t) + \kappa e_1^\top \tilde{X}(t)\tilde{X}(t)^\top e_1 - 2\kappa c_{\mathrm{c}}(t) e_1^\top \tilde{X}(t), \tag{4.19}$$

where $\tilde{X} = [\tilde{c}_{\mathrm{c}}(t) \quad \tilde{l}(t)]^\top$ and

$$\tilde{A} = \begin{bmatrix} \tilde{a}_1 & 0 \\ r_{\mathrm{g}} & 0 \end{bmatrix}. \tag{4.20}$$

4.1.2 Backstepping Transformation

As for the full-state feedback case, we now consider the following inverse backstepping transformation

$$\tilde{c}(x,t) = \tilde{w}(x,t) + \int_x^{l(t)} P(x,y)\tilde{w}(y,t)dy, \tag{4.21}$$

where $P(x,y) \in \mathbb{R}$ is the gain kernel to be solved on the time-varying domain $\Omega_0(t) = \{(x,y)|0 \leq y \leq x \leq l(t)\}$. Let the target system be

$$\tilde{w}_t(x,t) = D\tilde{w}_{xx}(x,t) - a\tilde{w}_x(x,t) - (g+\lambda)\tilde{w}(x,t) + \dot{l}(t)\left(Q(x,l(t)) - P(x,l(t))\right)\tilde{w}(l(t),t), \tag{4.22}$$

$$\tilde{w}_x(0,t) = \gamma_1 \tilde{w}(0,t), \tag{4.23}$$

$$\tilde{w}(l(t),t) = [1 \quad 0]\tilde{X}(t), \tag{4.24}$$

$$\dot{\tilde{X}}(t) = (A - LC)\tilde{X}(t) - f(\tilde{X}(t)) - c_{\mathrm{c}}(t)A_2\tilde{X}(t), \tag{4.25}$$

where $Q(x,y) \in \mathbb{R}$ is also the gain kernel obtained from direct backstepping transformation and

$$A_2 = \begin{bmatrix} 2\frac{r_g}{l_c} & 0 \\ 0 & 0 \end{bmatrix}. \tag{4.26}$$

Let the ODE observer gain L be described as $L = \begin{bmatrix} l_1 & l_2 \end{bmatrix}^\top$, so one can show the conditions for the gains as

$$l_1 > \frac{\tilde{a}_1 l_2}{r_g}, \quad l_2 > \tilde{a}_1. \tag{4.27}$$

which makes $A - LC$ Hurwitz.

4.1.3 Well-posedness of backstepping transformations

Taking the time and spatial derivatives of (4.21) together with the solution of (4.22)-(4.24) and the stability of $\tilde{X}(t)$, we obtain (4.9)-(4.11). However, these PDEs do not have an analytical solution. To ensure the well-posedness of the solution, we must prove that $P(x,y)$ is bounded. To achieve this, we apply the method of successive approximations, which allows us to obtain a numerical solution and to prove the boundedness of the solution.

Method of successive approximation

First, we present the lemma that establishes the well-posedness of (4.22)-(4.24).

Lemma 4.1. *If property* (3.33) *hold for all time t. Then, for an arbitrary constant,* $\lambda > 0$ *and a constant* $\frac{D}{a} \leq \gamma_1$*, the gain kernel PDE,*

$$DP_{yy}(x,y) - DP_{xx}(x,y) + aP_x(x,y) - aP_y(x,y) = \lambda P(x,y), \tag{4.28}$$

$$P(x,x) = \frac{\lambda}{2D}x + \gamma_1, \tag{4.29}$$

$$P_x(0,y) = 0, \tag{4.30}$$

has unique C^2 solutions which are bounded by

$$|P(x,y)| \leq \frac{\lambda}{2}\left(\frac{1}{a}+\frac{\bar{l}}{D}\left(e^{\frac{2a}{D}\bar{l}}+1\right)\right)e^{\lambda\left(\frac{1}{a}+\frac{\bar{l}}{D}\left(e^{\frac{2a}{D}\bar{l}}+1\right)\right)x}. \tag{4.31}$$

Proof. To prove this lemma, we apply the following transformation

$$P(x,y) = \tilde{P}(x,y)e^{\frac{a}{2D}(x+y)}, \tag{4.32}$$

so (4.9)-(4.11) become

$$\tilde{P}_{yy}(x,y) - \tilde{P}_{xx}(x,y) = \frac{\lambda}{2D}\tilde{P}(x,y), \tag{4.33}$$

$$\tilde{P}(x,x) = e^{-\frac{ax}{D}}\left(\frac{\lambda}{2D}x+\gamma_1\right), \tag{4.34}$$

$$\tilde{P}_x(0,y) = -\frac{a}{2D}\tilde{P}(0,y), \tag{4.35}$$

Now, we apply the spatial coordinate change which is

$$\bar{x} = y, \quad \bar{y} = x, \quad P^*(\bar{x},\bar{y}) = \tilde{P}(x,y) \tag{4.36}$$

Then, we have

$$P^*_{\bar{x}\bar{x}}(\bar{x},\bar{y}) - P^*_{\bar{y}\bar{y}}(\bar{x},\bar{y}) = \frac{\lambda}{2D}P^*(\bar{x},\bar{y}) \tag{4.37}$$

$$P^*(\bar{x},\bar{x}) = \frac{\lambda}{2D}e^{-\frac{a\bar{x}}{D}}\bar{x} + e^{-\frac{a\bar{x}}{D}}\gamma_1 \tag{4.38}$$

$$P^*_{\bar{y}}(\bar{x},0) = -\frac{a}{2D}P^*(\bar{x},0) \tag{4.39}$$

Next, we convert the gain kernel PDE into an integral equation by applying the following

transformation

$$\xi = x + y, \quad \eta = x - y, \quad P^*(\bar{x}, \bar{y}) = G(\xi, \eta) \tag{4.40}$$

where $(\xi, \eta) \in \mathcal{T}_1$ which is introduced as $\mathcal{T}_1 = \{\xi, \eta : 0 < \xi < 2l(t),\ 0 < \eta < \min(\xi, 2l(t) - \xi)\}$. This gives us

$$G_{\xi\eta}(\xi, \eta) = \frac{\lambda}{8D} G(\xi, \eta) \tag{4.41}$$

$$G(\xi, 0) = \frac{\lambda}{4D} e^{-\frac{a}{2D}\xi} \xi + e^{-\frac{a}{2D}\xi} \gamma_1 \tag{4.42}$$

$$G_\xi(\xi, \xi) - G_\eta(\xi, \xi) = -\frac{a}{2D} G(\xi, \xi) \tag{4.43}$$

When we take integral of (4.41) from 0 to η with respect to η, we get

$$G_\xi(\xi, \eta) = G_\xi(\xi, 0) + \int_0^\eta \frac{\lambda}{8D} G(\xi, s) ds \tag{4.44}$$

where

$$G_\xi(\xi, 0) = \frac{\lambda}{4D} e^{-\frac{a}{2D}\xi} \left(1 - \frac{a\xi}{2D}\right) - \frac{a}{2D} e^{-\frac{a}{2D}\xi} \gamma_1 \tag{4.45}$$

which leads us

$$G_\xi(\xi, \eta) = \frac{\lambda}{4D} e^{-\frac{a}{2D}\xi} \left(1 - \frac{a\xi}{2D}\right) - \frac{a}{2D} e^{-\frac{a}{2D}\xi} \gamma_1 + \int_0^\eta \frac{\lambda}{8D} G(\xi, s) ds. \tag{4.46}$$

Next, we integrate (4.46) from η to ξ with respect to ξ, so we get

$$\begin{aligned} G(\xi, \eta) =& G(\eta, \eta) + \int_\eta^\xi \frac{\lambda}{4D} e^{-\frac{a}{2D}\tau} \left(1 - \frac{a\tau}{2D}\right) - \frac{a}{2D} e^{-\frac{a}{2D}\tau} \gamma_1 d\tau \\ &+ \int_\eta^\xi \int_0^\eta \frac{\lambda}{8D} G(\tau, s) ds d\tau \end{aligned} \tag{4.47}$$

In order to find $G(\eta,\eta)$, we can use (4.43), so

$$\begin{aligned}\frac{d}{d\xi}G(\xi,\xi) &= G_{\xi}(\xi,\xi)+G_{\eta}(\xi,\xi)\\ &= 2G_{\xi}(\xi,\xi)+\frac{a}{2D}G(\xi,\xi)\end{aligned} \tag{4.48}$$

By using (4.46) with $\eta=\xi$, we get

$$G_{\xi}(\xi,\xi)=\frac{\lambda}{4D}e^{-\frac{a}{2D}\xi}\left(1-\frac{a\xi}{2D}\right)-\frac{a}{2D}e^{-\frac{a}{2D}\xi}\gamma_1+\int_0^{\xi}\frac{\lambda}{8D}G(\xi,s)ds \tag{4.49}$$

Now, we substitute (4.49) in (4.48), so we obtain

$$\frac{d}{d\xi}G(\xi,\xi)=\frac{\lambda}{2D}e^{-\frac{a}{2D}\xi}\left(1-\frac{a\xi}{2D}\right)-\frac{a}{D}e^{-\frac{a}{2D}\xi}\gamma_1+\int_0^{\xi}\frac{\lambda}{4D}G(\xi,s)ds+\frac{a}{2D}G(\xi,\xi) \tag{4.50}$$

We can integrate (4.50) by using the variation of constants formula. Then, we receive

$$G(\xi,\xi)=\int_0^{\xi}\left(\frac{\lambda}{2D}e^{-\frac{a}{2D}\tau}\left(1-\frac{a\tau}{2D}\right)-\frac{a}{D}e^{-\frac{a}{2D}\tau}\gamma_1+\int_0^{\tau}\frac{\lambda}{4D}G(\tau,s)ds\right)e^{\frac{a}{2D}(\tau-\xi)}d\tau \tag{4.51}$$

Substituting (4.51) in (4.47) with $\xi=\eta$, we get

$$\begin{aligned}G(\xi,\eta)=&\int_0^{\eta}\left(\frac{\lambda}{2D}e^{-\frac{a}{2D}\tau}\left(1-\frac{a\tau}{2D}\right)-\frac{a}{D}e^{-\frac{a}{2D}\tau}\gamma_1+\int_0^{\tau}\frac{\lambda}{4D}G(\tau,s)ds\right)e^{\frac{a}{2D}(\tau-\eta)}d\tau\\ &+\int_{\eta}^{\xi}\frac{\lambda}{4D}e^{-\frac{a}{2D}\tau}\left(1-\frac{a\tau}{2D}\right)-\frac{a}{2D}e^{-\frac{a}{2D}\tau}\gamma_1 d\tau+\int_{\eta}^{\xi}\int_0^{\eta}\frac{\lambda}{8D}G(\tau,s)dsd\tau\end{aligned} \tag{4.52}$$

This can be written in the form of

$$G(\xi,\eta)=G_0(\xi,\eta)+F[G](\xi,\eta) \tag{4.53}$$

which is

$$G_0(\xi,\eta) = \frac{\lambda}{2D}\int_0^\eta \left(e^{-\frac{a}{2D}\tau}\left(1-\frac{a\tau}{2D}\right)-\frac{2a}{\lambda}e^{-\frac{a}{2D}\tau}\gamma_1\right)e^{\frac{a}{2D}(\tau-\eta)}d\tau$$
$$+\frac{\lambda}{4D}\int_\eta^\xi e^{-\frac{a}{2D}\tau}\left(1-\frac{a\tau}{2D}\right)-\frac{2a}{\lambda}e^{-\frac{a}{2D}\tau}\gamma_1 d\tau \tag{4.54}$$

$$F[G](\xi,\eta) = \frac{\lambda}{4D}\int_0^\eta\left(\int_0^\tau G(\tau,s)ds\right)e^{\frac{a}{2D}(\tau-\eta)}d\tau+\frac{\lambda}{8D}\int_\eta^\xi\int_0^\eta G(\tau,s)dsd\tau \tag{4.55}$$

With the definition of G_0, we let

$$G_{n+1} = F[G_n] \tag{4.56}$$

and

$$\bar{c} = \sup_{x\in[0,\bar{l}[t]]}\left(1-\frac{ax}{2D}-\frac{2a\gamma_1}{\lambda}\right) = 1 \tag{4.57}$$

because $a,\ \gamma_1,\ D$, and λ are constants in $(0,\infty)$. We can simply find $G_0(\xi,\eta)$ as

$$\begin{aligned}|G_0(\xi,\eta)| &\le \frac{\lambda}{2D}\bar{c}\eta+\frac{\lambda}{2a}\bar{c}\\ &\le \frac{\lambda}{2a}+\frac{\lambda}{2D}l(t)\left(e^{\frac{2a}{D}l(t)}+1\right)\\ &\le \frac{\lambda}{2}\left(\frac{1}{a}+\frac{\bar{l}}{D}\left(e^{\frac{2a}{D}\bar{l}}+1\right)\right)\equiv M\end{aligned} \tag{4.58}$$

Now, suppose that

$$|G_n(\xi,\eta)| \le M^{n+1}\frac{(\xi+\eta)^2}{n!} \tag{4.59}$$

Then,

$$
\begin{aligned}
|G_{n+1}(\xi,\eta)| &\leq \frac{M^{n+1}}{n!}\frac{\lambda}{4D}\left\{\int_0^{\eta}\left(\int_0^{\tau}(\tau+s)^n ds\right)e^{\frac{a(\tau-\eta)}{2D}}d\tau+\frac{1}{2}\int_{\eta}^{\xi}\int_0^{\eta}(\tau+s)^n ds d\tau\right\} \\
&\leq \frac{M^{n+1}}{n!}\frac{\lambda}{4D}\left\{\frac{2D}{a}\bar{c}+2\bar{c}\bar{l}(t)\right\}\frac{(\xi+\eta)^{n+1}}{(n+1)} \\
&\leq \frac{M^{n+1}}{n!}\left\{\frac{\lambda}{2a}+\frac{\lambda}{2D}\bar{l}\right\}\frac{(\xi+\eta)^{n+1}}{(n+1)} \\
&\leq M^{n+2}\frac{(\xi+\eta)^{n+1}}{(n+1)!}
\end{aligned}
\tag{4.60}
$$

By induction, we proved the equation (4.59). Thus,

$$
G(\xi,\eta)=\sum_{n=0}^{\infty}G_n(\xi,\eta) \tag{4.61}
$$

which converges in $\mathcal{T}_1$ uniformly, and absolutely.In addition, it is a continuous and twice differentiable. Then, G has a bound

$$
|G(\xi,\eta)|\leq Me^{M(\xi+\eta)} \tag{4.62}
$$

Now, we suppose $G'(\xi,\eta)$ and $G''(\xi,\eta)$ are two different solutions of (4.41)-(4.43).Then,

$$
\begin{aligned}
|\Delta G(\xi,\eta)| &= G'(\xi,\eta)-G''(\xi,\eta) \\
&\leq 2Me^{2M}
\end{aligned}
\tag{4.63}
$$

Now, by using the (4.59), we get

$$
|\Delta G(\xi,\eta)|\leq 2M^{n+1}e^{2M}\frac{(\xi+\eta)^n}{n!} \tag{4.64}
$$

where

$$\lim_{n\to\infty} 2M^{n+1}e^{2M}\frac{(\xi+\eta)^n}{n!}=0 \tag{4.65}$$

Then, we can conclude the following result

$$|P(x,y)|\leq Me^{2Mx} \tag{4.66}$$

If (3.33) holds for all time, then (4.28)-(4.30) has a unique solution in C^2 which is bounded by (4.31). This completes the proof of Lemma 4.1. □

4.2 Stability proof of designed observer

In this section, we outline the proof of Theorem 4.1, starting with the inverse transformation that plays a crucial role in establishing the stability of the estimator.

4.2.1 Inverse Transformation

We use the following backstepping transformation

$$\tilde{w}(x,t)=\tilde{c}(x,t)-\int_x^{l(t)}Q(x,y)\tilde{u}(y,t)dy. \tag{4.67}$$

By applying (4.67) to the observer error system (4.16)–(4.19) and the target system (4.22)–(4.24), the conditions for the kernel function are obtained as

$$\begin{aligned} DQ_{xx}(x,y)-aQ_x(x,y)-DQ_{yy}(x,y)& \\ -aQ_y(x,y)&=\lambda Q(x,y), \end{aligned} \tag{4.68}$$

$$Q(x,x)=-\frac{\lambda}{2D}x+\gamma_1, \tag{4.69}$$

$$Q_x(0,y)=\gamma_1 Q(0,y). \tag{4.70}$$

We follow the same logic that we used for obtaining the solution of inverse backstepping transformation. First, we apply the following transformation $Q(x,y) = 2e^{\frac{a}{2D}(x-y)}\tilde{Q}(x,y)$ to (4.68)-(4.70). Thus, the transformed kernel PDE is well-posed, so the solution of $Q(x,y)$ exists, which means direct transformation exists. Similar to the inverse transformation, the closed-form solution of the direct kernel equation cannot be obtained. By applying the procedure in Section 4.1.3, we have the bound as $|Q(x,y)| \leq \Upsilon e^{2\Upsilon x}$.

4.2.2 Lyapunov analysis

We consider next the following Lyapunov function for the observer error target system

$$\tilde{V} = \tilde{V}_{11} + \tilde{V}_{12} + d_2\tilde{V}_2 + \frac{\gamma_1}{2}\tilde{w}(0,t)^2, \tag{4.71}$$

where

$$\tilde{V}_{11} = \frac{1}{2}d_1||\tilde{w}||^2, \tag{4.72}$$

$$\tilde{V}_{12} = \frac{1}{2}||\tilde{w}_x||^2, \tag{4.73}$$

$$\tilde{V}_2 = d_2\tilde{X}(t)^\top P_1\tilde{X}(t), \tag{4.74}$$

where

$$P_1 = \begin{bmatrix} \bar{\alpha}(1+\frac{2r_g}{l_2})+\frac{3}{2} & 2\bar{\alpha} \\ 2\bar{\alpha} & \bar{\alpha}(4+\frac{2l_1}{l_2}) \end{bmatrix}, \tag{4.75}$$

where $\bar{\alpha} > 0$, and makes P_1 a positive definite matrix. In addition, we can denote that

$$F(x,\tilde{X}(t)) = \left(P(x,\tilde{X}(t)+l_s) - Q(x,\tilde{X}(t)+l_s)\right)H^\top\tilde{X}(t). \tag{4.76}$$

Then, we state the following lemma.

Lemma 4.2. *Assume that assumptions* (3.33) *and* (3.34) *are satisfied for* $\bar{v} = \frac{D}{8\bar{l}}$*, for all time* $t \geq 0$*. Then, we conclude that for sufficiently large gain parameter* $\lambda > 0$*,* $d_1 > 0$*,* $d_2 > 0$*, and* $\bar{\alpha} > 0$*, there exists a positive constant* $\alpha_1 = \min\left\{d_1 \frac{D}{2}, d_1 (D + 2\lambda), (g + 2\lambda), \frac{\underline{\alpha}}{2\lambda_{\max}(P)}\right\}$ *and* $\tilde{\beta}_1 = d_2 \kappa \frac{\lambda_{\max}(P_1)}{\lambda_{\min}(P_1)^{3/2}}$ *which satisfy the following norm estimate hold for all* $t \geq 0$

$$\dot{\tilde{V}} \leq -\alpha_1 \tilde{V} + \beta_1 \tilde{V}^{3/2}. \tag{4.77}$$

Proof. Taking the time derivative of the Lyapunov functions along the target system (4.22)–(4.25), we have

$$\begin{aligned}
\dot{\tilde{V}}_{11} =& d_1 D \tilde{w}(l(t),t)\tilde{w}_x(l(t),t) - d_1\left(D\gamma_1 - \frac{a}{2}\right)\tilde{w}(0,t)^2 - d_1 \dot{l}(t)\int_0^{l(t)} \tilde{w}(x,t)F(x,\tilde{X}(t))dx \\
& - a\frac{d_1}{2}\tilde{w}(l(t),t)^2 - d_1 D||\tilde{w}_x||^2 - d_1(g+\lambda)||\tilde{w}||^2 + d_1\frac{\dot{l}(t)}{2}\tilde{w}(l(t),t)^2, \qquad (4.78) \\
\dot{\tilde{V}}_{12} =& H^\top (A - LC)\tilde{X}(t)\tilde{w}_x(l(t),t) - \frac{1}{2}\dot{l}(t)\tilde{w}_x(l(t),t)^2 - \tilde{w}_x(0,t)\tilde{w}_t(0,t) - D||\tilde{w}_{xx}(x,t)||^2 \\
& + \int_0^{l(t)} a\tilde{w}_{xx}(x,t)\tilde{w}_x(x,t)dx - (g+\lambda)\left(||\tilde{w}_x(x,t)||^2 + \gamma_1\tilde{w}(0,t)^2 - \tilde{w}(l(t),t)\tilde{w}_x(l(t),t)\right) \\
& - \dot{l}(t)\int_0^{l(t)} \tilde{w}_{xx}(x,t)F(x,\tilde{X}(t))dx, \qquad (4.79) \\
\dot{\tilde{V}}_2 =& d_2\tilde{X}^\top (A - LC)^\top P_1\tilde{X} + d_2\tilde{X}^\top P_1 (A - LC)\tilde{X} - d_2 2c_c(t)\tilde{X}^\top A_2 P_1\tilde{X} \\
& + d_2 f(\tilde{X})(P_1\tilde{X} + \tilde{X}^\top P_1), \qquad (4.80)
\end{aligned}$$

where $d_1 > 0$ and $d_2 > 0$. Applying Young's inequality, and by using (4.24)-(4.25) to the time derivative of $\tilde{V}_{11}$ in (4.78) leads to

$$\begin{aligned}
\dot{\tilde{V}}_{11} \leq & -d_1\left(D\gamma_1 - \frac{a}{2}\right)\tilde{w}(0,t)^2 - d_1 D||\tilde{w}_x(x,t)||^2 - d_1(g+\lambda)||\tilde{w}(x,t)||^2 + \frac{D\epsilon_1}{2}\tilde{w}_x(l(t),t)^2 \\
& - d_1\dot{l}(t)\int_0^{l(t)} \tilde{w}(x,t)F(x,\tilde{X}(t))dx, + \left(d_1^2\frac{D}{2\epsilon_1} + d_1\frac{l(t)}{2} - d_1\frac{a}{2}\right)\tilde{w}(l(t),t)^2, \qquad (4.81)
\end{aligned}$$

where $\epsilon_1 > 0$ is an arbitrarily small constant. Similarly, using Agmon's inequalities and Young's

inequality into the time derivative of $\tilde{V}_{12}$ in (4.79) gives us

$$\begin{aligned}\dot{\tilde{V}}_{12} \leq & \gamma_1^2\left(D\epsilon_1+\epsilon_2+\epsilon_3(g+\lambda)+\bar{v}+\frac{\bar{v}\epsilon_5}{2}\right)\tilde{w}(0,t)^2-\left(\gamma_1(g+\lambda)\right)\tilde{w}(0,t)^2-\left(D-\frac{D}{4}\right)||\tilde{w}_{xx}(x,t)||^2 \\ & -\left(-2\bar{l}(D\epsilon_1+\epsilon_2+\epsilon_3(g+\lambda)+\epsilon_4\bar{v}+\bar{v})\right)||\tilde{w}_{xx}(x,t)||^2-\left((g+\lambda)-\frac{a^2}{D}\right)||\tilde{w}_x(x,t)||^2 \\ & -\gamma_1\tilde{w}(0,t)\tilde{w}_t(0,t)+\left(\left(d_1^2\frac{D}{2\epsilon_1}+d_1\frac{a}{2}+d_1\frac{\bar{v}}{2}+\frac{(g+\lambda)}{2\epsilon_3}\right)+\frac{1}{2\epsilon_2}\lambda_{\max}((e_1^\top(A-LC))^2)\right)\tilde{X}^\top\tilde{X} \\ & +\frac{|\dot{l}(t)|}{2\epsilon_4}F(l(t),\tilde{X}(t))^2+\frac{|\dot{l}(t)|}{2\epsilon_5}\gamma_1F(0,\tilde{X}(t))^2+|\dot{l}(t)|\int_0^{l(t)}\tilde{w}_x(x,t)F_x(x,\tilde{X}(t))dx, \quad (4.82)\end{aligned}$$

where $\epsilon_i > 0$ for $i = \{1,...,5\}$ are arbitrarily small constants. By applying Young's inequality, using Lyapunov equation, (3.78) and (3.79), the time derivative of $\tilde{V}_2$ in (4.80) is obtained as

$$\dot{\tilde{V}}_2 \leq -8d_2\frac{r_{\mathrm{g}}^2\bar{\alpha}c_{\mathrm{c}}(t)}{l_{\mathrm{c}}l_2}\tilde{c}_{\mathrm{c}}(t)^2-d_2 4\bar{\alpha}l_2\tilde{l}(t)^2+d_2\kappa\lambda_{\max}(P_1)\left|\tilde{X}^\top\tilde{X}\right|^{3/2}, \quad (4.83)$$

by picking

$$l_2 \geq \max\left\{\frac{\tilde{a}}{\frac{2\bar{c}}{l_{\mathrm{c}}}+\frac{\tilde{a}^2+\tilde{a}}{2r_{\mathrm{g}}}+r_{\mathrm{g}}+1},\ \frac{2\bar{c}r_{\mathrm{g}}}{l_{\mathrm{c}}}+\tilde{a}^2+2r_{\mathrm{g}}\right\}, \quad (4.84)$$

$$\bar{\alpha} \leq \frac{3l_1l_2l_{\mathrm{c}}}{32\underline{c}r_{\mathrm{g}}+16\tilde{a}l_2l_{\mathrm{c}}}. \quad (4.85)$$

Note that there exists l_2 and $\underline{\alpha}$ for any physical values of $\underline{c}$ and $\bar{c}$. Now, we can derive the observer gain l_2 as

$$l_2 \geq \max\left\{\frac{\tilde{a}}{\frac{2\bar{c}}{l_{\mathrm{c}}}+\frac{\tilde{a}^2+\tilde{a}}{2r_{\mathrm{g}}}+r_{\mathrm{g}}+1},\ \frac{2\bar{c}r_{\mathrm{g}}}{l_{\mathrm{c}}}+\tilde{a}^2+2r_{\mathrm{g}},\tilde{a}\right\}. \quad (4.86)$$

In addition, one can show that

$$\underline{\alpha} = \min\left\{\frac{8r_{\mathrm{g}}^2\bar{\alpha}}{l_2l_{\mathrm{c}}},\ 2\bar{\alpha}l_2\right\}, \quad (4.87)$$

which leads to

$$\dot{\tilde{V}}_2 \leq -d_2\underline{\alpha}\tilde{X}^\top\tilde{X} + d_2\kappa\lambda_{\max}(P_1)\left|\tilde{X}^\top\tilde{X}\right|^{3/2}. \tag{4.88}$$

Then, we use Young's and Cauchy-Schwarz inequalities for F terms. There exist positive constants $L_i > 0$, for $i = 1,2,3,4$, which yield similar bounds as those in (3.57)-(3.60) for $F(.,.)$ terms. With these inequalities and (4.81)-(4.83), (4.82) becomes

$$\begin{aligned}
\dot{\tilde{V}}_{11} + \dot{\tilde{V}}_{12} + \dot{\tilde{V}}_2 \leq & -\frac{D}{2}||\tilde{w}_{xx}(x,t)||^2 - d_1\frac{D\gamma_1}{2}\tilde{w}(0,t)^2 - \left(d_1(g+\lambda) - \frac{\bar{v}\epsilon_6}{2}\right)||\tilde{w}(x,t)||^2 \\
& - d_1 D||\tilde{w}_x(x,t)||^2 - \left((g+\lambda) - \frac{a^2}{D} - \frac{\bar{v}\epsilon_7}{2}\right)||\tilde{w}_x(x,t)||^2 - \gamma_1\tilde{w}(0,t)\tilde{w}_t(0,t) \\
& + d_1\frac{\bar{v}}{2}L_1|\tilde{X}(t)|^2 + \left(\frac{\bar{v}L_2}{2\epsilon_4} + d_1^2\frac{\bar{v}L_3}{2\epsilon_6} + \frac{\bar{v}L_4}{2\epsilon_7} - d_2\underline{\alpha}\frac{d_1^2 D}{2\epsilon_1} + \frac{d_1 a}{2} + \frac{d_1\bar{v}}{2} + \frac{g+\lambda}{2\epsilon_3}\right)|\tilde{X}(t)|^2 \\
& + d_2\kappa\lambda_{\max}(P_1)(\tilde{X}^\top\tilde{X})^{3/2} + \frac{1}{2\epsilon_2}\lambda_{\max}((e_1^\top(A-LC))^2)|\tilde{X}(t)|^2.
\end{aligned} \tag{4.89}$$

By the positive definiteness of P_1, it holds that

$$\lambda_{\min}(P_1)\tilde{X}^\top\tilde{X} \leq \tilde{X}^\top P_1\tilde{X} \leq \lambda_{\max}(P_1)\tilde{X}^\top\tilde{X}, \tag{4.90}$$

where $\lambda_{\min}(P_1) > 0$ and $\lambda_{\max}(P_1) > 0$ are the smallest and the largest eigenvalues of P_1. Finally, by recalling $\gamma_1 \geq \frac{D}{a}$, and choosing constants d_1 and d_2 as

$$d_1 \geq \frac{2a^2 + D\bar{v}\epsilon_7}{D^2}, \tag{4.91}$$

$$\begin{aligned}
d_2 \geq & \frac{2}{\underline{\alpha}}\left(\frac{D}{2\epsilon_1} + d_1\frac{a+\bar{v}}{2} + \frac{(g+\lambda)}{2\epsilon_3} + \frac{\lambda_{\max}((e_1^\top(A-LC))^2)}{2\epsilon_2}\right. \\
& \left. + \left(\frac{d_1}{2}L_1 + \frac{1}{2\epsilon_4}L_2 + \frac{d_1^2}{2\epsilon_6}L_3 + \frac{1}{2\epsilon_7}L_4\right)\bar{v}\right),
\end{aligned} \tag{4.92}$$

one can show that (4.89) leads to

$$\begin{aligned}\dot{\tilde{V}} \leq & -d_1 \frac{D\gamma_1}{2}\tilde{w}(0,t)^2 - d_1\left(D+2\lambda\right)\tilde{V}_{12} - \left(g+2\lambda\right)\tilde{V}_{11} \\ & - \frac{\underline{\alpha}}{2\lambda_{\max}(P_1)}\tilde{V}_2 + d_2\kappa\frac{\lambda_{\max}(P_1)}{\lambda_{\min}(P_1)^{3/2}}\tilde{V}_2^{3/2} \\ \leq & -\alpha_1\tilde{V} + \tilde{\beta}_1\tilde{V}^{3/2}. \end{aligned} \tag{4.93}$$

Thus, Lemma 4.2 holds. □

By using the same approach in Lemma 3.2, we set $\tilde{M} = \min\left\{\tilde{M}_1, \tilde{m}_1\right\}$ where $\tilde{M}_1 = \frac{\lambda_{\min}(P_1)}{\tilde{d}_2}r^2$ and r is defined in (3.87). In addition, the inequality (4.93) ensures that $\tilde{V}(t) < \tilde{m}_1$ if $\tilde{V}(0) < \tilde{M}$ where $\tilde{m}_1 = \frac{\alpha_1^2}{4\tilde{\beta}_1^2}$. Thus, it leads to

$$\dot{\tilde{V}} \leq -\frac{\alpha_1}{2}\tilde{V}. \tag{4.94}$$

Thus, if $\tilde{V}(0) < \tilde{M}$, then $\tilde{V}(t) < \tilde{M}$ for all $t \geq 0$. This allows us to conclude that the target $\tilde{w}$-system (4.22)-(4.25) is locally exponentially stable in $\mathcal{H}_1$-norm, following a similar strategy utilized in state-feedback stability analysis.

Owing to backstepping transformation invertibility, the stability of $\tilde{w}$-system renders the original $\tilde{c}$-system (4.16)-(4.19) locally exponentially stable. This completes the proof of Theorem 4.1.

The estimation error flux in the cone is dominated by the length of the axon. It is bounded by $\mathcal{H}_1$-norm over the lengthy calculations of estimation error over the length of the axon and tubulin flux in the cone. Due to physically limited intuition, the axon cannot grow rapidly. This underscores the importance of considering both axon length and tubulin flux within the cone to ensure the convergence of the estimator.

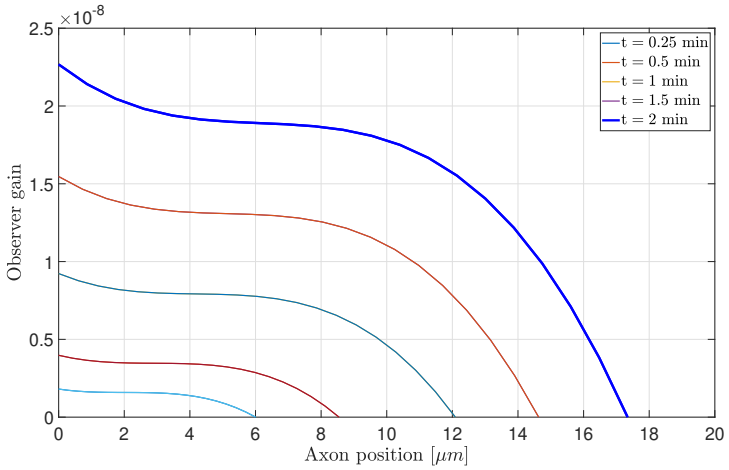

(a) The initial value of the gain, denoted as p, which starts at $p = 0.2 \times 10^{-8}$ when $x = 0\ m$ and $l(t) = 4\ \mu m$ at $t = 0\ min$, increases to $p = 2.25 \times 10^{-8}$ when $x = 0$ and $l(t) = 16\ \mu m$ at $t = 2\ min$.

Figure 4.1. Increase of the observer gain throughout the growth of the axon length.

4.3 Simulations: Estimation of unmeasured tubulin concentration profile in a 4× growth

We perform the simulation of the state estimation of the tubulin concentration by incorporating the biological parameters in Table 3.1. The observer gains for the decay rates of ODE states are set as $l_1 = 1$ and $l_2 = 12$. The parameter λ for the decay rate of the PDE state is chosen as 0.05 to obtain sufficiently fast convergence without causing a huge overshoot. In addition, the initial conditions for the observer are chosen $\hat{c}(x,0) = 0$. In Figure 4.2a and Figure 4.2b, the open-loop control, $U(t) = b_1 \sin(\omega t) + b_2$ where $b_1 = 200$, $b_2 = -10$, and $\omega = 1.256\ rad/s$, is applied to the plant and the estimator. Figure 4.2a and 4.2b show that the observer governed by (4.1)-(4.5) converges to the unmeasured tubulin concentration generated by (2.1)-(2.5), within $t = 1$min when the open-loop controller defined above is applied. In addition, the necessity of observer gain, $p_1(x, l(t))$, is demonstrated in Figure 4.1. In this figure, when the axon grows for a long distance, the observer gain, $p_1(x, l(t))$, increases because more time is needed to see the effect of the soma on the growth cone, which explains why observer gain becomes higher and higher when the axon expands.

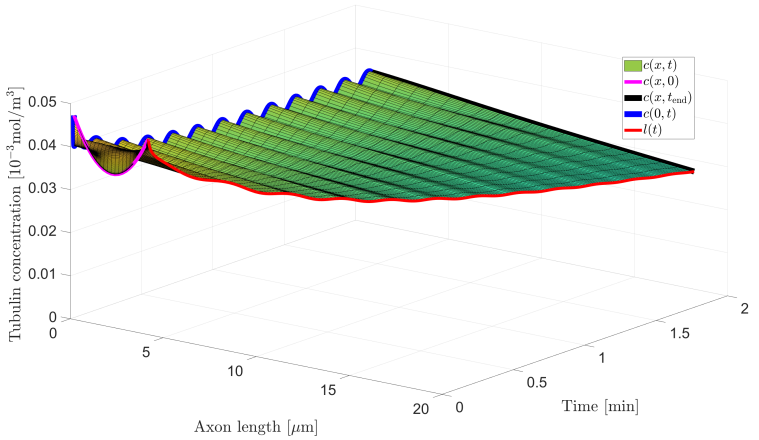

(a) The response of the tubulin concentration under the open-loop control signal $U(t) = b_1 \sin(\omega t) + b_2$.

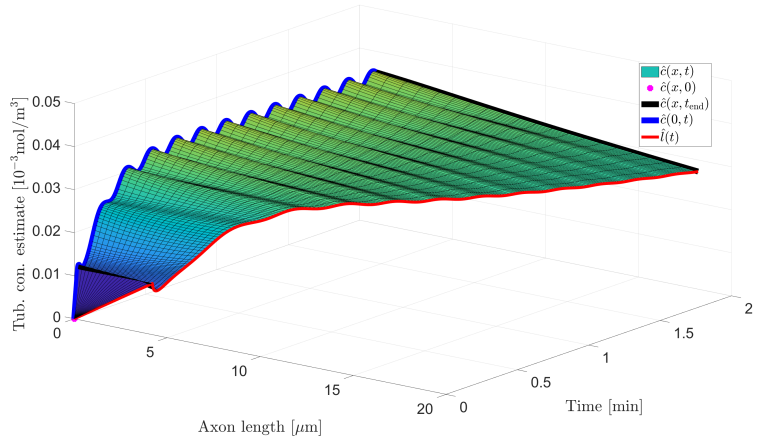

(b) The estimated tubulin concentration given by the observer in (4.1)-(4.5), successfully converges to the tubulin concentration and the axon length of the plant in Figure Note that the rate of convergence of estimator is faster than the rate of tubulin convergence of steady-state solution.4.2a.

Figure 4.2. Open-loop responses of the plant and observer.

Acknowledgements

Chapter 4 has been published in Automatica 2024 with the title “Neuron growth control and estimation by PDE backstepping” C. Demir, S. Koga, M. Krstic. Chapter 4, ‘also contains a partial adaptation of the work contained in the conference paper“Neuron growth output-feedback control by pde backstepping” C. Demir, S. Koga, M. Krstic, presented at American Control

Conference 2022. The dissertation author was the primary author of these publications.

Chapter 5

Observer-based Neuron Growth Control

5.1 Output-feedback design

In this section, an output feedback control law is developed based on the estimated tubulin concentration obtained through the observer proposed in 4, utilizing the measurements (4.6). The block diagram in Figure 5.1 illustrates the closed-loop system, which integrates the plant dynamics (2.1)–(2.5), the observer (4.1)–(4.5), and the control law (3.26).

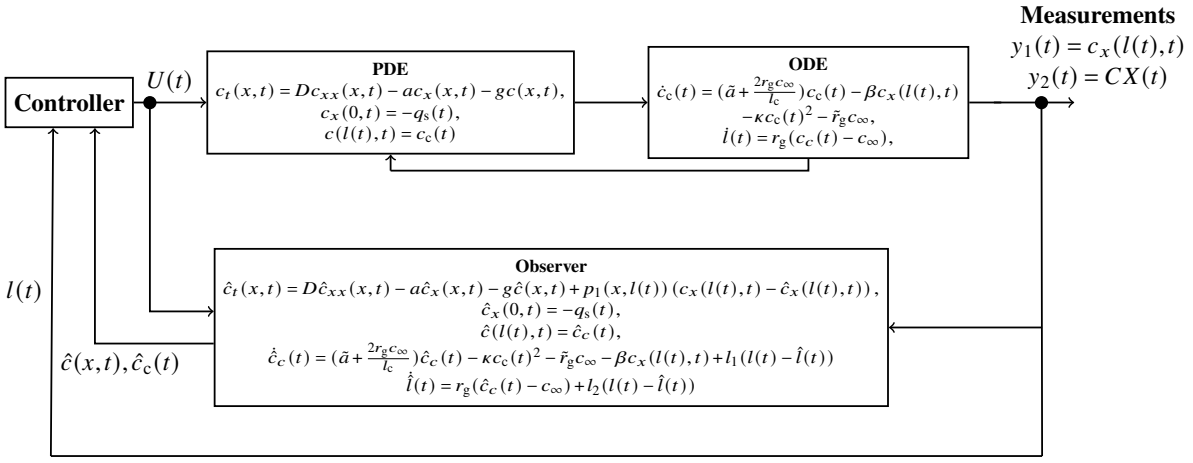

Figure 5.1. Block diagram of observer design and output feedback system

The following theorem applies to this control law:

Theorem 5.1. *Consider the closed-loop system* (2.14)-(2.18) *with the measurements* (4.6)*, and*

the observer (5.4)-(5.7) *under the output feedback control law:*

$$U(t) = \frac{D\gamma_2 - \beta}{D}\hat{u}(0,t) + \phi'(-l(t))^\top - \gamma_2\phi(-l(t))^\top \hat{X}(t) - \frac{1}{D}\int_0^{l(t)} (\phi'(-y)^\top - \gamma_2\phi(-y)^\top) B\hat{u}(y,t)dy, \tag{5.1}$$

where $\gamma_2 \geq \frac{a}{D}$ *and* $\phi(x)$ *is defined in* (3.24)*. Then, there exist* $\bar{M} > 0$*,* $\kappa > 0$ *and* $\zeta > 0$ *such that if* $\Gamma(0) < \bar{M}$ *then the following norm estimate holds:*

$$\Gamma(t) \leq \zeta\Gamma(0)\exp(-\kappa t). \tag{5.2}$$

where $\Gamma(t) := ||u||^2_{\mathcal{H}_1(0,l(t))} + |X|^2 + ||\hat{u}||^2_{\mathcal{H}_1(0,l(t))} + |\hat{X}|^2$*. Namely, the closed-loop system is locally stable in the sense of* $\mathcal{H}_1$*-norm.*

5.1.1 Reference error states

For the output feedback analysis, we first define the reference error state, $\hat{u}(x,t)$, for the observer as

$$\hat{u}(x,t) = \hat{c}(x,t) - c_{eq}(x). \tag{5.3}$$

By using (4.1)-(4.5), (2.10)-(2.13) and (5.3), we obtain the following nonlinear observer for the reference error system

$$\hat{u}_t(x,t) = D\hat{u}_{xx}(x,t) - a\hat{u}_x(x,t) - g\hat{u}(x,t) + p_1(x,l(t))\left(u_x(l(t),t) - \hat{u}_x(l(t),t)\right), \tag{5.4}$$

$$\hat{u}_x(0,t) = U(t), \tag{5.5}$$

$$\hat{u}(l(t),t) = e_1\hat{X}(t) + \tilde{h}(z_2(t)), \tag{5.6}$$

$$\dot{\hat{X}}(t) = A\hat{X}(t) + Bu_x(l(t),t) + LC(X(t) - \hat{X}(t)) + f(\hat{X}(t)). \tag{5.7}$$

5.1.2 Target reference error states

The following transformation from $(\hat{u}, \hat{X})$ into $(\hat{w}, \hat{X})$ is implemented by using (3.5) and (3.35). Taking the time and spatial derivatives of these transformations, the target $\hat{w}$-system is obtained as

$$\begin{aligned}\hat{w}_t =& D\hat{w}_{xx}(x,t) - a\hat{w}_x(x,t) - g\hat{w}(x,t) + \dot{l}(t)E(x,\hat{X}(t)) + p_1(x,l(t))\tilde{u}_x(l(t),t) \\ &- \int_x^{l(t)} k(x,y)p_1(y,l(t))\tilde{u}_x(l(t),t)dy - f(\hat{X}(t))\phi(x-l(t))^\top \\ &- \left(\phi'(x-l(t))^\top + \frac{a}{D}\phi(x-l(t))^\top\right)Bh^*(\hat{X}(t)), \end{aligned} \tag{5.8}$$

$$\hat{w}_x(0,t) = \gamma_2\hat{w}(0,t), \tag{5.9}$$

$$\hat{w}(l(t),t) = h^*(\hat{X}(t)), \tag{5.10}$$

$$\begin{aligned}\dot{\hat{X}}(t) =& (A+BK)\hat{X}(t) + B\hat{w}_x(l(t),t) + B\tilde{u}_x(l(t),t) \\ &+ LC\tilde{X}(t) + f(\hat{X}(t)), \end{aligned} \tag{5.11}$$

where h^* is defined in (3.32) and we denote $E(x,\hat{X}(t)) = (\phi'(x-\hat{X}(t)-l_s)^\top - k(x,\hat{X}(t)+l_s)H^\top)\hat{X}(t)$. By evaluating the spatial derivative of (3.5) at $x=0$, we derive the control law as in (5.1).

5.2 Stability under output-feedback control

In this section, Theorem 5.1 is proven for output feedback control law.

5.2.1 Lyapunov Analysis

Define the Lyapunov function for closed-loop systems as

$$V_{\text{tot}} = c_1\tilde{V}(t) + \frac{d_3}{2}||\hat{w}||^2 + \frac{1}{2}||\hat{w}_x||^2 + \frac{1}{2}\gamma_2\hat{w}(0,t)^2 + d_4\hat{X}(t)^\top\hat{P}\hat{X}(t), \tag{5.12}$$

where $c_1 > 0$ is chosen to be sufficiently large, $\tilde{V}(t)$ is defined in (4.71)–(4.74). Then, the total Lyapunov function for the closed-loop output feedback system is also written as

$$\begin{aligned} V_{\text{tot}}(t) =& c_1 \frac{1}{2}\left(d_1||\tilde{w}||^2 + ||\tilde{w}_x||^2\right) + \frac{1}{2}\left(d_3||\hat{w}||^2 + ||\hat{w}_x||^2\right) + c_1 d_2 \tilde{X}(t)^\top P \tilde{X}(t) + d_4 \hat{X}(t)^\top \hat{P} \hat{X}(t) \\ &+ \frac{1}{2}\left(c_1 \gamma_1 \tilde{w}(0,t)^2 + \gamma_2 \hat{w}(0,t)^2\right). \end{aligned} \tag{5.13}$$

We state the following lemma.

Lemma 5.1. *Properties* (3.33) *and* (3.34) *hold with,*

$$\bar{v} \leq \min\left\{\frac{g}{3\gamma_2}, \frac{D}{8\bar{l}}, \frac{g+\lambda}{2\gamma_1}\right\}, \tag{5.14}$$

for all time $t \geq 0$. Then, for sufficiently large enough $d_3 > 0$ and $d_4 > 0$, there exist positive constants $\alpha > 0$ and $\beta > 0$ such that the following norm estimate holds

$$\dot{V}_{\text{tot}} \leq -\alpha V_{\text{tot}} + \hat{\beta}_1 V_{\text{tot}}^{3/2} + \hat{\beta}_2 V_{\text{tot}}^2 + \hat{\beta}_3 V_{\text{tot}}^{5/2} + \hat{\beta}_4 V_{\text{tot}}^3. \tag{5.15}$$

Note that the properties (3.33) and (3.34) with (5.14) are enforced in our stability analysis by restricting the initial conditions.

Proof. By applying Young's, Cauchy-Schwarz, Poincare's, and Agmon's inequalities, with the help of the system properties (3.33) and (3.34) we obtain

$$\dot{V}_{\text{tot}} \leq -\alpha V_{\text{tot}} + \hat{\beta}_1 V_{\text{tot}}^{3/2} + \hat{\beta}_2 V_{\text{tot}}^2 + \hat{\beta}_3 V_{\text{tot}}^{5/2} + \hat{\beta}_4 V_{\text{tot}}^3, \tag{5.16}$$

for

$$\alpha = \min\left\{\frac{1}{2}\alpha_1, d_3\frac{D}{2}, \frac{g}{2}, d_4\frac{\lambda_{\min}(\hat{Q})}{4\lambda_{\max}(\hat{P})}\right\}, \tag{5.17}$$

$$\hat{\beta}_1 = \tilde{\beta} + \frac{r_{\mathrm{g}}}{\lambda_{\min}(\hat{P})}\left(\frac{L_5+L_6+L_8}{2} + d_3\frac{L_7}{2\varepsilon_3}\right) + \frac{2\kappa\left|\hat{P}\right|}{\lambda_{\max}(\hat{P})^{3/2}}, \tag{5.18}$$

$$\hat{\beta}_2 = \frac{8d_3^2D\left(L_{n_1}4k_n^2 + L_{n_2}\kappa^2\right) + 8D\left(L_{n_2}\kappa^2 + L_{n_3}4k_n^2\right)}{2\lambda_{\min}(\hat{P})^2}, \tag{5.19}$$

$$\hat{\beta}_3 = \frac{d_3 r_{\mathrm{g}}}{2\lambda_{\min}(\hat{P})^{5/2}}, \tag{5.20}$$

$$\hat{\beta}_4 = \frac{32DL_{n_2}k_m^2|P|^2(d_1^2+1)}{\lambda_{\min}(P)^3}, \tag{5.21}$$

where L_i for $i = \{5,6,7,8\}$ are bounds of the nonlinear terms as in (3.57)-(3.60) such that Lemma 5.1 holds. □

To prove local stability, we need to show Lemma 2 to ensure the convergence in all time. It satisfies that $V_{\mathrm{tot}}(t) < M_1$ holds for some $M > 0$, then $|\tilde{X}| < r$ where r is defined in (3.87). If $V_{\mathrm{tot}}(0) < M$, then $V_{\mathrm{tot}}(t) < M$ for all $t > 0$. In addition, $\dot{l}(t)$ can be written as $\dot{l}(t) = r_{\mathrm{g}}e_1^\top X(t)$, so we can bound $\dot{l}(t)$ to handle in the norm equivalence as

$$|\dot{l}(t)| \le r_{\mathrm{g}}\left(\sqrt{\frac{\tilde{V}_2}{\lambda_{\min}(P)}} + \sqrt{\frac{\hat{V}_2}{\lambda_{\min}(\hat{P})}}\right). \tag{5.22}$$

The inequality above leads to $|\dot{l}(t)|^2 \le \delta^2 V_{\mathrm{tot}}(t)$. Thus, it holds that

$$V_{\mathrm{tot}}(t) \le V_{\mathrm{tot}}(0)\exp\left(-\frac{\alpha}{2}t\right). \tag{5.23}$$

The norm equivalence between the target and original systems is shown using the direct and inverse transformations of both observer target and observer error target systems. First, let

$$\Psi = ||\hat{w}||^2_{\mathcal{H}_1(0,l(t))} + |\hat{X}|^2 + ||\tilde{w}||^2_{\mathcal{H}_1(0,l(t))} + |\tilde{X}|^2. \tag{5.24}$$

Using Agmon's inequalities for $\hat{w}(0,t)$ and $\tilde{w}(0,t)$ terms in $V_{\text{tot}}(t)$, one can obtain positive constants $\overline{M} > 0$ and $\underline{M} < 0$ such that

$$\underline{M}\Psi(t) \leq V_{\text{tot}}(t) \leq \overline{M}\Psi(t) \tag{5.25}$$

holds. Therefore, applying (5.25) to (5.23), we get

$$\Psi(t) \leq \frac{\overline{M}}{\underline{M}} \exp\left(-\frac{\alpha}{2}t\right)\Psi(0). \tag{5.26}$$

Now, we apply the norm equivalence argument to the transformations between the target systems, (4.22)-(4.25) and (5.8)-(5.11) and observer error (4.16)-(4.19) and the reference error systems (5.4)-(5.7). Let $\Phi(t)$ be defined as

$$\Phi(t) = ||\tilde{c}||^2_{\mathcal{H}_1(0,l(t))} + |\tilde{X}|^2 + ||\hat{u}||^2_{\mathcal{H}_1(0,l(t))} + |\hat{X}|^2. \tag{5.27}$$

Taking square of the transformations (4.21), (4.67), (3.5), and (3.35), and using Young's and Cauchy-Schwarz inequalities, one can see that there exist positive constants $\overline{N} > 0$, and $\underline{N} < 0$ such that

$$\underline{N}\Phi(t) \leq \Psi(t) \leq \overline{N}\Phi(t) \tag{5.28}$$

holds. Applying (5.28) to (5.26), we get

$$\Phi(t) \leq \frac{\overline{N}}{\underline{N}} \exp\left(-\frac{\alpha}{2}t\right)\Phi(0). \tag{5.29}$$

In the last step, we can apply norm equivalence argument between $(\tilde{c}, \tilde{X})$-system and (u, X)-system.

Let $\Gamma(t)$ defined as

$$\Gamma(t) = ||u||^2_{\mathcal{H}_1(0,l(t))} + |X|^2 + ||\hat{u}||^2_{\mathcal{H}_1(0,l(t))} + |\hat{X}|^2. \tag{5.30}$$

Now, by taking square of (2.10) and (4.13), one can show that there exists positive constants $\overline{K} > 0$ and $\underline{K} > 0$ such that

$$\underline{K}\Gamma(t) \leq \Gamma(t) \leq \overline{K}\Gamma(t) \tag{5.31}$$

holds. Applying (5.31) to (5.29), we get

$$\Gamma(t) \leq \frac{\overline{K}}{\underline{K}} \exp\left(-\frac{\alpha}{2}t\right)\Gamma(0). \tag{5.32}$$

Namely, since the backstepping transformation for the target error system and for the observer system are invertible, the local stability of $(\tilde{w}, \tilde{X}, \hat{w}, \hat{X})$ guarantees the local stability of $(u, X, \hat{u}, \hat{X})$, which completes the proof of Theorem 5.1.

5.3 Simulations: Axon elongation by up to *three orders of magnitude*

Under the closed-loop plant dynamics (2.1)-(2.5) with the output-feedback controller in (5.1) and the observer in (4.1)-(4.5), the axon length converges to the desired length, one order of magnitude higher than initial axon length, around by about $t = 3$ minutes as shown in Figure 5.2a. Also, Figure 5.2b illustrates that the estimated tubulin concentration $\hat{c}(x,t)$ converges to the unmeasured actual tubulin concentration, $c(x,t)$. After the convergence, both estimated and true tubulin concentrations converge to the steady-state solution, $c_{\text{eq}}(x)$, which shows the effectiveness of our proposed output feedback control law.

For three orders of magnitude of axon growth, the designed observer (4.1)-(4.5) and

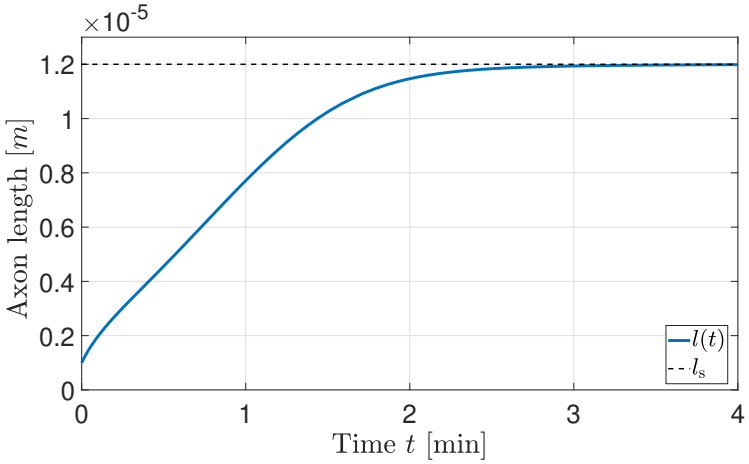

(a) The axon length $l(t)$ of the plant (2.1)-(2.5) converges to the desired length l_s by about $t = 3$min.

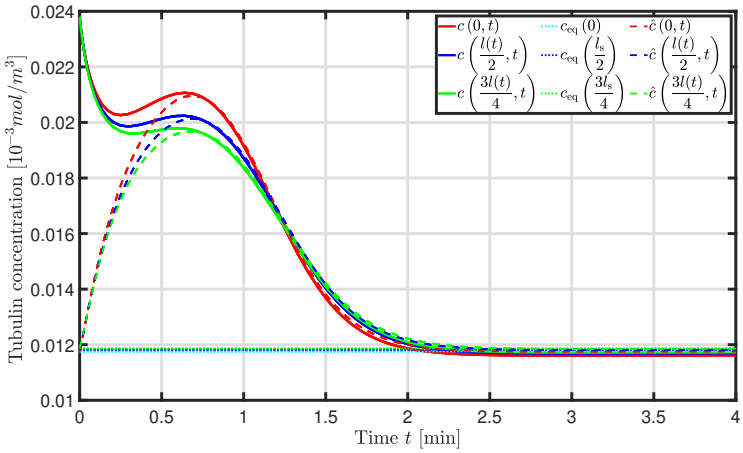

(b) The estimated tubulin concentration, $\hat{c}(x,t) = \hat{u}(x,t) + c_{\text{eq}}(x)$, generated by the observer in (4.1)-(4.5), converges to the true tubulin concentration, $c(x,t)$, generated by nonlinear plant dynamics (2.1)-(2.5), and then both converge to the steady-state solution, $c_{\text{eq}}(x)$ by about $t = 2.5$min. Note that the convergence of the estimator to the plant is achieved faster than the convergence of the plant to the desired equilibrium.

Figure 5.2. Close-loop response of the plant and observer.

output-feedback control law in (5.1) are applied to the plant (2.1)-(2.5) in Figure 5.3a and 5.3b. The observer gains are chosen as $l_1 = -3\times10^4$, $l_2 = 10$ and $\lambda = 1\times10^{-4}$ and the initial conditions are chosen $\hat{c}(x,0) = 0$. In Figure 5.3a, the initial axon length, $l_0 = 1\ \mu m$, converges to the desired axon length, $l_s = 1\ mm$ in $t = 37$ hours, nearly one and half days. In Figure 5.3b, the estimated tubulin concentration $\hat{c}(x,t)$ first converges to the plant tubulin concentration $c(x,t)$ around $t = 5$

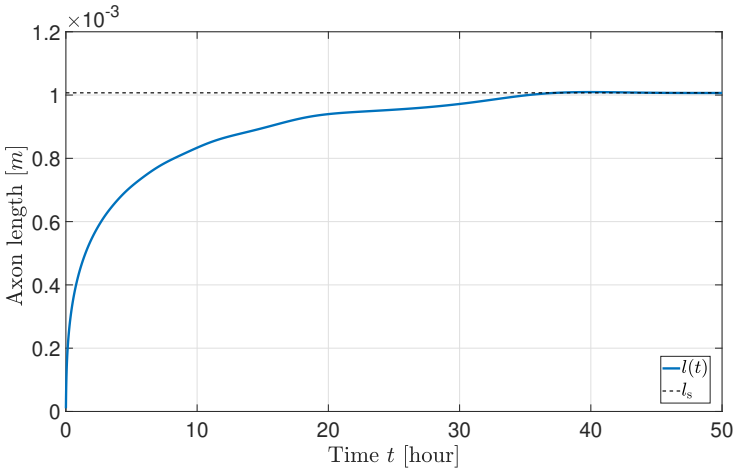

(a) The axon length $l(t)$ governed by the nonlinear ODE dynamics converges to the desired length $l_s = 1$ mm by about $t = 37$ hours.

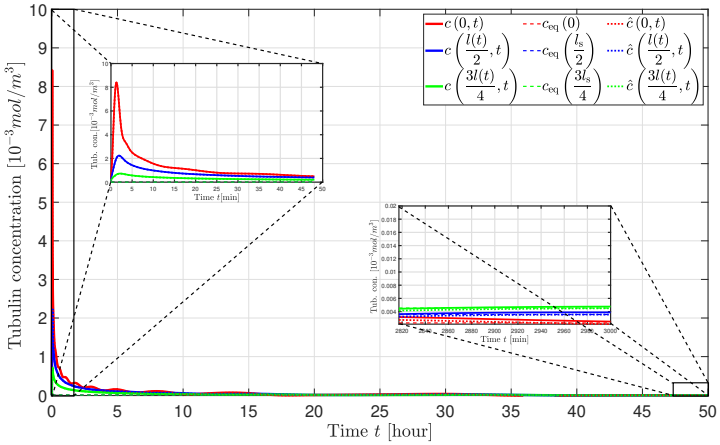

(b) Tubulin concentration $c(x,t)$ governed by the nonlinear PDE-ODE dynamics converges to the steady-state tubulin concentration, $c_{eq}(x)$ along the axon by about $t = 10$ hours.

Figure 5.3. The estimated tubulin concentration, $\hat{c}(x,t) = \hat{u}(x,t) + c_{eq}(x)$, generated by the observer in (4.1)-(4.5), converges to the unmeasured tubulin concentration, $c(x,t)$, generated by nonlinear plant dynamics (2.1)-(2.5), and then both converge to the steady-state solution, $c_{eq}(x)$ by about $t = 15$ hours. Note that the convergence of the estimator to the plant is achieved faster than the convergence of the plant to the desired equilibrium.

mins and then both converge to the steady-state solution $c_{eq}(x)$ around $t = 17$ hours. In addition, the tubulin concentration error, $\tilde{c}(x,t) = |c(x,t) - \hat{c}(x,t)|$, converges to zero uniformly along the spatial distribution in Figure 5.4.

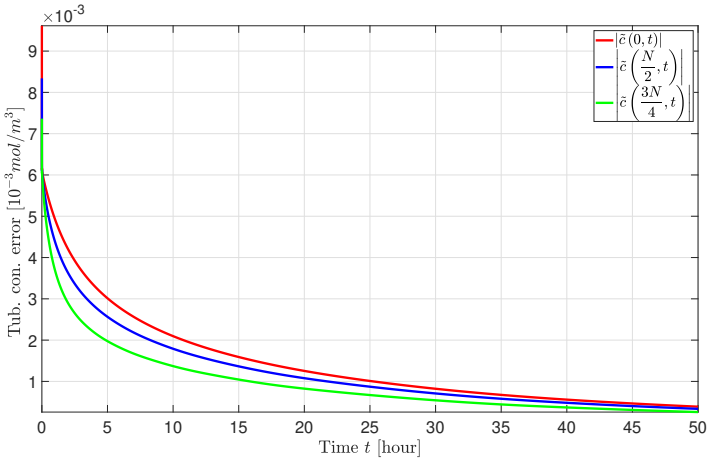

(a) When the length of axon, $l(t)$, increases the observer gain, $p_1(x, l(t))$ increases.

Figure 5.4. The estimation error, $\tilde{c}(x,t)$, between the estimated tubulin concentration $\hat{c}(x,t)$ and the plant tubulin concentration $c(x,t)$ converges to 0 uniformly along the axon length.

5.4 Robustness to Large Uncertainty in Diffusion, Advection, and Reaction

In this section, we illustrate the robustness of the proposed output-feedback control under parameter uncertainty. Figure 5.5a shows the simulation result under a mismatch between the parameters of the plant and those of the estimator. The plant parameters, D, a, and g, are set to have $+\%40$ errors in the upper figure, and to have -20% errors in the lower figure. Both plots show that the performance of the proposed observer-based output feedback controller is robust to the parameter mismatch. Figure 5.5a illustrates that the actual axon length converges successfully to the desired axon length. In addition, the convergence of the tubulin concentration is observed in Figure 5.5b under the same parameter mismatch. In this figure, the estimated tubulin concentration converges to the actual tubulin concentration and both converge to the steady-state tubulin concentration. Note that the convergence of the estimated tubulin concentration to the actual tubulin concentration is achieved before either one converges to the steady-state concentration. The simulation study demonstrates a robust performance of the proposed output-feedback controller under parameter mismatches.

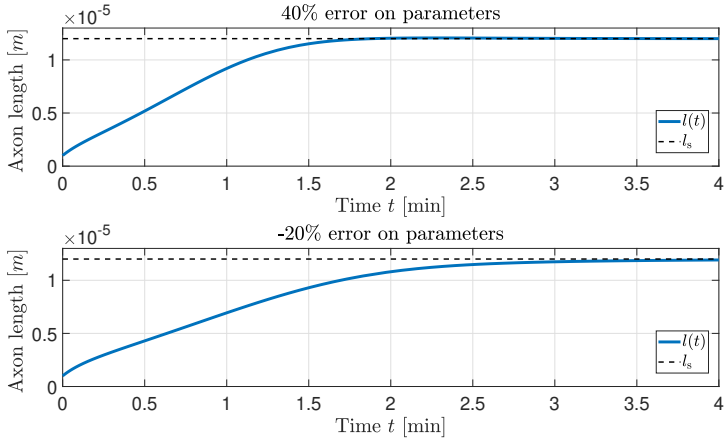

(a) Even when there is a parameters' error in D, a, and g, the proposed controller performs robustly enough for successfully achieving the convergence of the axon length to the desired axon length.

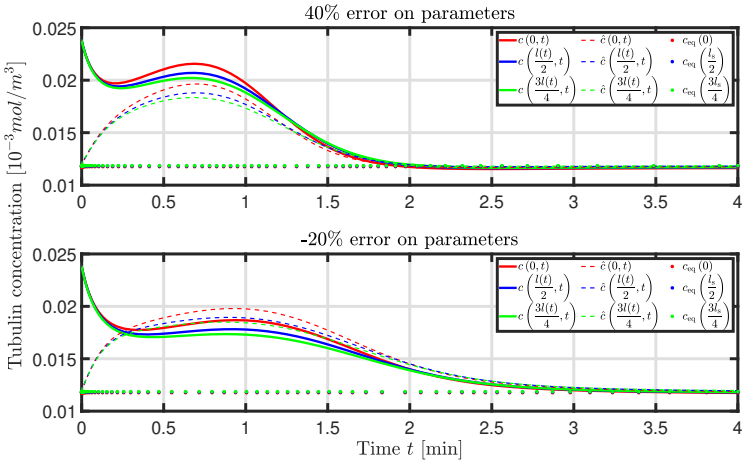

(b) The proposed observer also achieves an accurate estimation of the unmeasured tubulin concentration governed by nonlinear plant dynamics.

Figure 5.5. Robustness study of the proposed observer and the output feedback control under parameters' mismatch between the plant and the estimator.

Acknowledgements

Chapter 5 has been published in Automatica 2024 with the title "Neuron growth control and estimation by PDE backstepping" C. Demir, S. Koga, M. Krstic. Chapter 5, 'also contains a partial adaptation of the work contained in the conference paper"Neuron growth output-feedback control by pde backstepping" C. Demir, S. Koga, M. Krstic, presented at American Control

Conference 2022. The dissertation author was the primary author of these publications.

Chapter 6

Input Delay Compensation

In the previous chapter, feedback and output-feedback control laws were introduced; however, these did not account for any time delay between the injected input and the tubulin concentration dynamics. Time delays are common in biological processes and add complexity to the system. For example, the movement of essential proteins, such as tubulin, from the cell body to the axon's growth cone is not immediate, which introduces delays necessary for axon growth [65]. In this chapter, we address this issue by implementing an input delay compensation technique using a novel feedback control law. In this control law, the input time delay is modeled as a transport PDE, and with certain parameter changes, the problem transforms into a coupled neuron growth problem with a transport PDE as explicitly described in [55].

6.1 Axon Growth Model with Input Delay

The model presented in this section is nearly identical to the one in Chapter 2, with the key difference being the inclusion of an input time delay, D_e.

$$c_t(x,t) = Dc_{xx}(x,t) - ac_x(x,t) - gc(x,t), \tag{6.1}$$

$$c_x(0,t) = -q_{\mathrm{s}}(t-D_e), \tag{6.2}$$

$$c(l(t),t) = c_{\mathrm{c}}(t), \tag{6.3}$$

$$l_{\mathrm{c}}\dot{c}_{\mathrm{c}}(t) = (a-gl_{\mathrm{c}})c_{\mathrm{c}}(t) - Dc_x(l(t),t) - (r_{\mathrm{g}}c_{\mathrm{c}}(t)+\tilde{r}_{\mathrm{g}}l_{\mathrm{c}})(c_{\mathrm{c}}(t)-c_\infty), \tag{6.4}$$

$$\dot{l}(t) = r_{\mathrm{g}}(c_c(t)-c_\infty), \tag{6.5}$$

6.1.1 The reference error system with input delay

First, we derive the reference error states by taking into account the input time delay, where the states denoted as $u(x,t)$, $z_1(t)$, $z_2(t)$ and $U(t-D_e)$, are defined by

$$u(x,t) = c(x,t) - c_{\mathrm{eq}}(x), \tag{6.6}$$

$$z_1(t) = c_{\mathrm{c}}(t) - c_\infty, \tag{6.7}$$

$$z_2(t) = l(t) - l_{\mathrm{s}}, \tag{6.8}$$

$$U(t-D_e) = -(q_{\mathrm{s}}(t-D_e) - q_{\mathrm{s}}^*). \tag{6.9}$$

From (6.1)-(6.5), by using (2.6)-(2.9), and (6.6)-(6.9), we obtain

$$u_t(x,t) = Du_{xx}(x,t) - au_x(x,t) - gu(x,t), \tag{6.10}$$

$$u_x(0,t) = U(t - D_e), \tag{6.11}$$

$$u(l(t),t) = h(X(t)), \tag{6.12}$$

$$\dot{z}_1(t) = \tilde{a}_1 z_1(t) - \beta u_x(l(t),t) - \kappa z_1(t)^2 + \beta f_1(z_2(t)) - \beta \tilde{a}_2 z_2(t), \tag{6.13}$$

$$\dot{z}_2(t) = r_g z_1(t), \tag{6.14}$$

where all functions are parameters defined in Chapter 2.

6.1.2 Input delay as transport PDE

The dynamics of the delayed controller can be rigorously modeled using a transport PDE. This approach captures the time delay in the control system as a spatial-temporal process, providing a more accurate and comprehensive representation of how the delay impacts the system's performance. Thus, the delayed controller can be represented as

$$v_t(x,t) = v_x(x,t), \quad D_e \geq x \geq 0 \tag{6.15}$$

$$v(D_e,t) = U(t). \tag{6.16}$$

The solution to this equation is $v(x,t) = U(t + x - D_e)$ and thus the output $v(0,t) = U(t - D_e)$ gives the delayed input. Then, let $X \in \mathbb{R}^2$ be an ODE state vector for the reference error states $z_1(t)$ and $z_2(t)$, defined by

$$X(t) = [z_1(t) \quad z_2(t)]^\top. \tag{6.17}$$

By using (6.17), the systematic representation of (6.10)-(6.14) and (6.15)-(6.16) can be written as

$$u_t(x,t) = Du_{xx}(x,t) - au_x(x,t) - gu(x,t), \tag{6.18}$$

$$u_x(0,t) = v(0,t), \tag{6.19}$$

$$u(l(t),t) = h(X(t)), \tag{6.20}$$

$$\dot{X}(t) = AX(t) + f(X(t)) + Bu_x(l(t),t), \tag{6.21}$$

$$v_t(x,t) = v_x(x,t), \qquad D_e \geq x \geq 0 \tag{6.22}$$

$$v(D_e,t) = U(t). \tag{6.23}$$

6.1.3 Linearized reference error system

In order to obtain the control law, we first apply linearization around zero states to (6.18)-(6.23) which leads us to the following linearized system:

$$\dot{X}(t) = AX(t) + Bu_x(l(t),t), \tag{6.24}$$

$$u_t(x,t) = Du_{xx}(x,t) - au_x(x,t) - gu(x,t), \tag{6.25}$$

$$u(l(t),t) = H^\top X(t), \tag{6.26}$$

$$u_x(0,t) = v(0,t), \tag{6.27}$$

$$v_t(x,t) = v_x(x,t), \quad D_e \geq x \geq 0 \tag{6.28}$$

$$v(D_e,t) = U(t). \tag{6.29}$$

where H is defined in (2.36).

6.2 Backstepping Design of Delay Compensated Control

This section presents the theorem of the stability of the neuron growth problem with delay-compensated control law. We extended the delay-compensated backstepping method from

its application in the classical Stefan problem to a nonlinear moving boundary model that is coupled with a PDE-ODE system. We first state the theorem.

Theorem 6.1. *Let the system properties* (3.33) *and* (3.34) *hold. Consider the closed-loop system consisting of the plant* (6.18)–(6.23) *with the control law*

$$U(t) = -\int_{t-D_e}^{t} p(D_e, \vartheta + D_e - t)U(\vartheta)d\vartheta - \int_0^{l(t)} q(D_e, y)u(y,t)dy - \psi(D_e - l(t))X(t). \tag{6.30}$$

where $p(x,t)$, $q(x,t)$ *and* $\psi(x-l(t))$ *are gain kernel functions. Then, there exist positive parameters* $\bar{K} > 0$, $c > 0$, *and* $\kappa > 0$, *such that if* $Z(0) < \bar{K}$ *then the following norm estimate holds*

$$Z(t) \leq cZ(0)\exp(-\kappa t), \tag{6.31}$$

for all $t \geq 0$, *which guarantees the local exponential stability of the closed-loop system.*

The proof of this theorem is presented in the remainder of this section.

6.2.1 Transformation into target system

We consider two backstepping transformations of the following form:

$$w(x,t) = u(x,t) - \int_x^{l(t)} k(x,y)u(y,t)dy - \phi(x-l(t))X(t), \tag{6.32}$$

$$z(x,t) = v(x,t) + \int_0^x p(x,y)v(y,t)dy + \int_0^{l(t)} q(x,y)u(y,t)dy + \psi(x-l(t))X(t), \tag{6.33}$$

where the kernels $k(x,y)$, $\phi(x-l(t))$, $p(x,y)$, $q(x,y)$ and $\psi(x-l()t)$ are to be determined to transform the original system to a target system. Thus, the nonlinear desired target system is

proposed as

$$\dot{X}(t) = (A+BK)X(t) + Bw_x(l(t),t) + f(X(t)), \tag{6.34}$$

$$\begin{aligned} w_t(x,t) =& Dw_{xx}(x,t) - aw_x(x,t) - gw(x,t) - \dot{l}(t)F(x,X(t)) - \phi(x-l(t))^\top f(X(t)) \\ & - \left(\phi'(x-l(t))^\top + \frac{a}{D}\phi(x-l(t))^\top\right) Bh^*(X(t)), \end{aligned} \tag{6.35}$$

$$w(l(t),t) = h^*(X(t)), \tag{6.36}$$

$$w_x(0,t) = z(0,t), \tag{6.37}$$

$$z_t(x,t) = z_x(x,t) - \dot{l}(t)\left(q(x,l(t))H^\top - \psi'(x-l(t))\right)X(t), \tag{6.38}$$

$$z(D_e,t) = 0, \tag{6.39}$$

where the nonlinear terms are defined in (2.29) and (2.30). In this setting, $K \in \mathbb{R}^2$ is a selected feedback control gain vector, designed to ensure that the matrix $A+BK$ Hurwitz, meaning all its eigenvalues have negative real parts. Therefore, K is chosen as specified in (3.10). By applying linearization around zero states, one can obtain

$$\dot{X}(t) = (A+BK)X(t) + Bw_x(l(t),t), \tag{6.40}$$

$$\begin{aligned} w_t(x,t) =& Dw_{xx}(x,t) - aw_t(x,t) - gw(x,t) \\ & - \dot{l}(t)\left(k(x,l(t))u(l(t),t) - \phi'(x-l(t))^T X(t)\right), \quad 0 < x < l(t) \end{aligned} \tag{6.41}$$

$$w(l(t),t) = 0, \tag{6.42}$$

$$w_x(0,t) = z(0,t), \tag{6.43}$$

$$z_t(x,t) = z_x(x,t) - \dot{l}(t)\left(q(x,l(t))H^\top - \psi'(x-l(t))\right)X(t), \quad D_e \geq x \geq 0 \tag{6.44}$$

$$z(D_e,t) = 0 \tag{6.45}$$

6.2.2 Gain kernel solutions

The conditions of the kernel functions are obtained to satisfy both the governing equations. To achieve this, we take the time and spatial derivatives of (6.32) corresponding to the solutions of (6.24)-(6.27). As a result, the gain kernel solutions for $k(x,y)$ and $\phi(x)$, as detailed in Chapter 3.1.2, are obtained. Next, we derive the kernel functions for a different transformation, given by (6.33). Taking time and spatial derivatives of (6.33) along with (6.28)-(6.29), we have the following coupled PDE-ODE for gain kernels

$$q_x(x,y) = Dq_{yy}(x,y) + aq_y(x,y) - gq(x,y), \tag{6.46}$$

$$q(0,y) = -k_x(0,y), \tag{6.47}$$

$$q(x,l(t)) = -\frac{1}{D}\psi(x-l(t))B, \tag{6.48}$$

$$q_y(x,0) = -\frac{a}{D}q(x,0), \tag{6.49}$$

$$\psi'(x-l(t)) = \psi(x-l(t))A_1 - Dq_y(x,l(t))H^\top - aq(x,l(t))H^\top, \tag{6.50}$$

$$\psi(-l(t)) = -\phi'(-l(t)). \tag{6.51}$$

Through a variable change and the method of successive approximation, we can demonstrate that a unique classical solution exists for these equations. Subsequently, the final kernel function, $p(x,y)$, is the solution to the following transport PDE

$$p_x(x,y) = -p_y(x,y), \tag{6.52}$$

$$p(x,0) = -Dq(x,0). \tag{6.53}$$

6.2.3 Delay compensated backstepping control law

In this section, we design the control law that compensates for the input time delay. By using the boundary condition (6.39), substituting $x = D_e$ in (6.33) and defining $\vartheta = t + y - D_e$

where $\vartheta \in (t - D_e, t)$ and $v(y,t) = U(t + y - D_e)$, the control law becomes

$$U(t) = -\int_{t-D_e}^{t} p(D_e, \vartheta + D_e - t)U(\vartheta)d\vartheta - \int_0^{l(t)} q(D_e, y)u(y,t)dy - \psi(D_e - l(t))X(t). \tag{6.54}$$

where the gain kernels are discussed in the previous sections.

6.3 Stability proof under delay compensated control

In this section, we outline the proof of Theorem 6.1. We begin by formulating the nonlinear target system, which serves as the foundation for the subsequent analysis.

6.3.1 Transformed nonlinear target system

As the initial step in proving Theorem 6.1, we apply the following transformation to the system of equations (6.32)–(6.33). This transformation is crucial as it simplifies the equations, making it easier to analyze the system and proceed with the proof.

$$\varpi(x,t) = w(x,t) - xz(0,t) + l(t)z(0,t) - h^*(X(t)), \tag{6.55}$$

so we have

$$\dot{X}(t) = (A+BK)X(t) + B\varpi_x(l(t),t) + Bz(0,t) + f(X(t)), \tag{6.56}$$

$$\begin{aligned}\varpi_t(x,t) =& D\varpi_{xx}(x,t) - a\varpi_x(x,t) - g\varpi(x,t) - \dot{h}^*(X(t)) - gh^*(X(t)) - az(0,t) - gxz(0,t)\\ &+ gl(t)z(0,t) - xz_t(0,t) + \dot{l}(t)z(0,t) + l(t)z_t(0,t) - \dot{l}(t)F(x,X(t))\\ &- \phi(x-l(t))^\top f(X(t)) - \left(\phi'(x-l(t))^\top B + \frac{a}{D}\phi(x-l(t))^\top B\right)h^*(X(t)),\end{aligned} \tag{6.57}$$

$$\varpi(l(t),t) = 0, \tag{6.58}$$

$$\varpi_x(0,t) = 0, \tag{6.59}$$

$$z_t(x,t) = z_x(x,t) - \dot{l}(t)\left(\psi'(x-l(t)) - q(x,l(t))H^\top\right)X(t), \tag{6.60}$$

$$z(D_e,t) = 0, \tag{6.61}$$

where $x \in (0, l(t))$ for (6.57)-(6.59), and $x \in [0, D_e)$ for (6.60)-(6.61).

6.3.2 Inverse transformation

By performing a similar procedure to the derivation of the direct transformation, The inverse transformation of (6.32)-(6.33) is formulated as

$$u(x,t) = w(x,t) + \int_x^{l(t)} \iota(x,y)w(y,t)dy + \theta(x-l(t))X(t), \tag{6.62}$$

$$v(x,t) = z(x,t) - \int_0^x \varrho(x,y)z(y,t)dy - \int_0^{l(t)} \chi(x,y)w(y,t)dy - \varphi(x-l(t))X(t) \tag{6.63}$$

where the gain kernel functions $\iota(x,y)$, $\theta(x)$, $\varrho(x,y)$, $\chi(x,y)$ and $\varphi(x)$ are satisfy the following set of PDE-ODE equations:

$$\iota_{xx}(x,y)-\iota_{yy}(x,y)=\frac{a}{D}\left(\iota_x(x,y)+\iota_y(x,y)\right), \tag{6.64}$$

$$\iota_x(x,x)+\iota_y(y,y)=0, \tag{6.65}$$

$$\iota(x,l(t))=-\frac{1}{D}\theta(x-l(t))^{\top}B, \tag{6.66}$$

$$D\theta''(x-l(t))^{\top}+a\theta'(x-l(t))^{\top}+\left(gI+A_1+BK^{\top}\right)\theta(x-l(t))^{\top}=0, \tag{6.67}$$

$$\theta(0)=H, \tag{6.68}$$

$$\theta'(0)=K, \tag{6.69}$$

and

$$\chi_x(x,y)=-D\chi_{yy}(x,y)-a\chi_y(x,y)-g\chi(x,y), \tag{6.70}$$

$$\chi_y(x,o)=-\frac{a}{D}\chi(x,0), \tag{6.71}$$

$$\chi(x,l(t))=\frac{1}{D}\varphi(x-l(t))^{\top}B, \tag{6.72}$$

$$\chi(0,y)=-\iota_x(0,y), \tag{6.73}$$

$$\varphi'(x-l(t))^{\top}=\varphi(x-l(t))^{\top}\left(A_1+BK^{\top}\right), \tag{6.74}$$

$$\varphi(-l(t))^{\top}=\theta'(-l(t))^{\top}, \tag{6.75}$$

$$\varrho_x(x,y)=\varrho_y(x,y), \tag{6.76}$$

$$\varrho(0,t)=-\chi(x,0). \tag{6.77}$$

Note that the equations (6.64)–(6.69) are analytically solvable, and the solutions to these PDEs and ODEs are detailed in Chapter 3.1.2. Similarly, (6.70)-(6.77) are also analytically solvable, and the solutions are bounded.

6.3.3 System property to ensure local stability on a non-constant interval

To study the local stability of the target system we impose the following property for the system

$$\frac{D}{4\bar{l}} \geq a. \tag{6.78}$$

This property is physically valid and particularly relevant when the axon length is short. This condition applies to the majority of neurons, as the typical axon length falls within the range of 20 μm to 40 μm [11]. Given that most neurons have relatively short axons, the property described by (6.78) accurately reflects the physical characteristics observed in these biological systems.

6.3.4 Lyapunov analysis

We consider the following Lyapunov function for the target system

$$V = d_1 V_1 + V_2 + d_2 V_3 + d_3 V_4 + d_4 V_5, \tag{6.79}$$

where $d_1 > 0$, $d_2 > 0$, $d_3 > 0$ and $d_4 > 0$, and each Lyapunov function is

$$V_1 := \frac{1}{2}||\varpi||^2_{L_2}, \tag{6.80}$$

$$V_2 := \frac{1}{2}||\varpi_x||^2_{L_2}, \tag{6.81}$$

$$V_3 := \frac{1}{2}\int_0^{D_e} e^{cx} z^2(x,t)dx, \tag{6.82}$$

$$V_4 := \frac{1}{2}\int_0^{D_e} e^{cx} z_x^2(x,t)dx, \tag{6.83}$$

$$V_5 := X^\top P X, \tag{6.84}$$

where $c > 0$, and $P > 0$ is a positive definite matrix satisfying the Lyapunov equation:

$$(A+BK)^\top P + P(A+BK) = -Q, \tag{6.85}$$

for some positive definite matrix $Q > 0$. Since $A+BK^\top$ is Hurwitz, due to the positive definiteness of P and Q,

$$\lambda_{\min}(P)X^\top X \leq X^\top PX \leq \lambda_{\max}(P)X^\top X, \tag{6.86}$$

holds, where $\lambda_{\max}(P) > \lambda_{\min}(P) > 0$ are the largest and smallest eigenvalues in the positive definite matrix P. Then, we state the following lemma.

Lemma 6.1. *Let the system properties* (3.33)-(3.34) *and* (6.78) *are satisfied with*

$$\bar{v} = \frac{D}{16\bar{l}}, \tag{6.87}$$

Then, for sufficiently large $d_1 > 0$, $d_2 > 0$, $d_3 > 0$ and small $d_4 > 0$, there exist positive constants $\beta_1 > 0$, and $\beta_2 > 0$ such the following norm estimate holds for all $t \geq 0$:

$$\dot{V} \leq -\alpha V + \beta_1 V^{3/2} + \beta_2 V^2 + \beta_3 V^3, \tag{6.88}$$

where

$$\alpha = \min\left\{d_1\frac{D}{8}, \frac{g}{16}, \frac{\lambda_{\min}(Q)}{2\lambda_{\min}(P)}, c\right\}, \tag{6.89}$$

$$\beta_1 = \frac{1}{\lambda_{\min}(P)^{3/2}}\left(d_1\frac{r_{\mathrm{g}}\left(\bar{l}+1\right)}{2} + e^{cD_e}r_{\mathrm{g}}\left(d_2+d_3\right) + \frac{d_1r_{\mathrm{g}}L_3}{2} + \frac{r_{\mathrm{g}}L_2}{2} + \frac{d_1\bar{l}r_{\mathrm{g}}L_5^2}{2}\right.$$
$$\left. + 2d_4|P| + d_2r_{\mathrm{g}}L_{n_3} + d_3r_{\mathrm{g}}L_{n_3}\right), \tag{6.90}$$

$$\beta_2 = \frac{1}{\lambda_{\min}(P)^2}\left(d_1\frac{r_{\mathrm{g}}^2}{2} + \frac{1024D_e^2}{D^2}r_{\mathrm{g}}^4 + 8cD_e^4 + \frac{L_6}{\varepsilon}\kappa^2 + d_1\frac{L_{n_1}+L_{n_3}}{\varepsilon}k_n + \frac{64}{D}r_{\mathrm{g}}^2\left(\bar{l}^2+\frac{\bar{l}^3}{3}\right)L_5^2\right.$$
$$\left. + \frac{2r_{\mathrm{g}}^2L_4}{d_1D} + \frac{L_6}{\epsilon}\kappa^2 + \frac{L_{n_1}}{2\epsilon}k_n + 2h_n + 8k_n^2g^2\right), \tag{6.91}$$

$$\beta_3 = \frac{1}{\lambda_{\min}(P)^3}\left(\frac{2L_6k_m^2}{\varepsilon} + \frac{2L_6k_m^2}{\epsilon}\right) \tag{6.92}$$

Proof. Taking the time derivative of the Lyapunov function in (6.80), using Agmon's inequality, Poincare's inequality, Young's inequality, and satisfying (3.33), (3.34), (6.78), we obtain

$$\begin{aligned}
\dot{V}_1 =& -D||\varpi_x||^2 - g||\varpi||^2 + \frac{a}{2}\varpi(0,t)^2 - gz(0,t)l(t)\int_0^{l(t)} x\varpi(x,t)dx \\
&- \left[a + gl(t) + \dot{l}(t)\right]z(0,t)\int_0^{l(t)}\varpi(x,t)dx - z_x(0,t)\int_0^{l(t)}\left(l(t)+x\right)\varpi(x,t)dx \\
&+ \left(\dot{l}(t)\left(\psi'(-l(t)) - q(0,l(t))C^\top\right)X(t)\int_0^{l(t)}\left(l(t)+x\right)\varpi(x,t)dx\right) \\
&+ \dot{l}(t)\int_0^{l(t)}F(x,X(t))\varpi(x,t)dx + \int_0^{l(t)}\varpi(x,t)\phi(x-l(t))^\top f(X(t))dx \\
&+ \int_0^{l(t)}\varpi(x,t)\left(-\phi'(x-l(t))^\top - \frac{1}{D}\phi(x-l(t))^\top\right)Bh^*(X(t))dx \\
&- \int_0^{l(t)}\varpi(x,t)\left(\dot{h}^*(X(t)) + gh^*(X(t))\right)dx.
\end{aligned} \tag{6.93}$$

Similarly, (6.81) can be written as

$$\begin{aligned}\dot{V}_2 =& -D||\varpi_{xx}||^2 + a\int_0^{l(t)} \varpi_{xx}(x,t)\varpi_x(x,t)dx - g||\varpi_x||^2 - \frac{1}{2}\dot{l}(t)\varpi_x(l(t),t)^2 \\ &+ [a+gl(t)+\dot{l}(t)]z(0,t)\int_0^{l(t)} \varpi_{xx}(x,t)dx + z(0,t)\int_0^{l(t)} x\varpi_{xx}(x,t)dx \\ &+ z_x(0,t)\int_0^{l(t)} (l(t)+x)\,\varpi_{xx}(x,t)dx \\ &+ \dot{l}(t)\left(\psi'(-l(t)) - q(0,l(t))C^\top\right)X(t)\int_0^{l(t)} (l(t)+x)\,\varpi_{xx}(x,t)dx \\ &- \dot{l}(t)\left(F(l(t),X(t))\varpi_x(l(t),t) - \int_0^{l(t)} F_x(x,X(t))\varpi_x(x,t)dx\right) \\ &+ \int_0^{l(t)} \varpi_{xx}(x,t)\phi(x-l(t))^\top f(X(t))dx \\ &+ \int_0^{l(t)} \varpi_{xx}(x,t)\left(-\phi'(x-l(t))^\top - \frac{a}{D}\phi(x-l(t))^\top\right)Bh^*(X(t))dx \\ &- \int_0^{l(t)} \varpi_{xx}(x,t)\left(\dot{h}^*(X(t)) + gh^*(X(t))\right)dx \end{aligned} \tag{6.94}$$

(6.82) can be written as

$$\begin{aligned}\dot{V}_3 =& -z(0,t)^2 - c\int_0^{D_e} e^{cx}z^2(x,t)dx \\ &- \dot{l}(t)\int_0^{D_e} e^{cx}2z(x,t)\left(\psi'(x-l(t)) - q(x,l(t))C^\top\right)X(t)dx, \end{aligned} \tag{6.95}$$

(6.83) can be written as

$$\begin{aligned}\dot{V}_4 =& -z_x(0,t)^2 - c\int_0^{D_e} e^{cx}z_x^2(x,t)dx \\ &- \dot{l}(t)\int_0^{D_e} e^{cx}2z_x(x,t)\left(\psi''(x-l(t)) - q_x(x,l(t))C^\top\right)X(t)dx \end{aligned} \tag{6.96}$$

and (6.84) can be written as

$$\begin{aligned}\dot{V}_5 =& -X(t)^\top QX(t) + \varpi_x(l(t),t)2B^\top PX(t) + z(0,t)2B^\top PX(t)\\ &+\kappa X(t)^\top \left(Pe_1e_1^\top X(t)e_1^\top + e_1X(t)^\top e_1e_1^\top P\right)X(t).\end{aligned} \tag{6.97}$$

Now, we consider

$$V = d_1V_1 + V_2 + d_2V_3 + d_3V_4 + d_4V_5 \tag{6.98}$$

by taking a time derivative of V, substituting (6.93)-(6.97) into it, applying Wirtinger inequality, Young's inequality, and Agmon's inequality, one can obtain

$$\begin{aligned}\dot{V} \le& -\frac{D}{64}||\varpi_{xx}||^2 - d_1\frac{D}{4}||\varpi_x||^2 - d_1\frac{g}{16}||\varpi||^2 - \frac{d_2}{2}|z(0,t)|^2 - \frac{d_3}{2}|z_x(0,t)|^2 + d_1\frac{|\dot{l}(t)|^2}{2}||\varpi(t)||^2\\ &+\frac{8}{D}|\dot{l}(t)|^2|z(0,t)|^2 + d_1l(t)\left(\dot{l}(t)G_1(l(t))X(t)\int_0^{l(t)}\varpi(x,t)dx\right)\\ &+d_1\dot{l}(t)\int_0^{l(t)}F(x,X(t))\varpi(x,t)dx + \frac{1}{2\varepsilon}\int_0^{l(t)}\left(\phi(x-l(t))^\top f(X(t))\right)^2dx\\ &+d_1\frac{1}{2\varepsilon}\int_0^{l(t)}\left(G_2(x-l(t))B\bar{h}(X)\right)^2dx + \dot{l}(t)G_1(l(t)))X(t)\int_0^{l(t)}(l(t)+x)\,\varpi_{xx}(x,t)dx\\ &+\frac{|\dot{l}(t)|}{2}F(l(t),X(t))^2 + \dot{l}(t)\int_0^{l(t)}F_x(x,X(t))\varpi_x(x,t)dx\\ &+\frac{1}{2\epsilon}\int_0^{l(t)}\left(\phi(x-l(t))^\top f(X(t))\right)^2dx + \frac{1}{2\epsilon}\int_0^{l(t)}\left(G_3(x-l(t))B\bar{h}(X)\right)^2dx\\ &-d_2c\int_0^{D_e}e^{cx}z^2(x,t)dx - d_3c\int_0^{D_e}e^{cx}z_x^2(x,t)dx\\ &-2d_2\dot{l}(t)\int_0^{D_e}e^{cx}z(x,t)G_4(x-l(t))X(t)dx - 2d_3\dot{l}(t)\int_0^{D_e}e^{cx}z_x(x,t)G_5(x-l(t))X(t)dx\\ &-d_4\frac{\lambda_{\min}(Q)}{2}X^\top X + 2d_4\left|P\right|\left(X^\top X\right)^{3/2} + 2\bar{h}'(X)^2 + 2g^2\bar{h}(X)^2\end{aligned} \tag{6.99}$$

where

$$G_1(l(t)) := \psi'(-l(t)) - q(0, l(t))C^\top, \tag{6.100}$$

$$G_2(x - l(t)) := -\phi'(x - l(t))^\top - \frac{1}{D}\phi(x - l(t))^\top, \tag{6.101}$$

$$G_3(x - l(t)) := -\phi'(x - l(t))^\top - \frac{a}{D}\phi(x - l(t))^\top, \tag{6.102}$$

$$G_4(x - l(t)) := \psi'(x - l(t)) - q(x, l(t))C^\top, \tag{6.103}$$

$$G_5(x - l(t)) := \psi''(x - l(t)) - q_x(x, l(t))C^\top, \tag{6.104}$$

when we pick

$$d_1 \geq \frac{4a^2}{D^2}, \tag{6.105}$$

$$d_2 \geq d_1\left(g^2\frac{\bar{l}^5}{6D} + \frac{4(a^2 + g^2\bar{l}^2) + g}{g}\right) + \frac{32(a^2 + g^2\bar{l}^2)}{D} + \frac{32\bar{l}^3}{3D} + d_4\frac{4\left|B^T P\right|^2}{\lambda_{\min}(Q)}, \tag{6.106}$$

$$d_3 \geq d_1\frac{4\bar{l}^2}{g} + d_1\frac{4\bar{l}^3}{3g} + \frac{32\bar{l}^5}{3D} + \frac{32\bar{l}^3}{3D}, \tag{6.107}$$

$$d_4 \leq \frac{D\lambda_{\min}(Q)}{512\bar{l}\left|B^T P\right|^2}. \tag{6.108}$$

By using the system property (3.33), we can show that there exist positive constants $L_i > 0$ for $i = 1, 2, \ldots, 8$ such that the inequalities (3.57)-(3.60), (3.62)-(3.64) and the following inequalities hold:

$$\left|\psi'(-l(t)) - q(0, l(t))C^\top\right| \leq L_5, \tag{6.109}$$

$$\int_0^{l(t)} \phi(x - l(t))^2 dx \leq L_6, \tag{6.110}$$

In addition, $\dot{l}(t)$ can be rewritten as in (3.61). For the nonlinear terms, the upper bound for $f(X)$ is derived as in (3.79) and $h^*(X(t))$ is bounded as in (3.78) and similarly, the upper bound for

$\bar{h}'(X)$ term is obtained for $x < 1.79$ as

$$\dot{h}^*(X(t))^2 \leq h_n(X^\top X)^2 \tag{6.111}$$

where $h_n = \max\left\{2c_\infty r_g^2 K_+^2 \lambda_+^4, 2c_\infty r_g^2 K_-^2 \lambda_-^4\right\}$. Now, by using Cauchy-Schwarz, Agmon's, Young's inequalities, and the following inequality

$$||z_x(x,t)||^2 \leq \int_0^{D_e} e^{cx} z_x(x,t)^2 dx \leq e^{cD_e}||z_x(x,t)^2||, \tag{6.112}$$

we obtain

$$\begin{aligned}
\dot{V} \leq & -d_1\frac{D}{8}V_2 - d_1\frac{g}{16}V_1 - d_4\frac{\lambda_{\min}(Q)}{2\lambda_{\min}(P)}V_5 - d_2cV_3 - d_3cV_4 \\
& + \frac{1}{\lambda_{\min}(P)^{3/2}}\left(d_1\frac{r_g\left(\bar{l}+1\right)}{2} + e^{cD_e}r_g\left(d_2+d_3\right) + \frac{d_1 r_g L_3}{2} + \frac{r_g L_2}{2} + \frac{d_1\bar{l}r_g L_5^2}{2}\right)V^{3/2} \\
& + \frac{1}{\lambda_{\min}(P)^{3/2}}\left(2d_4|P| + d_2 r_g L_{n_3} + d_3 r_g L_{n_3}\right)V^{3/2} \\
& + \frac{1}{\lambda_{\min}(P)^2}\left(d_1\frac{r_g^2}{2} + \frac{1024D_e^2}{D^2}r_g^4 + 8cD_e^4 + \frac{L_6}{\varepsilon}\kappa^2\right)V^2 \\
& + \frac{1}{\lambda_{\min}(P)^2}\left(d_1\frac{L_{n_1}+L_{n_3}}{\varepsilon}k_n + \frac{64}{D}r_g^2\left(\bar{l}^2 + \frac{\bar{l}^3}{3}\right)L_5^2\right)V^2 \\
& + \frac{1}{\lambda_{min}(P)^2}\left(\frac{2r_g^2 L_4}{d_1 D} + \frac{L_6}{\epsilon}\kappa^2 + \frac{L_{n_1}}{2\epsilon}k_n + 2h_n + 8k_n^2 g^2\right)V^2 \\
& + \frac{1}{\lambda_{\min}(P)^3}\left(\frac{2L_6 k_m^2}{\varepsilon} + \frac{2L_6 k_m^2}{\epsilon}\right)V^3.
\end{aligned} \tag{6.113}$$

The inequality above can be written as

$$\dot{V} \leq -\alpha V + \beta_1 V^{3/2} + \beta_2 V^2 + \beta_3 V^3, \tag{6.114}$$

where α, β_1, β_2 and β_3 are defined in (6.89)-(6.92), which completes the proof of Lemma 6.1. □

6.3.5 Guaranteeing the conditions for all time

Next, we prove the following lemmas to conclude Theorem 6.1 by ensuring the local stability of the closed-loop system.

Lemma 6.2. *With the system property* (6.78)*, there exists a positive constant* $K_1 > 0$ *such that in* $\Omega_1 := \{(\varpi, z, X) \in H_1 \times H_1 \times \mathbb{R}^2 | V(t) < K_1\}$*, and the system properties* (3.33) *and 3.34 are satisfied.*

Proof. Following the proof of Lemma 3.2, the proof of Lemma 6.2 is trivial. Thus, it is not explicitly given here. □

Lemma 6.3. *With the system property* (6.78)*, there exists a positive constant* $K_2 > 0$ *such that if* $V(0) < K_2$ *then the system properties* (3.33) *and 3.34 are satisfied and the following norm estimate holds:*

$$V(t) \leq V(0) e^{-\frac{\alpha}{2}t}. \tag{6.115}$$

Proof. For a positive constant $K_2 > 0$, let $\Omega := \{(\varpi, z, X) \in H_1 \times H_1 \times \mathbb{R}^2 | V(t) < K_2\}$. If $K_2 \leq K_1$ then $\Omega \subset \Omega_1$, and thus the assumptions are satisfied in Ω. Moreover, due to Lemma 6.1, the norm estimate (6.88) holds. Hence, by setting

$$K_2 \leq \frac{-\beta_2^2 \sqrt{\frac{\beta_1^2(2\alpha\beta_2+\beta_1^2)}{\beta_2^4}} + \alpha\beta_2 + \beta_1^2}{2\beta_2^2}, \tag{6.116}$$

we can see that applying $V(t) < K_2$ to (6.88) leads to

$$\dot{V} \leq -\frac{\alpha}{2} V, \tag{6.117}$$

by which the norm estimate (6.115) is deduced. Since (6.115) is a monotonically decreasing function in time, by setting $K_3 = \min\{K_1, K_2\}$, the region Ω is shown to be an invariant set. Thus,

if $V(0) < K_3$, then $V(t) < K_3$ for all $t \geq 0$, and one can conclude with Lemma 6.3. □

Finally, we show that (w, z, X) system is locally exponentially stable. Taking the square of (6.55) and applying Young's and Cauchy-Schwarz inequalities, we obtain

$$||\varpi(\cdot,t)||^2_{H_1} \leq 3||w(\cdot,t)||^2_{H_1} + M_1||z(\cdot,t)||^2_{H_1} + M_2|X|^2, \tag{6.118}$$

$$||w(\cdot,t)||^2_{H_1} \leq 3||\varpi(\cdot,t)||^2_{H_1} + M_1||z(\cdot,t)||^2_{H_1} + M_2|X|^2, \tag{6.119}$$

where $M_1 = 4D_e^3\bar{l} + 4D_e\bar{l}^3$ and $M_2 = 12k_n^2$. Consider the norm

$$\Pi(x,t) = ||w(x,t)||^2_{H_1} + ||z(x,t)||^2_{H_1} + |X(t)|^2. \tag{6.120}$$

By using (6.112), we can show that

$$||z(.,t)||^2_{H_1} \leq V_3 + V_4 \leq e^{cD_e}||z(.,t)||^2_{H_1}, \tag{6.121}$$

and

$$M_3||w(.,t)||^2_{H_1} \leq 2V_1 + 2V_2 \leq M_4||w(.,t)||^2_{H_1}, \tag{6.122}$$

where $M_3 = \max\{\bar{l}^2, 1\}$ and $M_4 = \max\{\frac{1}{\bar{l}^2}, 1\}$. Then, we have

$$\begin{aligned}\Pi(t) \leq & (1+M_1)\,||z_x(x,t)||^2_{H_1} + 3||\varpi(x,t)||^2_{H_1} \\ & + (1+M_2)|X(t)|^2 \\ \leq & (2+2M_1)(V_3+V_4) + 12(V_1+V_2) + \frac{1+M_2}{\lambda_{\min}(P)}V_5\end{aligned} \tag{6.123}$$

By using (6.79), we have

$$\begin{aligned} V \leq & \left(\max\{d_2, d_3\} e^{cD_e} + \frac{M_1 M_3}{2} \max\{d_1, 1\} \right) ||z(.,t)||^2_{H_1} \\ & + \frac{3M_3}{2} \max\{d_1, 1\} ||w(.,t)||^2_{H_1} \\ & + \left(\frac{d_4}{\lambda_{\min}(P)} + \frac{M_2 M_3}{2} \max\{d_1, 1\} \right) |X(t)|^2 \\ \leq & \Sigma_1 ||z(.,t)||^2_{H_1} + \Sigma_2 ||w(.,t)||^2_{H_1} + \Sigma_3 |X(t)|^2 \end{aligned} \tag{6.124}$$

where

$$\Sigma_1 = \max\{d_2, d_3\} e^{cD_e} + \frac{M_1 M_3}{2} \max\{d_1, 1\}, \tag{6.125}$$

$$\Sigma_2 = \frac{3M_3}{2} \max\{d_1, 1\}, \tag{6.126}$$

$$\Sigma_3 = \frac{d_4}{\lambda_{\min}(P)} + \frac{M_2 M_3}{2} \max\{d_1, 1\}. \tag{6.127}$$

Therefore, (6.123) and (6.124) leads us the following norm equivalence

$$\underline{\delta} V(t) \leq \Pi(t) \leq \bar{\delta} V(t) \tag{6.128}$$

where

$$\underline{\delta} = \frac{1}{\max\{\Sigma_1, \Sigma_2, \Sigma_3\}}, \tag{6.129}$$

$$\bar{\delta} = \max\left\{ (2 + 2M_1), 12, \frac{1 + M_2}{\lambda_{\min}(P)} \right\}. \tag{6.130}$$

With the inequalities (6.115) and (6.128), we show that

$$\Pi(t) \leq \frac{\bar{\delta}}{\underline{\delta}} \Pi(0) e^{-\frac{\alpha}{2}}, \tag{6.131}$$

which ensures the exponential stability of (w, z, X)-system. Finally, owing to Lemma 6.3 and

(6.131), and using the similar norm equivalent estimate in the $\mathcal{H}_1$-norm between the target system (w, z, X) and the closed-loop system (u, v, X), the local stability of the closed-loop system is proved, which completes the proof of Theorem 6.1.

Acknowledgements

Chapter 6 contains a partial adaptation of the work contained in the conference paper "Input Delay Compensation for Neuron Growth by PDE Backstepping" C. Demir, S. Koga, M. Krstic, presented at the 17th IFAC Workshop on Time Delay Systems 2022. The dissertation author was the primary author of these publications.

Chapter 7

Event-triggered Control

In this chapter, we propose an event-triggered control mechanism for the feedback control law of neuron growth control. For parabolic moving boundary problems, specifically for Stefan problem, both static and dynamic event-triggering mechanisms are developed in [76, 77]. These enhancements encouraged us to use this technique for the neuron growth problem. Event-triggered control is particularly beneficial in the context of neuron growth regulation as it allows for more efficient and responsive management of neuronal development. By activating the control law only in response to specific events or conditions, this approach optimizes resource utilization and conserves energy, making the control process more effective and sustainable. This mechanism enhances the practical applicability of the feedback control system, ensuring that interventions occur precisely when necessary, thus improving the overall regulation of neuron growth. In order to design this control law, we adjust the neuron growth model in a manner that facilitates convergence analysis.

7.1 Axon Growth Model with Actuation at Robin Boundary Condition

In this section, the neuron growth model is modified for actuation at the Robin boundary condition. Thus, the model is

$$c_t(x,t) = Dc_{xx}(x,t) - ac_x(x,t) - gc(x,t), \tag{7.1}$$

$$c_x(0,t) + c(0,t) = -q_{\mathrm{s}}(t), \tag{7.2}$$

$$c(l(t),t) = c_{\mathrm{c}}(t), \tag{7.3}$$

$$l_{\mathrm{c}}\dot{c}_{\mathrm{c}}(t) = (a - gl_{\mathrm{c}})c_{\mathrm{c}}(t) - Dc_x(l(t),t) - (r_{\mathrm{g}}c_{\mathrm{c}}(t) + \tilde{r}_{\mathrm{g}}l_{\mathrm{c}})(c_{\mathrm{c}}(t) - c_\infty), \tag{7.4}$$

$$\dot{l}(t) = r_{\mathrm{g}}(c_c(t) - c_\infty), \tag{7.5}$$

For this boundary condition, the steady-state solution needs to be redefined, so in the next section, we provide the steady-state solution for the Robin boundary condition.

Steady-state analysis of the model

To achieve a desired axon length l_{s}, we examine the steady-state solution $(c_{\mathrm{eq}}(x), c_\infty, l_{\mathrm{s}})$. By setting the time derivatives in (7.1), (7.4), and (7.5) to zero, one can derive the steady state solution of (7.1)-(7.5) as

$$c_{\mathrm{eq}}(x) = c_\infty \left(K_+ e^{\lambda_+(x-l_{\mathrm{s}})} + K_- e^{\lambda_-(x-l_{\mathrm{s}})} \right), \tag{7.6}$$

where $\lambda_\pm$ and $K_\pm$ are defined in (2.7) and (2.8). The steady-state input for the concentration flux in the soma is then obtained as

$$q_{\mathrm{s}}^* = -c_\infty \left(K_+(1+\lambda_+)e^{-\lambda_+ l_{\mathrm{s}}} + K_-(1+\lambda_-)e^{-\lambda_- l_{\mathrm{s}}} \right). \tag{7.7}$$

Reference error system

The reference error system defined in Chapter 2.2.1 is similar to the system under consideration, with the only difference being the location where actuation occurs. Consequently,

the condition (2.15) is modified and substituted with the following Robin boundary:

$$u_x(0,t)+u(0,t)=U(t) \tag{7.8}$$

Note that this boundary condition remains unaffected by the process of linearization. Therefore, we derive the control law by utilizing the linearized reference error system in (2.14), (2.16), (2.17), (2.18) and (7.8).

7.2 Sample-based Control of Neuron Growth Problem

This section presents the sample-based control law for a nonlinear moving boundary model that is coupled with a PDE-ODE system. We first design the control law by deriving the target system using a backstepping transformation.

7.2.1 Transformation into target system

The backstepping transformation and associated kernel functions are given in this section. By applying the backstepping transformation that is defined in (3.5), one can transfer (2.14), (2.16), (2.17), (2.18) and (7.8) to the following desired target system:

$$w_t(x,t)=Dw_{xx}(x,t)-aw_x(x,t)-gw(x,t)-\dot{l}(t)F(x,X(t)), \tag{7.9}$$

$$w_x(0,t)+w(0,t)=-\frac{1}{D}(H-\epsilon)^\top Bu(0,t), \tag{7.10}$$

$$w(l(t),t)=\epsilon^\top X(t), \tag{7.11}$$

$$\dot{X}(t)=(A_1+BK^\top)X(t)+Bw_x(l(t),t), \tag{7.12}$$

where $K\in\mathbb{R}^2$ is chosen as in (3.10) to make A_1+BK Hurwitz and $\epsilon=[\epsilon_1,\epsilon_2]$ will be designed later to prove convergence.

7.2.2 Gain kernel solutions

The approach for obtaining gain kernels in (3.5), namely $k(x,y)$ and $\phi(x)$, is detailed in Section 3.1.2. However, due to the use of a different boundary condition, these solutions will exhibit slight modifications. As a result, the gain kernels $k(x,y)$ and $\phi(x)$ are obtained as follows:

$$k(x,y) = -\frac{1}{D}\phi(x-y)^\top B, \tag{7.13}$$

$$\phi(x)^\top = \left[(H-\epsilon)^\top K^\top - \tfrac{1}{D}H^\top BH^\top\right] e^{N_1 x}\begin{bmatrix} I \\ 0 \end{bmatrix}, \tag{7.14}$$

where the matrix $N_1 \in R^{4\times 4}$ is defined as

$$N_1 = \begin{bmatrix} 0 & \frac{1}{D}\left(gI + A + \frac{a}{D}BH^\top\right) \\ I & \frac{1}{D}\left(BH^\top + aI\right) \end{bmatrix}. \tag{7.15}$$

We also need to introduce the inverse transformation in this section, which is essential for both designing the event-triggering mechanism and the convergence analysis. The inverse backstepping transformation (3.35) is used, with solutions in Section 3.1.2.

7.2.3 Continuous-time and sampled-data control law

By taking the spatial derivative of the transformation and substituting $x = 0$ into both the backstepping transformation and its spatial derivative, and setting boundary condition (3.7), the control law is derived as

$$U(t) = -\frac{1}{D}\int_0^{l(t)} p(x)Bu(x,t)dx + p(l(t))X(t), \tag{7.16}$$

where

$$p(x) = \phi'(-x)^\top + \phi(-x)^\top. \tag{7.17}$$

The system outlined in (7.1)-(7.5), with the continuous-time controller input (7.16), is locally exponentially stable in the L^2-norm sense, as demonstrated in Chapter 3. To develop the event-triggered control mechanism, the CTC input is sampled at discrete intervals, which holds it constant between events. This approach yields the following sampled-data control.

$$U_k^c(t) := U(t_k^c), \tag{7.18}$$

where is employed at

$$u_x(0,t) + u(0,t) = U_k^c(t) \tag{7.19}$$

for $\forall t \in [t_k^c, t_{k+1}^c)$, $k \in \mathbb{N}$ with the increasing time sequence, $I^c = \{t_k^c\}_{k\in\mathbb{N}}$, where $t_0^c = 0$. The notations "c" represent CETC. It's important to note that at each sampling time, the control input is sampled from (3.1), in other words, the sampled-data control law is the emulation of the continuous-time controller that is to be implemented in a Zero-Order Hold fashion.

7.3 Event-Triggered based Control

In this section, we introduce the event-triggered state-feedback control approach, deriving sampling times for our control law to trigger events. We begin by defining the event-triggering mechanism.

Definition 7.1. *The design parameters are $\gamma > 0$, $\eta > 0$, $\rho > 0$ and $\beta_i > 0$ where $i \in \{1, ...5\}$. The event-based controller consists of two trigger mechanisms:*

1. *The event-trigger: The set of all event times are in increasing sequence and they are denoted as $I^c = \{t_0^c, t_1^c, ...\}$ where $t_0^c = 0$ with the following rule*

   - *If $S(t, t_k^c) = \emptyset$, then the set of the times of the events is $\{t_0^c, ..., t_k^c\}$.*

- *If* $S(t,t_k^c) \neq \emptyset$*, the next event time is* $t_{k+1}^c = \inf\left(S(t,t_k^c)\right)$ *where*

$$S(t,t_k^c) = \{t \in \mathbb{R}_+ | t > t_k^c \wedge \Gamma^c(t) > 0\} \tag{7.20}$$

where

$$\Gamma^c(t) = d^2(t) + \gamma m(t) \tag{7.21}$$

for all $t \in [t_k^c, t_{k+1}^c)$*,* $d(t)$ *is given as*

$$d(t) = U(t) - U(t_k^c) \tag{7.22}$$

and $m(t)$ *satisfies the ODE*

$$\begin{aligned}\dot{m}(t) = &-\eta m(t) + \rho d(t)^2 - \beta_1 X(t)^2 - \beta_2 X(t)^4 - \beta_3 X(t)^6 - \beta_4 |w(0,t)|^2 \\ &- \beta_5 ||w(x,t))||^2\end{aligned} \tag{7.23}$$

2. *The control action: The feedback control law that is derived in* (7.16) *for all* $t \in [t_k^c, t_{k+1}^c)$ *where* $k \in \mathbb{N}$*.*

Lemma 7.1. *Under the definition of the state feedback event-triggered boundary control, it holds that* $d^2(t) \leq -\gamma m(t)$ *and* $m(t) > 0$ *for* $t \in [0, F)$*, where* $F = \sup(I^c)$*.*

Proof. From the definition of the event-trigger approach, it is guaranteed that $d^2(t) \leq -\gamma m(t)$, $t \in [0, F)$. It yields

$$\dot{m}(t) \leq -(\eta + \gamma\rho) m(t) - \beta_1 X(t)^2 - \beta_2 X(t)^4 - \beta_3 X(t)^6 - \beta_4 |w(0,t)|^2 - \beta_5 ||w(x,t))||^2 \tag{7.24}$$

for $t \in (t_k^c, t_{k+1}^c),\ k \in \mathbb{N}$. Considering time continuity of $m(t)$, we can obtain

$$\begin{aligned} m(t) \leq & m(t_k^c) e^{-(\eta+\rho\sigma)(t-t_k^c)} - \int_{t_k^c}^{t} e^{-(\eta+\rho\sigma)(t-\tau)} \left(\beta_1 X(\tau)^2 + \beta_2 X(\tau)^4 + \beta_3 X(\tau)^6\right) d\tau \\ & - \int_{t_k}^{t} e^{-(\eta+\rho\sigma)(t-\tau)} (\beta_4 |w(0,\tau)|^2 + \beta_5 ||w(l(x,\tau)||^2) d\tau \end{aligned} \tag{7.25}$$

From the event-trigger mechanism definition, we have that $m(t_0^c) = m(0) < 0$. Therefore, the estimate of $m(t)$ in (7.25) ensures that $m(t) < 0$ for all $t \in [0, t_1^c]$. This can be generalized for all t. which means it can be shown that $m(t) < 0$ for $t \in [0, F)$. □

Lemma 7.2. *For all $t \in (t_k^c, t_{k+1}^c)$ where $k \in \mathbb{N}$, it holds that*

$$(\dot{d}(t))^2 \leq \rho_1 d^2(t) + \alpha_1 X(t)^2 + \alpha_2 X(t)^4 + \alpha_3 X(t)^6 + \alpha_4 w(0,t)^2 + \alpha_5 ||w(x,t)||^2, \tag{7.26}$$

for the following positive constants and defined functions:

$$\rho_1 = 7|p(0)B|^2, \tag{7.27}$$

$$\begin{aligned}\alpha_1 = {} & \frac{21}{2}\left|\frac{1}{D}\zeta(y)B\int_0^{l(t)}\varphi(x-l(t))^\top dx\right|^2 + 28(p(0)Bp(l(t)))^2 \\ & +21\left(\left(p(0)\left(1-\frac{a}{D}\right)+\dot{p}(0)\right)B\right)^2(\varphi(0)^\top)^2 + 28(p(l(t))A)^2 \\ & +14\left(\left|\dot{p}(l(t))+\frac{a}{D}p(l(t))+\frac{r_{\mathrm{g}}}{D}e_1 p(l(t))\right|BH^\top\right)^2,\end{aligned} \tag{7.28}$$

$$\alpha_2 = 7\left(r_{\mathrm{g}}e_1\dot{p}(l(t)) + 2k_n\left|\dot{p}(l(t))+\frac{a}{D}p(l(t))\right|B + p(l(t))\kappa\right)^2 \tag{7.29}$$

$$\alpha_3 = 7\left(\frac{2k_n}{D}r_{\mathrm{g}}e_1 p(l(t))B\right)^2 + 28\left(k_m p(l(t))\right)^2, \tag{7.30}$$

$$\alpha_4 = 21\left(\left(p(0)\left(1-\frac{a}{D}\right)+\dot{p}(0)\right)B\right)^2, \tag{7.31}$$

$$\begin{aligned}\alpha_5 = {} & 7\left|\frac{1}{D}\zeta(y)B\right|^2\left(\frac{9}{2}+\frac{9}{2}\left(\int_0^{l(t)}\int_x^{l(t)}q(x,y)^2dydx\right)\right) \\ & +21\left(\left(p(0)\left(1-\frac{a}{D}\right)+\dot{p}(0)\right)B\right)^2\bar{G}(l(t))^2,\end{aligned} \tag{7.32}$$

$$\zeta(y) := \int_0^{l(t)} D\ddot{p}(y) - a\dot{p}(y) + gp(y) - p(0)Bp(y)dy, \tag{7.33}$$

$$\bar{G}(l(t)) := \int_0^{l(t)} q(0,x)dx \tag{7.34}$$

Proof. By taking the time derivative of (7.22), along with the nonlinear reference error system (2.24), (2.26), (2.27) and (7.19), we get

$$\begin{aligned}\dot{d}(t) = {} & -\frac{1}{D}\dot{l}(t)p(l(t))Bh(X(t)) + \dot{l}(t)\dot{p}(l(t))X(t) \\ & +\int_0^{l(t)}\left(\ddot{p}(y)-\frac{a}{D}\dot{p}(y)+\frac{g}{D}p(y)\right)Bu(y,t)dy - \int_0^{l(t)}\frac{1}{D}p(0)Bp(y)Bu(y,t)dy \\ & -p(0)Bd(t) - \left(p(0)\left(1-\frac{a}{D}\right)+\dot{p}(0)\right)Bu(0,t) + \left(p(0)Bp(l(t))+p(l(t))A\right)X(t) \\ & +p(l(t))f(X(t)) + \left(\dot{p}(l(t))B+\frac{a}{D}p(l(t))B\right)h(X(t))\end{aligned} \tag{7.35}$$

By using inverse transformation of backstepping in (3.35), Young's and Cauchy Schwarz's

inequalities, one can show

$$||u||^2 \leq \left(\frac{3}{2}+\frac{3}{2}\left(\int_0^{l(t)}\int_x^{l(t)} q(x,y)^2 dydx\right)^{1/2}\right)^2 ||w||^2 + \frac{3}{2}\left(\int_0^{l(t)} \varphi(x-l(t))^\top dx\right)^2 X(t)^2 \tag{7.36}$$

Applying the same procedure, we can also demonstrate that

$$u(0,t)^2 \leq 3w(0,t)^2 + 3(\varphi(0)^\top)^2 X(t)^2 + 3\left(\int_0^{l(t)} q(0,y)w(y,t)dy\right)^2, \tag{7.37}$$

The nonlinear terms can be shown to satisfy the inequalities defined in (3.78) and (3.79). Then, using Young's and Cauchy-Schwarz's inequalities, one can obtain

$$\dot{d}(t)^2 \leq \rho_1 d(t)^2 + \alpha_1 X(t)^2 + \alpha_2 X(t)^4 + \alpha_3 X(t)^6 + \alpha_4 w(0,t)^2 + \alpha_5 ||w(x,t)||^2 \tag{7.38}$$

where ρ_1 and α_i are defined in(7.27)-(7.32). □

7.4 Avoidance of zeno phenomena and stability proof under event-triggering Control

7.4.1 Avoidance of Zeno phenomena

The event-triggering mechanism dictates when to sample the continuous-time control signal, reducing computational and communication complexity. However, defining these sampling times is challenging due to the potential for Zeno behavior, where specific instances may result in infinite triggering within finite time intervals, limiting the mechanism's applicability. To address this, we prove the existence of a minimum dwell-time in the following theorem.

Theorem 7.1. *Consider the closed-loop system of* (2.1)-(2.5) *incorporating the control law given*

by

$$U(t_k^c) = -\frac{1}{D}\int_0^{l(t_k^c)} p(x)Bu(x,t_k^c)dx + p(l(t_k^c))X(t_k^c), \tag{7.39}$$

and the triggering mechanism in Definition 1. There exists a minimum dwell-time denoted as τ *between two consecutive triggering times* t_k^c *and* t_{k+1}^c*, satisfying* $t_{k+1}^c - t_k^c \geq \tau$ *for all* $k \in \mathbb{N}$ *when* β_i *is selected as follows:*

$$\beta_i = \frac{\alpha_i}{\gamma(1-\sigma)} \tag{7.40}$$

where $\sigma \in (0,1)$*,* $i = \{1,...,5\}$ *and the values of* α_i *are provided in equations* (7.28)-(7.32)*.*

Proof. By using Lemma 7.1, we define the continuous function $\psi(t)$ in $[t_k^c, t_{k+1}^c)$ to derive the lower bound between interexecution times as follows:

$$\psi(t) := \frac{d^2(t) + \gamma(1-\sigma)m(t)}{-\gamma\sigma m(t)} \tag{7.41}$$

As described in [30], one can show that

$$\dot{m}(t) = -\eta m(t) + \rho d(t)^2 - \beta_1 X(t)^2 - \beta_2 X(t)^4 - \beta_3 X(t)^6 - \beta_4 |w(0,t)|^2 - \beta_5 ||w||^2 \tag{7.42}$$

Taking the time derivative of (7.41) and using Lemma 7.1, we can choose β_i as described in (7.40). Thus, we get

$$\dot{\psi}(t) \leq a_1\psi(t)^2 + a_2\psi(t) + a_3, \tag{7.43}$$

where

$$a_1 = \rho\sigma\gamma > 0, \tag{7.44}$$

$$a_2 = 1 + 2\rho_1 + (1-\sigma)\rho + \eta > 0, \tag{7.45}$$

$$a_3 = (1 + \rho_1 + \gamma(1-\sigma)\rho + \eta)\frac{1-\sigma}{\sigma} > 0. \tag{7.46}$$

Using the comparison principle and the argument in [30], one can prove that there exists a time minimum dwell-time τ as follows:

$$\tau = \int_0^1 \frac{1}{a_1 s^2 + a_2 s + a_3} ds \tag{7.47}$$

which completes the proof. □

7.4.2 Stability proof under event-triggering control law

In this section, we initially introduce the theorem, which establishes the local exponential convergence.

Theorem 7.2. *Consider the closed-loop system comprising the plant described by* (7.1)-(7.5) *along with the control law specified by* (7.16) *and employing an event-triggering mechanism that is defined in Definition 7.1. Let*

$$\rho \geq \frac{d_1^2 D}{\delta_1} \tag{7.48}$$

and $\eta > 0$ *be design parameters,* $\sigma \in (0,1)$ *while* β_i *for* $i = \{1,2,3,4,5\}$ *are chosen as in* (7.28)-(7.32). *Then, there exist constants* $M > 0$, $c > 0$ *and* Γ, *such that, if initial conditions is such that* $Z(0) < M$ *then the following norm estimate is satisfied:*

$$Z(t) \leq cZ(0)exp(-\Gamma t), \tag{7.49}$$

for all $t \geq 0$, *in* L_2*-norm* $Z(t) = ||u(.,t)||_{L_2}^2 + X^\top X$ *which establishes the local exponential*

convergence of the origin of the closed-loop system.

In the remainder of this section, we provide the proof of Theorem 7.2.

7.4.3 Nonlinear target system

We first apply the following transformation to the system of equations (7.9)-(7.12) to simplify the analysis of system convergence.

$$\varpi(x,t) = w(x,t) - h^*(X(t)) \tag{7.50}$$

so this transformation gives us the following nonlinear target system

$$\begin{aligned}\varpi_t(x,t) =& D\varpi_{xx}(x,t) - a\varpi_x(x,t) - g\varpi(x,t) + gh^*(X(t)) - \dot{l}(t)F(x,X(t)) \\ & - \dot{h}^*(X(t))B\varpi_x(l(t),t) - \phi(x-l(t))^\top f(X(t)) - G(x,l(t))h^*(X) \\ & - \dot{h}^*(X(t))\left((A+BK)X(t) + f(X(t))\right), \end{aligned} \tag{7.51}$$

$$\varpi_x(0,t) + \varpi(0,t) = d(t) - \frac{1}{D}(H-\epsilon)^\top Bu(0,t) + h^*(X(t)), \tag{7.52}$$

$$\varpi(l(t),t) = \epsilon^\top X(t), \tag{7.53}$$

$$\dot{X}(t) = (A+BK)X(t) + f(X(t)) + B\varpi_x(l(t),t) \tag{7.54}$$

7.4.4 Lyapunov analysis

We consider the following Lyapunov functionals

$$V_1 = \frac{1}{2}||\varpi||^2 := \frac{1}{2}\int_0^{l(t)} \varpi(x,t)^2 dx, \tag{7.55}$$

$$V_2 = X(t)^\top P_1 X(t), \quad V_3 = \frac{1}{2}X(t)^\top P_2 X(t) \tag{7.56}$$

where $P_1 \succ 0$ and $P_2 \succeq 0$ are positive definite and positive semidefinite matrices satisfying the Lyapunov equations:

$$(A+BK^\top)^\top P_1 + P_1(A+BK^\top) = -Q_1, \tag{7.57}$$

$$(A+BK^\top)^\top (P_1+P_2) + (P_1+P_2)(A+BK^\top) = -Q_2 \tag{7.58}$$

where

$$P_1 = \begin{bmatrix} p_{1,1} & p_{1,2} \\ p_{1,2} & p_{2,2} \end{bmatrix}, \quad P_2 = \begin{bmatrix} \frac{D\epsilon_1}{\beta} - 2p_{1,1} & 0 \\ 0 & 0 \end{bmatrix} \tag{7.59}$$

where we pick $\epsilon \in \mathbb{R}^2$ as $\epsilon_1 \geq 2l_c p_{1,1}$ and $\epsilon_2 = \frac{p_{1,2}}{l_c d_1}$ for some positive definite matrices $Q_1 \succ 0$ and $Q_2 \succ 0$. We define the total Lyapunov function as

$$V(t) = d_1 V_1(t) + d_2 V_2(t) + V_3(t) - m(t), \tag{7.60}$$

where $d_1 > 0$ and $d_2 > 0$ are parameters to be determined.

Lemma 7.3. *Assume that the conditions in* (3.33) *and* (3.34) *are satisfied with* $\bar{v} = \frac{D}{16(D+1)}$*, for all* $t \geq 0$*. Then, for sufficiently large* $d_1 > 0$ *and sufficiently small* $d_2 < 0$*, there exist positive constants* ξ_i *for* $i = \{1,2,3,4,5\}$ *such that the following norm estimate holds for* $t \in (t_k^c, t_{k+1}^c)$*,* $k \in \mathbb{N}$*:*

$$\dot{V} \leq -\alpha^* V + \sum_{i=1}^{4} \xi_i V^{(1+\frac{i}{2})} \tag{7.61}$$

where $\alpha^* = \min\left\{\frac{g}{2}, \frac{1}{2\lambda_{\min}(P_1+P_2)}, \eta\right\}$.

Proof. When we take the time derivative of the Lyapunov functional (7.55)-(7.56) along the

target system, we get

$$\begin{aligned}
\dot{V} =& D d_1 \varpi(x,t)\varpi_x(x,t)|_{x=0}^{x=l(t)} - d_1 D||\varpi_x(x,t)||^2 d_1 a \frac{1}{2}\varpi(x,t)^2|_{x=0}^{x=l(t)} - d_1 g||\varpi(x,t)||^2 \\
&+ \frac{d_1}{2}\dot{l}(t)\varpi(l(t),t)^2 + d_1\dot{l}(t)\int_0^{l(t)} F(x,X(t))\varpi(x,t)dx \\
&+ d_1\int_0^{l(t)} \varpi(x,t)\phi(x-l(t))^\top f(X(t))dx + d_1\int_0^{l(t)} \varpi(x,t)G(x,l(t))h^*(X)dx \\
&- d_1\int_0^{l(t)} \frac{d}{dt}h^*(X(t))\varpi(x,t)dx \\
&+ d_2 X(t)^\top (A^\top + (BK)^\top)P_1 X(t) + d_2 X(t)^\top P_1 (A+BK)X(t) \\
&+ d_2 B^\top \varpi_x(l(t),t)P_1 X(t) + d_2 X(t)^\top P_1 B\varpi_x(l(t),t) + d_2 f(X(t))^\top P_1 X(t) \\
&+ d_2 X(t)^\top P_1 f(X(t)) + X(t)^\top P_2 \dot{X}(t) + \eta m(t) - \rho d(t)^2 + \beta_1 X(t)^2 + \beta_2 X(t)^4 + \beta_3 X(t)^6 \\
&+ 2\beta_4|\varpi(0,t)|^2 + 2\beta_5||\varpi(x,t))||^2 + 16k_n^2(\beta_4+\beta_5)(X^\top X)^2,
\end{aligned} \tag{7.62}$$

where we used

$$||\varpi(x,t)||^2 + h^*(X(t))^2 \geq \frac{1}{2}||w(x,t)||^2. \tag{7.63}$$

Now, substituting boundary conditions for $t \in (t_k^c + t_{k+1}^c)$, $k \in \mathbb{N}$ with

$$\varpi_x(l(t),t) = \bar{B}\left(\dot{X} - (A+BK)X(t) - f(X(t))\right) \tag{7.64}$$

where $\bar{B} = [-\beta^{-1}\ 0]$, we obtain

$$\begin{aligned}
\dot{V} \leq & -d_1 D||\varpi_x(x,t)||^2 - (d_1 g - 2\beta_5)||\varpi(x,t)||^2 \\
& + \left(\delta_1\left(\frac{3D}{2}+2\right) + Dd_1 + \frac{d_1 a}{2} + 2\beta_4 + d_1(H-\epsilon)^\top B\right)\varpi(0,t)^2 \\
& - \left(\rho - \frac{d_1^2 D}{2\delta_1}\right)d(t)^2 + \left(\frac{d_1^2}{2\delta_1}\left(\beta^2(1-\epsilon_1)^2(1+G_2(l(t))) + D\right) + 2\beta_4\right)h^*(X(t))^2 \\
& + \frac{d_1}{2}\dot{l}(t)\left(\epsilon^\top X(t)\right)^2 + d_1\dot{l}(t)\int_0^{l(t)} F(x,X(t))\varpi(x,t)dx \\
& + d_1\int_0^{l(t)} \varpi(x,t)\phi(x-l(t))^\top f(X(t))dx + d_1\int_0^{l(t)} \varpi(x,t)G(x,l(t))h^*(X)dx \\
& - d_1\int_0^{l(t)} \frac{d}{dt}h^*(X(t))\varpi(x,t)dx - (Dd_1\epsilon^\top + 2B^\top P)X(t)\left(\bar{B}(A+BK)X(t) + \bar{B}f(X(t))\right) \\
& - d_2 X(t)^\top Q X(t) + d_2 f(X(t))^\top P X(t) + d_2 X(t)^\top P f(X(t)) + \eta m(t) + \beta_1 X(t)^2 + \beta_2 X(t)^4 \\
& + \beta_3 X(t)^6 + 16k_n^2(\beta_4+\beta_5)(X^\top X)^2. \qquad (7.65)
\end{aligned}$$

Then, applying Poincaré's, Agmon's, and Young's inequalities, (7.48), along with (7.23), and using the inequalities (3.78) and (3.79), the expression for (7.65) can be transformed into:

$$\dot{V} \leq -\alpha^* V + \xi_1 V^{3/2} + \xi_2 V^2 + \xi_3 V^{5/2} + \xi_4 V^3 \qquad (7.66)$$

where

$$\xi_1 = \frac{\left(Dd_1|\epsilon\bar{B}| + 2d_2\left|P_1^\top B\bar{B}\right|\right)\kappa^2 + \frac{d_1 r_g}{2}(1+L_1) + r_g}{d_2^{3/2}\lambda_{\min}(P_1+P_2)^{3/2}} \qquad (7.67)$$

$$\xi_2 = \frac{\Xi_1}{d_2^2\lambda_{\min}(P_1+P_2)^2}, \qquad (7.68)$$

$$\xi_3 = \frac{4d_2 k_m|P_1|}{d_2^{5/2}\lambda_{\min}(P_1+P_2)^{5/2}}, \qquad (7.69)$$

$$\xi_4 = \frac{\Xi_2}{d_2^3\lambda_{\min}(P_1+P_2)^3}, \qquad (7.70)$$

taking into account (3.61) and choosing the constants d_1 and d_2 to satisfy

$$d_1 \geq \max\left\{\frac{8\bar{l}(D+2)+16\bar{l}\beta_4}{D}, \frac{4\beta_5+7}{g}\right\}, \tag{7.71}$$

$$d_2 \geq \frac{4}{\lambda_{\min}(Q_2)}\left(Dd_1\left|\epsilon\bar{B}|(A+BK)\right|+\beta_1\right)+\frac{4}{\lambda_{\min}(Q_2)}\left(\left(D+2+Dd_1+\frac{d_1 a}{2}+2\beta_4\right)\frac{2}{\beta^2}\right). \tag{7.72}$$

Note that the positive constants in (7.67)-(7.70) are given as

$$\begin{aligned}\Xi_1 =&4Dd_1|\epsilon\bar{B}|k_m^2|P_1|^2+8d_2\left|P_1^\top B\bar{B}\right|k_m^2|P_1|^2+\beta_2+2d_1^2L_{n_3}k_n^2+\frac{d_1^2}{2}L_{n_2}\kappa^2\\ &+d_1^2c_\infty^2r_{\mathrm{g}}^2k_l+8d_2\kappa|P|\beta_5k_l\ +2d_2\kappa|P|\left(d_1^2\left(\beta^2(1-\epsilon_1)^2\left(1+\bar{G}(l(t))^2\right)+D\right)\right)k_l,\end{aligned} \tag{7.73}$$

$$\Xi_2 =d_1^2c_\infty^2r_{\mathrm{g}}^2k_l+\frac{d_1^2}{2}L_{n_2}4k_m^2|P_1|^2+\beta_3+\left(d_1^2\left(\beta^2(1-\epsilon_1)^2\left(1+\bar{G}(l(t))^2\right)+D\right)+4\beta_5\right)k_l, \tag{7.74}$$

$$k_l =\max\{|K_+\lambda_+|,|K_-\lambda_-|\}^2 \tag{7.75}$$

and the inequalities are

$$F(0,X(t))^2 \leq L_1X^\top X, \tag{7.76}$$

$$\int_0^{l(t)}\left(\phi(x-l(t))^\top\right)^2dx \leq L_{n_2}, \tag{7.77}$$

$$\int_0^{l(t)}\left(\phi'(x-l(t))^\top B-ak(x,l(t))\right)^2dx \leq L_{n_3} \tag{7.78}$$

which completes the proof of Lemma 7.3. □

In this next section, we ensure the local stability of the closed-loop system with the event-triggering mechanism.

Lemma 7.4. *In the region* $\Omega_1 := \{(\varpi, X) \in L_2 \times \mathbb{R}^2 | V(t) < M_0\}$ *where* $t \in (t_k^c, t_{k+1}^c)$ $k \in \mathbb{N}$*, there exists a positive constant* $M_0 > 0$ *such that the conditions in* (3.34) *hold.*

Proof. The proof of Lemma 7.4 is a straightforward case of the proof of Lemma 3.2. □

From the proof of Lemma 7.4, we have $M_0 = \frac{\lambda_{\min}(P)}{d_2} r^2$ for $t \in (t_k^c, t_{k+1}^c)$, $k \in \mathbb{N}$. Next, we analyze stability within the time interval $t \in (t_k^c, t_{k+1}^c)$ for $k \in \mathbb{N}$, and subsequently for $t \in (0, t)$. Within this interval, we establish the following lemma:

Lemma 7.5. *There exists a positive constant M_k such that if $V(t_k^c) < M_k^c$ then the following norm estimate holds for $t \in (t_k^c, t_{k+1}^c)$, where $k \in \mathbb{N}$:*

$$V(t_{k+1}^c) \leq V(t_k^c) e^{-\frac{\alpha^*}{2}(t_{k+1}^c - t_k^c)} \tag{7.79}$$

Proof. For $M_k > 0$, we easily demonstrate that $M_k < M_0$ using Lemma 7.4, ensuring the norm estimate from Lemma 7.3 holds. Thus, we set $M_k \leq p^*$, where p^* is a non-zero root of the polynomial for $V > 0$.

$$-\alpha^* V + \xi_1 V^{3/2} + \xi_2 V^2 + \xi_3 V^{5/2} + \xi_4 V^3 = 0 \tag{7.80}$$

Since α^*, and ξ_i are all positive, at least one positive root exists for the polynomial in (7.80). Therefore, (7.66) implies

$$\dot{V}(t) \leq -\frac{\alpha^*}{2} V(t) \tag{7.81}$$

for $t \in (t_k^c, t_{k+1}^c)$, $k \in \mathbb{N}$ where $M_k = \min\{M_0, p^*\}$. The continuity of $V(t)$ in this interval implies $V(t_{k+1}^{c^-}) = V(t)$ and $V(t_k^{c^+}) = V(t_k^c)$ where $t_k^{c^+}$ and $t_k^{c^-}$ are right and left limits of $t = t_k^c$, respectively. Thus, we have

$$V(t_{k+1}^c) \leq \exp(-\alpha^*(t_{k+1}^c - t_k^c)) V(t_k^c) \tag{7.82}$$

which completes the proof of Lemma 7.5. □

For any $t \geq 0$ in $t \in [t_k^c, t_{k+1}^c)$, $k \in \mathbb{N}$, we obtain

$$V(t) \leq e^{-\alpha^*(t-t_k)} V(t_k) \leq e^{-\alpha^* t} V(0) \tag{7.83}$$

Recalling $m(t) < 0$ and (3.44), we have

$$d_1 V_1(t) + V_2(t) + d_2 V_3(t) \leq e^{-\alpha^* t} V(0). \tag{7.84}$$

which means that

$$d_1 \frac{1}{2} ||\varpi(x)||^2 + d_2 X(t)^\top \left(P_1 + \frac{1}{d_2} P_2 \right) X(t) \leq e^{-\alpha t} \left(\frac{d_1}{2} ||\varpi(0)||^2 + d_2 X(0)^\top \left(P_1 + \frac{1}{d_2} P_2 \right) X(0) - m(0) \right). \tag{7.85}$$

Utilizing the norm equivalence principle between the (ϖ, X) system and the (w, X) system, and leveraging the invertibility of the backstepping transformation, we establish the local exponential convergence of (u, X) in the L_2-norm.

7.5 Simulations

In this section, we numerically analyze the plant dynamics (7.1)-(7.5) using the control law (7.16) and the event triggering mechanism as defined in Definition 7.1. The model employs biological constants and control parameters from Table 3.1, with initial conditions set to $c_0(x) = 1.5c_\infty$ for the tubulin concentration along the axon and $l_0 = 1\mu m$ for the initial axon length. The control gain parameters are chosen as $k_1 = -0.001$ and $k_2 = 3 \times 10^{13}$. The event-triggering mechanism parameters are set as follows: $m(0) = -0.5$, $\beta_1 = 4.0849 \times 10^8$, $\beta_2 = 1.307 \times 10^{10}$, $\beta_3 = 1.642 \times 10^{11}$, $\beta_4 = 6.536 \times 10^{11}$, $\beta_5 = 7.35 \times 10^{11}$, $\rho = 4 \times 10^{22}$, $\eta = 800$ and $\sigma = 0.5$. In Figure 7.2a and 7.2b, we present the evolution of tubulin concentration along

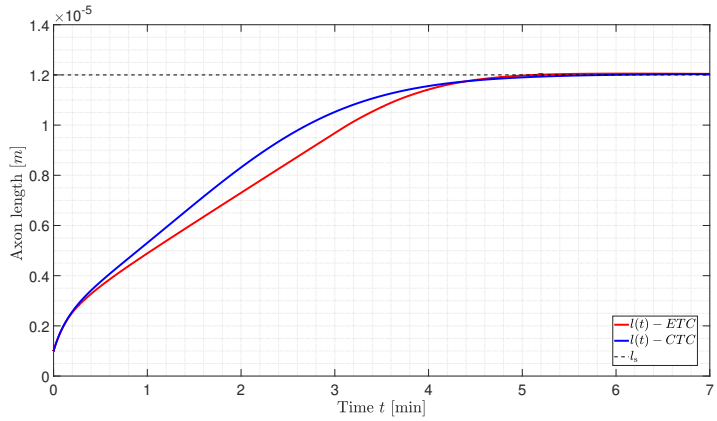

(a) The axon length, $l(t)$ successfully converges to the desired length by $t = 4.5$ mins for both event-triggered and continuous-time control law.

Figure 7.1. The closed-loop response of the continuous-time and event-triggered control law for $l_s = 12\mu m$

the axon for both continuous-time control law and event-triggered control. Figure 7.1 shows axon growth convergence under continuous-time and event-triggered control laws. Both methods achieve the desired $12\mu m$ length from an initial $1\mu m$ in about 4.5 minutes.

Acknowledgements

Chapter 7 is being prepared for publication under the title “Adaptive Event-Triggered and Periodic Event-Triggered Boundary Control of Neuron Growth with Actuation at Soma” C. Demir, M. Diagne, M. Krstic. Chapter 7, ‘also contains a partial adaptation of the work contained in the conference paper “Event-Triggered Control of Neuron Growth with Dirichlet Actuation at Soma” C. Demir, S. Koga, M. Krstic, presented at American Control Conference 2024. The dissertation author was the primary author of these publications.

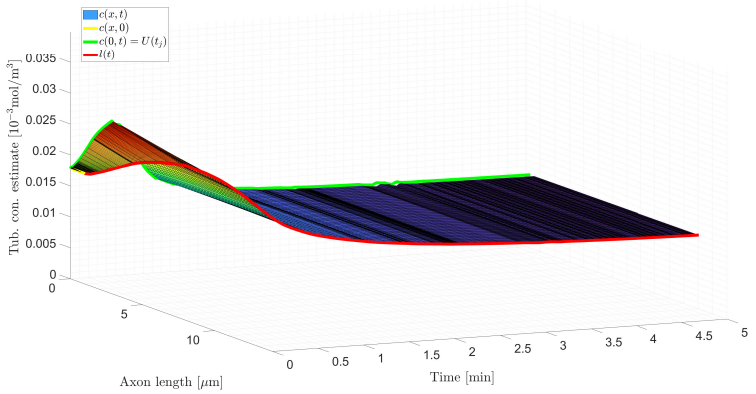

(a) Event-triggered control

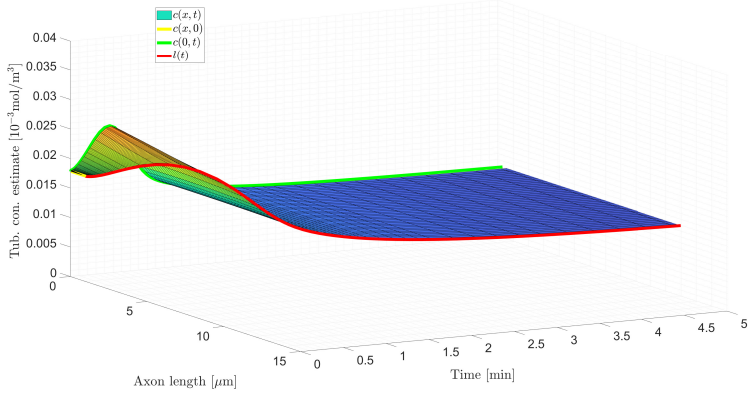

(b) Continuous-time control

Figure 7.2. The closed-loop response of the designed full-state feedback control system for continuous-time and event-triggered control law.

Chapter 8

Periodic Event-triggered Control

Motivated by the feasibility challenges encountered in real-time implementation when applying feedback control to biological systems for medical treatments, we convert the continuous time event-triggered control (CETC) design by supplementing a periodic sampling rule. This introduces a dynamic periodic event-triggering control (PETC) approach, where the triggering function is only checked periodically while the control input is updated aperiodically. The concepts in this chapter build upon the pioneering work of [78], who first extended event-triggering mechanisms to moving boundary PDEs. The authors' innovative contributions in [78] provided the foundation for the methods developed here, and this chapter continues to evolve the ideas presented in this work. The PETC improves the practical implementation of the control law because it can be applied to standard time-sliced actuators (like ChABC) for axon growth. The strategy involves deriving a novel triggering condition and establishing an upper bound on the continuous-time event trigger between two periodic examinations, explicitly derived as a sampling period in our study.

8.1 Periodic event-triggered based control

In this section, we propose a periodic event-triggering mechanism for axonal growth by deriving periodic sampling times for our control law. First, we give the definition of periodic event-triggering mechanism.

Definition 8.1. *Consider the event-triggering function $\Gamma^p(t)$, which undergoes periodic evaluation with a period of $h > 0$. The PETC that generates the events are characterized by two parts:*

1. *The event-trigger mechanism: A periodic event-trigger that determines the event times*

$$t_{k+1}^p = \inf\{t \in \mathbb{R}_+ | t > t_k^p, \Gamma^p(t) > 0,\ t = nh,\ h > 0,\ n \in \mathbb{N}\}, \tag{8.1}$$

with $t_0^p = 0$ where h is sampling period and

$$\Gamma^p(t) = \upsilon_1 d^2(t) - \upsilon_2 m(t) \tag{8.2}$$

where $\upsilon_1 > 0$ and $\upsilon_2 > 0$.

2. *The feedback control law that is derived as*

$$U_k^p(t) = -\frac{1}{D}\int_0^{l(t_k^p)} p(x)Bu(x,t_k^p)dx + p(l(t_k^p))X(t_k^p) \tag{8.3}$$

for all $t \in [t_k^p, t_{k+1}^p)$ for $k \in \mathbb{N}$.

Note that periodicity in the triggering conditions (8.1), allows us to monitor the triggering function *periodically* and update the control laws *aperiodically,* removing the continuous monitoring of the PDE-ODE state variables. Then, the boundary condition (7.8) becomes

$$u_x(0,t) + u(0,t) = U(t_k^p). \tag{8.4}$$

8.1.1 Selection of the sampling period

The sampling period, denoted as h, represents the unit of time during which the control input is updated. Let the periodic event-triggered function given by (8.1), along with the boundary condition in (8.4) and the plant dynamics from (7.1)-(7.5), satisfy the condition $\Gamma^p(t) \leq 0$ for all t within the interval $t \in [t_k^p, t_{k+1}^p)$ for $k \in \mathbb{N}$. Hence, it follows that $m(t) < 0$ for all $t > 0$. The

parameter h is selected to satisfy

$$0 < h \leq \tau, \tag{8.5}$$

where the upper bound, τ, is the minimum inter-event time of the CETC design defined in (7.44)-(7.47).

8.1.2 Design of the periodic event triggering function $\Gamma^p(t)$

Proposition 8.1. *Under the definition of the periodic event-triggered boundary control* (8.4)*, with the sampling period $h < \tau$, it holds that*

$$\Gamma^c(t) \leq \frac{1}{q}\left((a+\gamma\rho)d^2(nh)e^{q(t-nh)} - \gamma\rho d^2(nh) + q\gamma m(nh)e^{-\eta(t-nh)}\right), \tag{8.6}$$

for all $t \in [nh,(n+1)h)$ and any $n \in [t_k^p/h, t_{k+1}^p/h) \subset \mathbb{N}$, where $q = 1+\eta+\rho_1$ and $\Gamma^c(t) = d^2(t) - \gamma m(t)$ for $\gamma > 0$.

Proof. Taking the time derivative of $\Gamma^c(t)$ in $t \in [nh,(n+1)h)$ and $n \in [t_k^p/h, t_{k+1}^p/h) \subset \mathbb{N}$, one can show that

$$\dot{\Gamma}^c(t) = 2d(t)\dot{d}(t) - \gamma\dot{m}(t) \tag{8.7}$$

$$\leq d^2(t) + \dot{d}^2(t) - \gamma\dot{m}(t). \tag{8.8}$$

By using Lemma 7.1 and 7.2, we get

$$\begin{aligned}\dot{\Gamma}^c(t) \leq & (1+\rho_1+\gamma\rho)d^2(t) - (\gamma\beta_1-\alpha_1)X(t)^2 - (\gamma\beta_2-\alpha_2)X(t)^4 - (\gamma\beta_3-\alpha_3)X(t)^6 \\ & - (\gamma\beta_4-\alpha_4)u(0,t)^2 - (\gamma\beta_5-\alpha_5)||u(x,t)||^2 + \eta\gamma m(t).\end{aligned} \tag{8.9}$$

By using the definition of $\Gamma^c(t)$, we get

$$\begin{aligned}\dot{\Gamma}^c(t) \leq & (1+\rho_1+\gamma\rho)\Gamma^c(t) - (\gamma\beta_1-\alpha_1)\,X(t)^2 - (\gamma\beta_2-\alpha_2)\,X(t)^4 - (\gamma\beta_3-\alpha_3)\,X(t)^6 \\ & - (\gamma\beta_4-\alpha_4)\,u(0,t)^2 - (\gamma\beta_5-\alpha_5)\,||u(x,t)||^2 + ((1+\rho_1+\gamma\rho)\,\gamma+\eta\gamma)\,m(t). \end{aligned} \tag{8.10}$$

Since $m(t)$ satisfies Lemma 7.1 and (7.1)-(7.5) with the event-triggered control law (7.18) is locally exponentially convergen, (8.10) exhibit smooth behavior in the interval $t \in [nh,(n+1)h)$ and for any $n \in [t_k^p/h, t_{k+1}^p/h) \subset \mathbb{N}$. This establishes the existence of a non-negative function $\iota(t) \in C^0((t_k^p, t_{k+1}^p);\mathbb{R}_+)$ such that:

$$\begin{aligned}\dot{\Gamma}^c(t) = & (1+\rho_1+\gamma\rho)\Gamma(t) - (\gamma\beta_1-\alpha_1)\,X(t)^2 - (\gamma\beta_2-\alpha_2)\,X(t)^4 - (\gamma\beta_3-\alpha_3)\,X(t)^6 \\ & - (\gamma\beta_4-\alpha_4)\,u(0,t)^2 - (\gamma\beta_5-\alpha_5)\,||u(x,t)||^2 + ((1+\rho_1+\gamma\rho)\,\gamma+\eta\gamma)\,m(t) - \iota(t), \end{aligned} \tag{8.11}$$

for all $t \in [nh,(n+1)h)$ and for any $n \in [t_k^p/h, t_{k+1}^p/h) \subset \mathbb{N}$. Moreover, through the substitution of $d^2(t) = \Gamma^c(t) + \gamma m(t)$, we can rephrase the dynamics of $m(t)$ as follows:

$$\begin{aligned}\dot{m}(t) = & -\rho\Gamma^c(t) - (\eta+\rho\gamma)\,m(t) + \beta_1 X(t)^2 + \beta_2 X(t)^4 + \beta_3 X(t)^6 + \beta_4 |u(0,t)|^2 \\ & + \beta_5 ||u(x,t))||^2, \end{aligned} \tag{8.12}$$

for all $t \in [nh,(n+1)h)$ and for any $n \in [t_k^p/h, t_{k+1}^p/h) \subset \mathbb{N}$. Subsequently, by combining (8.11) with (8.12), we can derive the subsequent system of ODEs:

$$\dot{r}(t) = A_1 r(t) + v(t),$$

where

$$r(t) = \begin{bmatrix} \Gamma^c(t) \\ m(t) \end{bmatrix}, A_1 = \begin{bmatrix} q-\eta+\gamma\rho & \gamma(q+\gamma\rho) \\ -\rho & -\eta-\rho\gamma \end{bmatrix},$$
$$v(t) = \begin{bmatrix} f_1(t) \\ f_2(t) \end{bmatrix}, \tag{8.13}$$

where

$$\begin{aligned} f_1(t) =& -(\gamma\beta_1-\alpha_1)X(t)^2-(\gamma\beta_2-\alpha_2)X(t)^4-(\gamma\beta_3-\alpha_3)X(t)^6-(\gamma\beta_4-\alpha_4)u(0,t)^2 \\ & -(\gamma\beta_5-\alpha_5)||u(x,t)||^2-\iota(t), \end{aligned} \tag{8.14}$$

$$f_2(t) = \beta_1 X(t)^2+\beta_2 X(t)^4+\beta_3 X(t)^6+\beta_4|u(0,t)|^2+\beta_5||u(x,t))||^2, \tag{8.15}$$

and

$$q = 1+\eta+\rho_1. \tag{8.16}$$

The solution to (8.13) for all $t \in [nh,(n+1)h)$ and for any $n \in [t_k^p/h, t_{k+1}^p/h) \subset \mathbb{N}$ can be expressed as:

$$r(t) = e^{A_1(t-nh)}r(nh)+\int_{nh}^{t} e^{A_1(t-\xi)}v(\xi)d\xi, \tag{8.17}$$

which gives us

$$\Gamma^c(t) = C_1 e^{A_1(t-nh)}r(nh)+C_1\int_{nh}^{t} e^{A_1(t-\xi)}v(\xi)d\xi, \tag{8.18}$$

where $C_1 = [1 \quad 0]$. Since matrix A_1 has two distinct eigenvalues, we can diagonalize the matrix

exponential $e^{A_1 t}$ as it is defined in [79]. Thus, we can derive the second part of (8.18) as

$$C_1 e^{A_1(t-\xi)} v(\xi) = \begin{bmatrix} g_1(t) & g_2(t) \end{bmatrix} \begin{bmatrix} f_1(t) \\ f_2(t) \end{bmatrix}, \tag{8.19}$$

where

$$g_1(t) = \frac{q+\gamma\rho}{q} e^{(1+\rho_1)t} - \frac{\rho\gamma}{q} e^{-\eta t}, \tag{8.20}$$

$$g_2(t) = \frac{\gamma(q+\gamma\rho)}{q} \left(e^{(1+\rho_1)t} - e^{-\eta t} \right). \tag{8.21}$$

Since we have the following relationship

$$1 + \eta + 7|p(0)B|^2 > 0, \tag{8.22}$$

we can get

$$g_1(t) = \frac{1}{q} \left(-\gamma\rho + (q+\rho\gamma) e^{qt} \right) e^{-\eta t}, \tag{8.23}$$

$$g_2(t) = \frac{\gamma(q+\gamma\rho)}{q} \left(-1 + e^{qt} \right) e^{-\eta t}. \tag{8.24}$$

It's apparent that $g_1(t)$ remains positive for $t > 0$. Furthermore, considering the relation (7.40), and using ascending order of triggering times that is the solution of (7.47) is represented by

$$\tau = \frac{1}{q} \ln \left(1 + \frac{\sigma q}{(1-\sigma)(q+\gamma\rho)} \right), \tag{8.25}$$

one can show that

$$
\begin{aligned}
C_1 e^{A_1(t-\xi)} v(\xi) = & \frac{\alpha_1(q+\gamma\rho)}{q}\left(e^{q\tau} - e^{q(t-\xi)}\right) e^{-\eta(t-\xi)} X(t)^2 \\
& + \frac{\alpha_2(q+\gamma\rho)}{q}\left(e^{q\tau} - e^{q(t-\xi)}\right) e^{-\eta(t-\xi)} X(t)^4 \\
& + \frac{\alpha_3(q+\gamma\rho)}{q}\left(e^{q\tau} - e^{q(t-\xi)}\right) e^{-\eta(t-\xi)} X(t)^6 \\
& + \frac{\alpha_4(q+\gamma\rho)}{q}\left(e^{q\tau} - e^{q(t-\xi)}\right) e^{-\eta(t-\xi)} u(0,t)^2 \\
& + \frac{\alpha_5(q+\gamma\rho)}{q}\left(e^{q\tau} - e^{q(t-\xi)}\right) e^{-\eta(t-\xi)} ||u(x,t)||^2. \qquad (8.26)
\end{aligned}
$$

Given the stipulated intervals $nh \le \xi \le t \le (n+1)h$, and $h \le \tau$, upon thorough examination of (8.26), it emerges that the inequality $(\gamma\beta_i - \alpha_i)g_1(t-\xi) - \beta_i g_2(t-\xi) > 0$ satisfied for all $i = 1,2,3,4,5$. This observation prompts us to establish $C_1 e^{A_1(t-\xi)} v(\xi)$ which holds for all t and ξ within the range of $nh \le \xi \le t \le (n+1)h$, and for $n \in [t_k^p/h, t_{k+1}^p/h) \subset \mathbb{N}$. Taking this observation into account alongside (8.18), we can derive the following expression for $t \in [nh, (n+1)h)$:

$$
\Gamma^c(t) \le \frac{1}{q}\left(-\gamma(q+\gamma\rho)m(nh) - \gamma\rho\Gamma^c(nh) + (q+\gamma\rho)\left(\Gamma^c(nh) + \gamma m(nh)\right) e^{q(t-nh)}\right). \qquad (8.27)
$$

Upon performing the substitution $\Gamma^c(nh)$ into (8.27), we are able to derive the inequality (8.6) which is valid for all $t \in [nh, (n+1)h)$. This concludes the proof. □

Building upon Proposition 8.1, the update time for the control input can be determined by identifying when the subsequent condition is met for any $t \in [nh, (n+1)h)$, thereby challenging the positive definiteness of $\Gamma^c(t)$.

$$
(q+\gamma\rho)d^2(nh)e^{q(t-nh)} - \gamma\rho d^2(nh) + q\gamma m(nh) > 0, \qquad (8.28)
$$

Thus, one can choose this condition as $\Gamma^p(t)$ such that

$$\Gamma^p(t) = (q+\gamma\rho)e^{qh}d^2(t) - \gamma\rho d^2(t) + q\gamma m(t), \tag{8.29}$$

which completes the design process. Next, we state the following theorem that guarantees $\Gamma^c(t) \leq 0$ for all $t \in [t_k^p, t_{k+1}^p)$, $k \in \mathbb{N}$.

Theorem 8.1. *Let the design parameters, ρ_1 and β_i as defined in* (7.27)-(7.40)*, set the sampling rate in accordance with* (8.5)*, let $\rho, \gamma, \eta > 0$ and $\sigma \in (0,1)$. Let us consider the periodic event-triggering mechanism* (8.1)-(8.3) *with the $\Gamma^p(t)$ as defined in* (8.29) *which generates the increasing sequence of times $\{t_k^p\}_{k\in\mathbb{N}}$ with $t_0^p = 0$. Then, for $\Gamma^c(t)$ and $m(t)$ with $m(t) < 0$, it holds that $\Gamma^c(t) \leq 0$ and $m(t) < 0$ for all $t > 0$.*

Proof. We omit this proof, which is trivial when one follows the steps of the proof of Theorem 2 in [79]. □

8.2 Convergence proof under periodic event-triggering control law

In this section, we begin by introducing the theorem that establishes the local exponential convergence of the closed-loop system under the periodic event-triggering mechanism.

Theorem 8.2. *Let the design parameters, ρ, ρ_1 and β_i given as defined in Theorem 8.1. Consider the periodic event-triggering rule* (8.1)-(8.3) *with the periodic event-triggering function* (8.29) *and sampling rate h defined in* (8.5)*, which generates an increasing event-times $\{t_k^p\}_{k\in\mathbb{N}}$. Assuming the well-posedness, the closed-loop system of* (7.1)-(7.5) *with the boundary control law* (8.3) *and* (8.29) *is locally exponentially convergent in L^2-norm sense.*

In the remainder of this section, we provide the proof of Theorem (8.2).

8.2.1 Nonlinear target system

In order to prove that the closed-loop system (7.1)-(7.5) with the control law (7.16) and the periodic event-triggering mechanism (8.1) and (8.29), is locally exponentially convergent, we first obtain the following target system by applying transformation (3.5) and (7.50), one can obtain the same nonlinear target system, (7.51)-(7.54).

8.2.2 Lyapunov analysis

To demonstrate the local convergence of the system, we initially establish the system properties in a non-constant spatial interval as derived in (3.33) and (3.34). As demonstrated in Chapter 7, $m(t) < 0$ for all $t \in [t_k^p, t_{k+1}^p)$ where $k \in \mathbb{N}$, implying $\Gamma^c(t) \leq 0$ for $t \in [t_k^p, t_{k+1}^p)$. Assuming the well-posedness of the closed-loop system and following the methodology outlined in Chapter 7, the subsequent Lyapunov functional is considered

$$V(t) = V_1(t) - m(t), \tag{8.30}$$

where

$$V_1(t) = d_1 \frac{1}{2} \int_0^{l(t)} \varpi(x,t)^2 dx + X(t)^\top \left(d_2 P_1 + \frac{1}{2} P_2 \right) X(t) \tag{8.31}$$

and $d_1 > 0$, $d_2 > 0$, $P_1 \succ 0$ and $P_2 \succeq 0$ are positive definite and positive semidefinite matrices satisfying the Lyapunov equations:

$$(A + BK^\top)^\top P_1 + P_1 (A + BK^\top) = -Q_1, \tag{8.32}$$

$$(A + BK^\top)^\top (P_1 + P_2) + (P_1 + P_2)(A + BK^\top) = -Q_2 \tag{8.33}$$

where P_1 and P_2 are chosen as in (7.59) and we pick $\epsilon \in \mathbb{R}^2$ as $\epsilon_1 \geq 2 l_c p_{1,1}$ and $\epsilon_2 = \frac{p_{1,2}}{l_c d_1}$ for some positive definite matrices $Q_1 \succ 0$ and $Q_2 \succ 0$.

Proof. Similar to the strategy used in Chapter 7, by taking the time derivative of (8.31), applying Poincaré's, Agmon's, and Young's inequalities, we first derive the following expression:

$$\dot{V} \leq -\alpha^* V + \xi_1 V^{3/2} + \xi_2 V^2 + \xi_3 V^{5/2} + \xi_4 V^3 \tag{8.34}$$

where α^* and ξ_i are defined in (7.67)-(7.70) and where d_1 and d_2 are chosen to satisfy (7.71)-(7.72). Note that the positive constant parameters and the inequalities are also defined in (7.73)-(7.78). Given (8.34), we can demonstrate that within the region $\Omega_1 := \{(\varpi, X) \in L^2 \times \mathbb{R}^2 | V(t) < M_0\}$ where $t \in (t_k^p, t_{k+1}^p)$ for $k \in \mathbb{N}$, there exists a positive constant $M_0 > 0$ ensuring the satisfaction of the system properties (3.33) and (3.34). The existence of such $M_0 > 0$ is established in Lemma 7.4. From this result, we have $M_0 = \frac{\lambda_{\min}(P_1)}{d_2} r^2$ where $r = \min\left\{\frac{\bar{v}}{r_g}, l_s, \bar{l} - l_s\right\}$ for $t \in (t_k^p, t_{k+1}^p)$, $k \in \mathbb{N}$. Next, we analyze the convergence within the time interval $t \in (t_k^p, t_{k+1}^p)$ for $k \in \mathbb{N}$, and subsequently for $t \in (0, t)$. Then, a positive constant M exists such that when $V(t_j) < M$, the following norm estimate is valid for $t \in [t_k^p, t_{k+1}^p)$, where $k \in \mathbb{N}$:

$$V(t_{k+1}^p) \leq V(t_k^p) e^{-\frac{\alpha^*}{2}(t_{k+1}^p - t_k^p)}. \tag{8.35}$$

For $M > 0$, we define the set $\Omega := \{(\varpi, X) \in L^2 \times \mathbb{R}^2 | V(t) < M\}$. From Lemma 7.4, it is clear that if $M \leq M_0$, then $\Omega \subset \Omega_1$ which satisfy the system properties (3.33) and (3.34) and the norm estimate defined in (8.35) for $t \in [t_k^p, t_{k+1}^p)$, where $k \in \mathbb{N}$. Hence, we set $M \leq p^*$, where p^* is a non-zero root of the following polynomial

$$-\alpha^* V + \xi_1 V^{3/2} + \xi_2 V^2 + \xi_3 V^{5/2} + \xi_4 V^3 = 0 \tag{8.36}$$

for $V > 0$. Given that all coefficients of this polynomial are positive, at least one positive root p^*

exists. Thus, (8.34) implies

$$\dot{V} \leq -\frac{\alpha^*}{2}V(t) \tag{8.37}$$

for $t \in [t_k^p, t_{k+1}^p)$, where $k \in \mathbb{N}$ and $M = \min\{M_0, p^*\}$. The smoothness of $V(t)$ within this interval ensures that $V(t_{k+1}^{p^-}) = V(t)$ and $V(t_k^{p^+}) = V(t_k^p)$, where $t_k^{p^+}$ and $t_k^{p^-}$ denote the right and left limits of $t = t_k^p$, respectively. Thus, we can have the norm estimate in (8.35). Then, for any $t \geq 0$ in $t \in [t_k^p, t_{k+1}^p)$ where $k \in \mathbb{N}$, we have

$$V(t) \leq e^{-\alpha^*(t-t_k^p)}V(t_k^p) \leq e^{-\alpha^* t}V(0). \tag{8.38}$$

Recalling $m(t) < 0$ and (8.30), we can write

$$V_1(t) - m(t) \leq e^{-\alpha^* t}V(0) \tag{8.39}$$

by applying the comparison principle one can obtain the following norm estimate for the target system (ϖ, X):

$$\begin{aligned} d_1\frac{1}{2}||\varpi(x)||^2 + d_2X(t)^\top\left(P_1 + \frac{1}{d_2}P_2\right)X(t) \\ \leq e^{-\alpha^* t}\left(\frac{d_1}{2}||\varpi(0)||^2 + d_2X(0)^\top\left(P_1 + \frac{1}{d_2}P_2\right)X(0) - m(0)\right) \end{aligned} \tag{8.40}$$

Utilizing the invertibility of the transformation (7.50), we subsequently prove that the target system (w, X) is also locally exponentially convergent. For the original system (u, X), we leverage the invertibility of the backstepping transformation given in (3.5). Consequently, we conclude that the closed-loop system is also locally exponentially convergent. This completes the proof. □

8.3 Simulations

In this section, we conduct numerical simulations for the system represented by equations (7.1)-(7.5), employing the control law (7.16) along with the designed periodic event-triggering mechanism (8.1) utilizing the triggering function (8.29). The model parameters are detailed in Table 3.1. Initial conditions are specified as $c_0(x) = 1.5c_\infty$ for the tubulin concentration along the axon and $l_0 = 1\mu m$ for the initial axon length. Control gain parameters are set as $k_1 = -0.001$ and $k_2 = 3 \times 10^{13}$. The event-triggering parameters are set as follows $m(0) = -0.5$, $\beta_1 = 2.5 \times 10^8$, $\beta_2 = 8 \times 10^9$, $\beta_3 = 1 \times 10^{11}$, $\beta_4 = 4 \times 10^{11}$, $\beta_5 = 4.5 \times 10^{11}$, $\rho = 1.5 \times 10^{-15}$, $\gamma = 1$, $\eta = 2$ and $\sigma = 0.8$. Moreover, the sampling period for the periodic event-triggering mechanism is selected as $h = 0.5\ ms$ which is smaller than the minimal dwell time $\tau \approx 0.54\ ms$.

Figure 8.1 illustrates the evolution of the continuous-time control input, $U(t)$, the event-triggering control input, $U_k^c(t)$, as defined in (7.18) with the triggering mechanism given by Definition 7.1, and the periodic event-triggering control input, $U_k^p(t)$, as defined in (8.3) with the triggering condition in (8.1) and triggering function in (8.29). While PETC closely emulates the CETC control input behavior, both PETC and CETC minimized the necessity of control law updates by maintaining comparable performance. In Figure 8.2, tubulin concentration, $c(x,t)$, and axon length, $l(t)$, converge to the steady-state solution of the tubulin concentration and the desired axon length. Note that tubulin concentration exhibits smoother changes with the PETC mechanism compared to the CETC mechanism which enhances the practical applicability.

Acknowledgements

Chapter 8 is being prepared for publication under the title “Adaptive Event-Triggered and Periodic Event-Triggered Boundary Control of Neuron Growth with Actuation at Soma” C. Demir, M. Diagne, M. Krstic. Chapter 7, ‘also contains a partial adaptation of the work contained in the conference paper “Periodic Event-Triggered Boundary Control of Neuron Growth with Actuation at Soma” C. Demir, M. Diagne, M. Krstic, accepted and will be presented at the 63rd

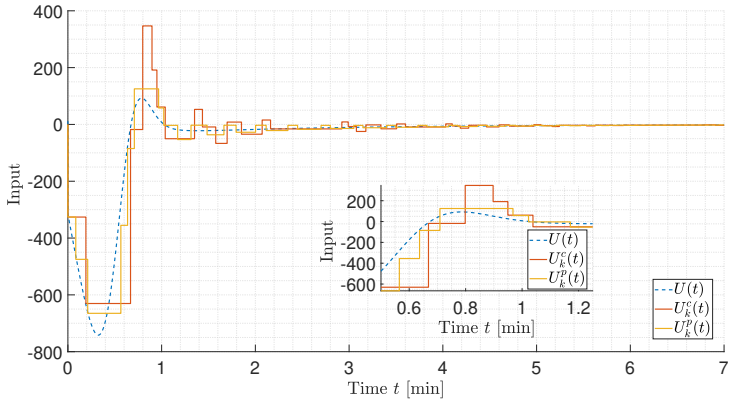

Figure 8.1. Comparison between periodic-event triggering control input $U_k^p(t)$, continuous time event triggering control input $U_k^c(t)$ and the continuous control law $U(t)$

IEEE Conference on Decision and Control 2024. The dissertation author was the primary author of these publications.

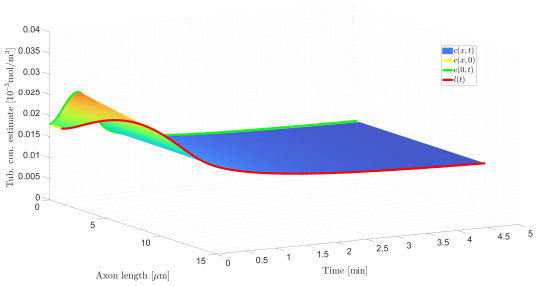

(a) Continous time control input.

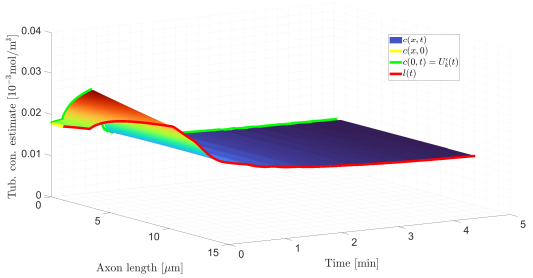

(b) Event-triggered control input.

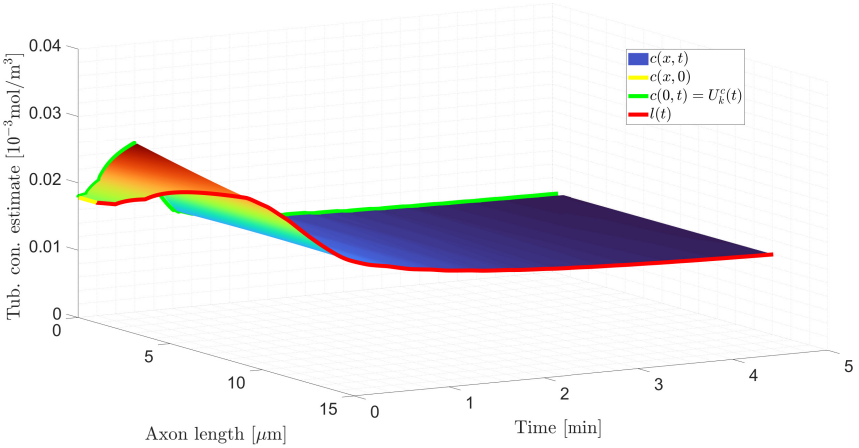

(c) Periodic event-triggered control input.

Figure 8.2. The tubulin concentration governed by (2.1)-(2.5), $c(x,t)$, converges to the steady-state tubulin concentration, $c_{\text{eq}}(t)$ by about $t = 4.5$min for both continuous control input, CETC and PETC. The axon length, $l(t)$, also converges to the desired axon length, l_s, by about $t = 4$min.

Chapter 9

Conclusion and Future Work

9.1 Summary

This dissertation bridges the fields of neurobiology and control systems by introducing new mechanisms for control laws. In Chapter 1, we began by explaining how neurons function and why the growth of neurons is crucial for maintaining their functionality. Neuron growth is essential for the proper functioning of vertebrate animals, so we explored the biological processes that support this growth. We also examined the potential therapeutic approaches that could address problems arising from disruptions in neuron growth. Understanding the mechanics of neuron growth is key to developing these therapies. Therefore, we discussed various mathematical models that help explain how neurons grow. Among these models, one stands out: the moving boundary model. This model is particularly effective in capturing the behavior of axon elongation, which is a process driven by the dynamics of a protein called tubulin. In the field of control systems, there is a similar concept known as the Stefan problem. This problem has been the focus of recent research in several areas, including feedback control, state estimation, compensation for delays, and event-triggering mechanisms. In this chapter, we provided an overview of these studies, highlighting how the Stefan problem relates to the moving boundary model in neurobiology and the broader implications for both fields. In the next chapter, we delve into the moving boundary neuron growth problem. We begin by explaining the steady-state solution, which describes the long-term behavior of the system, and then we define

the reference error system, which is used to measure deviations from the desired growth pattern. After establishing these foundational concepts, we introduce the main objective of the control law, which is to guide the system towards a desired state. We also discuss how this objective is achieved in the context of the Stefan problem, drawing parallels between the control strategies used in neurobiology and those in control systems engineering.

In Chapter 3, we focused on developing a state feedback control law, assuming the availability of full state measurements. Our approach began with a backstepping transformation, which allowed us to map the nonlinear neuron growth model onto a more manageable stable target system. Due to the complexity of the nonlinear model and the absence of existing backstepping methods for such systems, we opted to linearize the target system. This linearization enabled us to derive the control law and calculate the gain kernels needed for effective control. Importantly, this linearization did not affect the stability of the overall system, as our stability analysis was conducted using the original nonlinear model. As a result, we achieved local stability, which is adequate because minor variations in tubulin concentration do not pose a significant risk to axon viability. To validate our control law, we conducted simulations for both long and short-length axon elongation scenarios. The results confirmed that our control law performs effectively, demonstrating its potential to manage neuron growth under various conditions.

As previously mentioned, the availability of full state measurements is a critical aspect of the state feedback design in Chapter 3. However, in most biological systems, such complete measurements are rarely available. To address this challenge, we designed a state estimator in Chapter 4, considering the availability of only two key measurements: axon length and the flux of tubulin concentration from the axon to the growth cone. This estimator allows us to estimate the tubulin concentration along the entire axon. We began by defining the observer, which includes observer gains. These gains determine the balance between relying on the observer's predictions and the actual measurements. Next, we formulated the observer error dynamics, which are critical for ensuring that the observer's estimates converge to the actual system states. The goal is to demonstrate that the error in these estimates eventually becomes zero, meaning the

observer accurately converges the true state of the system. To design the observer, we applied a backstepping transformation, similar to the approach used in the state feedback control design. This transformation helped us map the observer error dynamics onto a target system, from which we derived the observer gains. These gains are functions of the backstepping transformation's gain kernels. We then proved that the target observer error system is locally exponentially stable, ensuring that the estimation process is reliable. We conducted simulations to evaluate the effectiveness of our method in accurately estimating the actual states of the neuron growth system. As an extension of this work, Chapter 4 introduces the output-feedback control law. This control law leverages the state estimates from Chapter 4 within the control law framework developed in Chapter 3. We also provided a stability analysis for the closed-loop system, which includes the plant dynamics, the observer, and the control law. Finally, simulations were performed to demonstrate that this control law successfully guides neuron growth to both short and long desired axon lengths.

In Chapter 6, we developed a control law that compensates for input delays caused by biological processes. These delays were modeled using a transport partial differential equation (PDE), which resulted in the neuron growth dynamics being coupled with a transport PDE. To address this coupled PDE-ODE-PDE system, we defined a backstepping transformation and formulated the corresponding target system. We then demonstrated the existence of gain kernel solutions of this transformation. Utilizing the backstepping transformation and the transport PDE, we derived a control law that effectively compensates for the input delay, guiding the neuron to converge to the steady-state solution. Following this, we first analyzed the stability of the target system and then verified the stability of the original plant.

To enhance the practicality of the proposed control laws, we introduced dynamic event-triggering mechanisms in Chapters 7 and 8. These mechanisms allow the control signal to be sampled only when a specific event occurs, which increases the efficiency of the control law by reducing the frequency of communication needed for neuron growth regulation. We first defined an event-triggering mechanism that monitors the system for events—such as when the

system approaches instability—and triggers control law updates in an aperiodic manner. Between events, a zero-order hold is used to maintain the control signal at a constant value. However, since this aperiodic checking can be challenging to implement in practice, we also designed a periodic event-triggering mechanism. This mechanism checks for events at regular intervals but samples the control law periodically. For both mechanisms, we analyzed the avoidance of Zeno behavior (an undesirable situation where events are triggered infinitely often in a finite period) and ensured the convergence of the system under these mechanisms. Finally, we demonstrated the performance of these control mechanisms through simulations and provided a comparison of their effectiveness in the later sections.

9.2 Future Work

The problem and solution presented in this dissertation represent a pioneering effort in applying control systems theory to the neuron growth problem. This work opens up numerous potential research opportunities, not only from a control systems perspective but also in the fields of neurobiology, neuroscience, and medicine. From a control system design perspective, one promising area for future research is to consider the neuron growth model parameters as unknown. This is a realistic scenario, given the vast number of neurons, each with different physical properties that may vary over time or be difficult to determine for specific neurons. To address this challenge, adaptive control strategies could be employed. These strategies are designed to estimate unknown parameters in real-time and update the control mechanism accordingly, allowing the system to adapt to these varying parameters effectively. This approach could lead to more robust and flexible control methods for managing neuron growth with unknown parameters. Developing an adaptive control law is our ongoing project. These unknown parameters could also vary over time and across different spatial domains due to the inherent complexity and dynamic nature of biological processes, which would provide a more accurate representation of the neuron growth process. To address these variations, adaptive mechanisms could be

developed that adjust the control strategy in response to these changing parameters. Moreover, this adaptive mechanism could be integrated with event-triggering mechanisms or, more advanced, self-triggering mechanisms. These approaches would further enhance the applicability of the control law by making it more efficient and responsive to the real-time needs of the system, thereby reducing unnecessary computations and communications. This integration would allow the control system to dynamically adjust not only to parameter variations but also to changes in the environment or the state of the neuron, leading to more robust and effective control in complex biological systems. Another major direction would be designing a control law for a bundle of neurons instead of a single neuron which captures the collective behavior and emergent properties of neural networks, which are essential for brain functions like perception, learning, and decision-making. However, there is not any model that captures the behavior of a bundle of neurons. From the perspective of designing medical therapy for neurodegenerative diseases, it is essential to develop a mathematical model that accurately represents the dynamic behavior of the therapy, which would serve as the actuator of the control law. This model is crucial for predicting how the therapy will interact with the patient's neural system over time, allowing for the fine-tuning of treatment strategies. By capturing the complexities of the disease's progression and the therapy's effects, the model enables the control law to adjust the therapeutic interventions dynamically, ensuring optimal dosing and timing to maximize efficacy and minimize side effects. Such a model would be instrumental in creating personalized treatment plans that adapt to the individual needs of patients, potentially slowing or even halting the progression of neurodegenerative conditions. These are just a couple of possible future research directions, and the potential is by no means limited to these areas. The intersection of control systems theory with neurobiology opens up a vast landscape of opportunities for exploration and innovation.

Bibliography

[1] K.-E. Åarzén, "A simple event-based pid controller," *IFAC Proceedings Volumes*, vol. 32, no. 2, pp. 8687–8692, 1999.

[2] W. W. Ahmed and T. A. Saif, "Active transport of vesicles in neurons is modulated by mechanical tension," *Scientific reports*, vol. 4, no. 1, p. 4481, 2014.

[3] J. R. Anderson, *Cognitive psychology and its implications*. Macmillan, 2005.

[4] J. B. Angevine and C. W. Cotman, *Principles of neuroanatomy*. Oxford University Press, USA, 1981.

[5] M. Anthonisen and P. Grutter, "Growth and elasticity of mechanically-created neurites," *arXiv preprint arXiv:1912.05735*, 2019.

[6] E. J. Bradbury and L. M. Carter, "Manipulating the glial scar: chondroitinase ABC as a therapy for spinal cord injury," *Brain research bulletin*, vol. 84, no. 4-5, pp. 306–316, 2011.

[7] E. J. Bradbury and S. B. McMahon, "Spinal cord repair strategies: why do they work?" *Nature Reviews Neuroscience*, vol. 7, no. 8, pp. 644–653, 2006.

[8] M. Buisson-Fenet, S. Koga, and M. Krstic, "Control of piston position in inviscid gas by bilateral boundary actuation," in *2018 IEEE Conference on Decision and Control (CDC)*. IEEE, 2018, pp. 5622–5627.

[9] Z. Chen, J. Bentsman, and B. G. Thomas, "Enthalpy-based output feedback control of the Stefan problem with hysteresis," in *2020 American Control Conference (ACC)*, 2020, pp. 2661–2666.

[10] A. Citri and R. C. Malenka, "Synaptic plasticity: multiple forms, functions, and mechanisms," *Neuropsychopharmacology*, vol. 33, no. 1, pp. 18–41, 2008.

[11] B. D. Clark, E. M. Goldberg, and B. Rudy, "Electrogenic tuning of the axon initial segment," *The Neuroscientist*, vol. 15, no. 6, pp. 651–668, 2009.

[12] J.-M. Coron, R. Vazquez, M. Krstic, and G. Bastin, "Local exponential H^2 stabilization of a 2\times2 quasilinear hyperbolic system using backstepping," *SIAM Journal on Control and Optimization*, vol. 51, no. 3, pp. 2005–2035, 2013.

[13] C. M. Cowan and L. A. Raymond, "Selective neuronal degeneration in huntington's disease," *Current topics in developmental biology*, vol. 75, pp. 25–71, 2006.

[14] W. Dauer and S. Przedborski, "Parkinson's disease: mechanisms and models," *Neuron*, vol. 39, no. 6, pp. 889–909, 2003.

[15] P. Day, N. Alves, E. Daniell, D. Dasgupta, R. Ogborne, A. Steeper, M. Raza, C. Ellis, J. Fawcett, R. Keynes *et al.*, "Targeting chondroitinase ABC to axons enhances the ability of chondroitinase to promote neurite outgrowth and sprouting," *PloS one*, vol. 15, no. 1, 2020.

[16] P. Dayan and L. F. Abbott, *Theoretical neuroscience: computational and mathematical modeling of neural systems*. MIT press, 2005.

[17] D. Debanne, E. Campanac, A. Bialowas, E. Carlier, and G. Alcaraz, "Axon physiology," *Physiological reviews*, vol. 91, no. 2, pp. 555–602, 2011.

[18] C. Demir, M. Diagne, and M. Krstic, "Periodic event-triggered boundary control of neuron growth with actuation at soma," *arXiv preprint arXiv:2404.19206*, 2024.

[19] C. Demir, S. Koga, and M. Krstic, "Neuron growth control by PDE backstepping: Axon length regulation by tubulin flux actuation in soma," in *2021 60th IEEE Conference on Decision and Control (CDC)*, 2021, pp. 649–654.

[20] ——, "Input delay compensation for neuron growth by pde backstepping," *IFAC-PapersOnLine*, vol. 55, no. 36, pp. 49–54, 2022.

[21] ——, "Neuron growth output-feedback control by PDE backstepping," in *2022 American Control Conference (ACC)*, 2022, pp. 4159–4164.

[22] ——, "Event-triggered control of neuron growth with dirichlet actuation at soma," *arXiv preprint arXiv:2310.00131*, 2023.

[23] ——, "Neuron growth control and estimation by pde backstepping," *Automatica*, vol. 165, p. 111669, 2024.

[24] T. J. Dennerll, P. Lamoureux, R. E. Buxbaum, and S. R. Heidemann, "The cytomechanics of axonal elongation and retraction." *The Journal of cell biology*, vol. 109, no. 6, pp. 3073–3083, 1989.

[25] S. Diehl, E. Henningsson, and A. Heyden, "Efficient simulations of tubulin-driven axonal growth," *Journal of computational neuroscience*, vol. 41, no. 1, pp. 45–63, 2016.

[26] S. Diehl, E. Henningsson, A. Heyden, and S. Perna, "A one-dimensional moving-boundary model for tubulin-driven axonal growth," *Journal of theoretical biology*, vol. 358, pp. 194–207, 2014.

[27] W. B. Dunbar, N. Petit, P. Rouchon, and P. A. Martin, "Motion planning for a nonlinear Stefan problem," *ESAIM: Control, Optimisation and Calculus of Variations*, vol. 9, pp. 275–296, 2003. [Online]. Available: http://www.numdam.org/articles/10.1051/cocv:2003013/

[28] S. Ecklebe, F. Woittennek, C. Frank-Rotsch, N. Dropka, and J. Winkler, "Toward model-based control of the vertical gradient freeze crystal growth process," *IEEE Transactions on Control Systems Technology*, 2021.

[29] N. Espitia, I. Karafyllis, and M. Krstic, "Event-triggered boundary control of constant-parameter reaction–diffusion pdes: A small-gain approach," *Automatica*, vol. 128, p. 109562, 2021.

[30] N. Espitia, A. Girard, N. Marchand, and C. Prieur, "Event-based boundary control of a linear 2×2 hyperbolic system via backstepping approach," *IEEE Transactions on Automatic Control*, vol. 63, no. 8, pp. 2686–2693, 2018.

[31] K. L. Fink, F. López-Giráldez, I.-J. Kim, S. M. Strittmatter, and W. B. Cafferty, "Identification of intrinsic axon growth modulators for intact cns neurons after injury," *Cell reports*, vol. 18, no. 11, pp. 2687–2701, 2017.

[32] C. Frantz, K. M. Stewart, and V. M. Weaver, "The extracellular matrix at a glance," *Journal of cell science*, vol. 123, no. 24, pp. 4195–4200, 2010.

[33] S. Gierke, P. Kumar, and T. Wittmann, "Analysis of microtubule polymerization dynamics in live cells," *Methods in cell biology*, vol. 97, pp. 15–33, 2010.

[34] A. Goriely, *The mathematics and mechanics of biological growth*. Springer, 2017, vol. 45.

[35] A. Goriely, S. Budday, and E. Kuhl, "Neuromechanics: from neurons to brain," *Advances in applied mechanics*, vol. 48, pp. 79–139, 2015.

[36] B. P. Graham, K. Lauchlan, and D. R. Mclean, "Dynamics of outgrowth in a continuum model of neurite elongation," *Journal of computational neuroscience*, vol. 20, pp. 43–60, 2006.

[37] Y. Hara, "Brain plasticity and rehabilitation in stroke patients," *Journal of Nippon Medical School*, vol. 82, no. 1, pp. 4–13, 2015.

[38] W. P. Heemels, K. H. Johansson, and P. Tabuada, "An introduction to event-triggered and self-triggered control," in *2012 ieee 51st ieee conference on decision and control (cdc)*. IEEE, 2012, pp. 3270–3285.

[39] W. Heemels, J. Sandee, and P. Van Den Bosch, "Analysis of event-driven controllers for linear systems," *International journal of control*, vol. 81, no. 4, pp. 571–590, 2008.

[40] T. A. Hely, B. Graham, and A. Van Ooyen, "A computational model of dendrite elongation and branching based on map2 phosphorylation," *Journal of theoretical biology*, vol. 210, no. 3, pp. 375–384, 2001.

[41] E. J. Huang and L. F. Reichardt, "Neurotrophins: roles in neuronal development and function," *Annual review of neuroscience*, vol. 24, no. 1, pp. 677–736, 2001.

[42] M. Izadi, J. Abdollahi, and S. S. Dubljevic, "PDE backstepping control of one-dimensional heat equation with time-varying domain," *Automatica*, vol. 54, pp. 41–48, 2015.

[43] E. M. Izhikevich, *Dynamical systems in neuroscience*. MIT press, 2007.

[44] E. R. Kandel, J. H. Schwartz, T. M. Jessell, S. Siegelbaum, A. J. Hudspeth, and S. Mack, *Principles of neural science*. McGraw-hill New York, 2000, vol. 4.

[45] I. Karafyllis and M. Krstic, "Sampled-data boundary feedback control of 1-d parabolic pdes," *Automatica*, vol. 87, pp. 226–237, 2018.

[46] S. Karimi-Abdolrezaee, E. Eftekharpour, J. Wang, D. Schut, and M. G. Fehlings, "Synergistic effects of transplanted adult neural stem/progenitor cells, chondroitinase, and growth factors promote functional repair and plasticity of the chronically injured spinal cord," *Journal of Neuroscience*, vol. 30, no. 5, pp. 1657–1676, 2010.

[47] R. A. Koene, B. Tijms, P. Van Hees, F. Postma, A. De Ridder, G. J. Ramakers, J. Van Pelt, and A. Van Ooyen, "Netmorph: a framework for the stochastic generation of large scale neuronal networks with realistic neuron morphologies," *Neuroinformatics*, vol. 7, pp. 195–210, 2009.

[48] E. Kofman and J. H. Braslavsky, "Level crossing sampling in feedback stabilization under data-rate constraints," in *Proceedings of the 45th IEEE Conference on Decision and Control*. IEEE, 2006, pp. 4423–4428.

[49] S. Koga, C. Demir, and M. Krstic, "Event-triggered safe stabilizing boundary control for the stefan pde system with actuator dynamics," in *2023 American Control Conference (ACC)*. IEEE, 2023, pp. 1794–1799.

[50] S. Koga, M. Diagne, and M. Krstic, "Control and state estimation of the one-phase Stefan problem via backstepping design," *IEEE Transactions on Automatic Control*, vol. 64, no. 2, pp. 510–525, 2018.

[51] S. Koga and M. Krstic, *Materials Phase Change PDE Control and Estimation: From Additive Manufacturing to Polar Ice*. Springer Nature, 2020.

[52] S. Koga, D. Straub, M. Diagne, and M. Krstic, "Stabilization of Filament Production Rate for Screw Extrusion-Based Polymer Three-Dimensional-Printing," *Journal of Dynamic Systems, Measurement, and Control*, vol. 142, no. 3, 12 2019.

[53] M. Krstic, "Compensating actuator and sensor dynamics governed by diffusion PDEs," *Systems & Control Letters*, vol. 58, no. 5, pp. 372–377, 2009.

[54] ——, "Control of an unstable reaction–diffusion pde with long input delay," *Systems & Control Letters*, vol. 58, no. 10-11, pp. 773–782, 2009.

[55] ——, "Delay compensation for nonlinear, adaptive, and pde systems," 2009.

[56] M. Krstic and A. Smyshlyaev, *Boundary control of PDEs: A course on backstepping designs*. SIAM, 2008.

[57] T. M. Laleg Kirati, H. Arabi, M. Tadjine, and C. Zayane, "Estimation of the neuronal activation using fMRI data: An observer-based approach," in *2013 Amer. Control Conf.*, 2013, pp. 5457–5461.

[58] H. Lee, R. J. McKeon, and R. V. Bellamkonda, "Sustained delivery of thermostabilized chABC enhances axonal sprouting and functional recovery after spinal cord injury," *Proceedings of the National Academy of Sciences*, vol. 107, no. 8, pp. 3340–3345, 2010.

[59] M. L. Lemons, D. R. Howland, and D. K. Anderson, "Chondroitin sulfate proteoglycan immunoreactivity increases following spinal cord injury and transplantation," *Experimental neurology*, vol. 160, no. 1, pp. 51–65, 1999.

[60] G.-H. Li and C.-D. Qin, "A model for neurite growth and neuronal morphogenesis," *Mathematical biosciences*, vol. 132, no. 1, pp. 97–110, 1996.

[61] G.-H. Li, L.-W. Wang *et al.*, "Computer model of growth cone behavior and neuronal morphogenesis," *Journal of Theoretical Biology*, vol. 174, no. 4, pp. 381–389, 1995.

[62] O. Lindvall and Z. Kokaia, "Stem cells for the treatment of neurological disorders," *Nature*, vol. 441, no. 7097, pp. 1094–1096, 2006.

[63] X. Z. Liu, X. M. Xu, R. Hu, C. Du, S. X. Zhang, J. W. McDonald, H. X. Dong, Y. J. Wu, G. S. Fan, M. F. Jacquin *et al.*, "Neuronal and glial apoptosis after traumatic spinal cord injury," *Journal of Neuroscience*, vol. 17, no. 14, pp. 5395–5406, 1997.

[64] R. B. Maccioni, J. P. Muñoz, and L. Barbeito, "The molecular bases of Alzheimer's disease and other neurodegenerative disorders," *Archives of medical research*, vol. 32, no. 5, pp. 367–381, 2001.

[65] S. Maday, A. E. Twelvetrees, A. J. Moughamian, and E. L. Holzbaur, "Axonal transport: cargo-specific mechanisms of motility and regulation," *Neuron*, vol. 84, no. 2, pp. 292–309, 2014.

[66] A. Maidi and J.-P. Corriou, "Boundary geometric control of a linear Stefan problem," *Journal of Process Control*, vol. 24, no. 6, pp. 939–946, 2014.

[67] D. R. McLean, A. van Ooyen, and B. P. Graham, "Continuum model for tubulin-driven neurite elongation," *Neurocomp.*, vol. 58, pp. 511–516, 2004.

[68] J. Mercado, J. Pérez-Rigueiro, D. González-Nieto, P. Lozano-Picazo, P. López, F. Panetsos, M. Elices, A. Gañán-Calvo, G. Guinea, and M. Ramos-Gómez, "Regenerated silk fibers obtained by straining flow spinning for guiding axonal elongation in primary cortical neurons," *ACS Biomaterials Science & Engineering*, vol. 6, no. 12, pp. 6842–6852, 2020.

[69] K. E. Miller and D. C. Samuels, "The axon as a metabolic compartment: protein degradation, transport, and maximum length of an axon," *Journal of theoretical biology*, vol. 186, no. 3, pp. 373–379, 1997.

[70] D. M. O'Connor and N. M. Boulis, "Gene therapy for neurodegenerative diseases," *Trends in molecular medicine*, vol. 21, no. 8, pp. 504–512, 2015.

[71] M. O'Toole, P. Lamoureux, and K. E. Miller, "A physical model of axonal elongation: force, viscosity, and adhesions govern the mode of outgrowth," *Biophysical journal*, vol. 94, no. 7, pp. 2610–2620, 2008.

[72] M. O'Toole, R. Latham, R. M. Baqri, and K. E. Miller, "Modeling mitochondrial dynamics during in vivo axonal elongation," *Journal of theoretical biology*, vol. 255, no. 4, pp. 369–377, 2008.

[73] N. Petit, "Control problems for one-dimensional fluids and reactive fluids with moving interfaces," in *Advances in the theory of control, signals and systems with physical modeling*. Springer, 2010.

[74] B. Petrus, J. Bentsman, and B. G. Thomas, "Enthalpy-based feedback control algorithms for the Stefan problem," in *2012 IEEE 51st IEEE Conference on Decision and Control (CDC)*, 2012, pp. 7037–7042.

[75] M. Pool, J. Thiemann, A. Bar-Or, and A. E. Fournier, "Neuritetracer: a novel imagej plugin for automated quantification of neurite outgrowth," *Journal of neuroscience methods*, vol. 168, no. 1, pp. 134–139, 2008.

[76] B. Rathnayake and M. Diagne, "Event-based boundary control of one-phase Stefan problem: A static triggering approach," in *2022 American Control Conference (ACC)*. IEEE, 2022, pp. 2403–2408.

[77] ——, "Event-based boundary control of the stefan problem: A dynamic triggering approach," in *2022 IEEE 61st Conference on Decision and Control (CDC)*. IEEE, 2022, pp. 415–420.

[78] ——, "Observer-based periodic event-triggered boundary control of the one-phase stefan problem," *IFAC-PapersOnLine*, vol. 56, no. 2, pp. 11 415–11 422, 2023.

[79] ——, "Periodic event-triggered boundary control of a class of reaction-diffusion pdes," in *2023 American Control Conference (ACC)*. IEEE, 2023, pp. 1800–1806.

[80] P. Recho, A. Jerusalem, and A. Goriely, "Growth, collapse, and stalling in a mechanical model for neurite motility," *Physical Review E*, vol. 93, no. 3, p. 032410, 2016.

[81] L. Ribar and R. Sepulchre, "Neuromorphic control: Designing multiscale mixed-feedback systems," *IEEE Control Systems Magazine*, vol. 41, no. 6, pp. 34–63, 2021.

[82] D. C. Samuels, H. Hentschel, and A. Fine, "The origin of neuronal polarization: a model of axon formation," *Philosophical Transactions of the Royal Society of London. Series B: Biological Sciences*, vol. 351, no. 1344, pp. 1147–1156, 1996.

[83] A. Selivanov and E. Fridman, "Distributed event-triggered control of diffusion semilinear pdes," *Automatica*, vol. 68, pp. 344–351, 2016.

[84] C. J. Shatz, "The developing brain," *Scientific American*, vol. 267, no. 3, pp. 60–67, 1992.

[85] N. A. Silva, N. Sousa, R. L. Reis, and A. J. Salgado, "From basics to clinical: a comprehensive review on spinal cord injury," *Progress in neurobiology*, vol. 114, pp. 25–57, 2014.

[86] A. Smyshlyaev and M. Krstic, "Closed-form boundary state feedbacks for a class of 1-D partial integro-differential equations," *IEEE Transactions on Automatic Control*, vol. 49, no. 12, pp. 2185–2202, 2004.

[87] L. Squire, D. Berg, F. E. Bloom, S. Du Lac, A. Ghosh, and N. C. Spitzer, *Fundamental neuroscience*. Academic press, 2012.

[88] G. B. Stokin and L. S. Goldstein, "Axonal transport and alzheimer's disease," *Annu. Rev. Biochem.*, vol. 75, no. 1, pp. 607–627, 2006.

[89] G. A. Susto and M. Krstic, "Control of PDE–ODE cascades with Neumann interconnections," *Journal of the Franklin Institute*, vol. 347, no. 1, pp. 284–314, 2010.

[90] D. M. Suter and K. E. Miller, "The emerging role of forces in axonal elongation," *Progress in neurobiology*, vol. 94, no. 2, pp. 91–101, 2011.

[91] S. Tang and C. Xie, "State and output feedback boundary control for a coupled PDE–ODE system," *Syst. Contr. Lett.*, vol. 60, no. 8, pp. 540–545, 2011.

[92] S. Thuret, L. D. Moon, and F. H. Gage, "Therapeutic interventions after spinal cord injury," *Nature Reviews Neuroscience*, vol. 7, no. 8, pp. 628–643, 2006.

[93] T. Trappenberg, *Fundamentals of computational neuroscience*. OUP Oxford, 2009.

[94] D. Tsubakino, M. Krstic, and S. Hara, "Backstepping control for parabolic pdes with in-domain actuation," in *2012 American Control Conference (ACC)*. IEEE, 2012, pp. 2226–2231.

[95] A. Van Ooyen, B. P. Graham, and G. J. Ramakers, "Competition for tubulin between growing neurites during development," *Neurocomputing*, vol. 38, pp. 73–78, 2001.

[96] M. P. Van Veen and J. Van Pelt, "Neuritic growth rate described by modeling microtubule dynamics," *Bulletin of mathematical biology*, vol. 56, no. 2, pp. 249–273, 1994.

[97] S. Wang and F. Woittennek, "Backstepping-method for parabolic systems with in-domain actuation," *IFAC Proceedings Volumes*, vol. 46, no. 26, pp. 43–48, 2013.

[98] H. Yu, M. Diagne, L. Zhang, and M. Krstic, "Bilateral boundary control of moving shockwave in LWR model of congested traffic," *IEEE Transactions on Automatic Control*, 2020.

[99] F. Zubler and R. Douglas, "A framework for modeling the growth and development of neurons and networks," *Frontiers in computational neuroscience*, vol. 3, p. 757, 2009.